DESIGN AND CALIBRATION OF A RAPID-RESPONSE THIN-FILM HEAT FLUX GAGE

by

David Scott Campbell

Thesis submitted to the Faculty of the

Virginia Polytechnic Institute and State University

in partial fulfillment of the requirements for the degree of

Master of Science

in

Mechanical Engineering

APPROVED:

T. E. Diller, Chairman

D. P. Telionis

A. Moutsoglou

June 1985

Blacksburg, Virginia

DESIGN AND CALIBRATION OF A RAPID-RESPONSE THIN-FILM HEAT FLUX GAGE

by

David Scott Campbell

T. E. Diller, Chairman

Mechanical Engineering

(ABSTRACT)

A local heat-flux measurement system was built, calibrated and tested for use in unsteady flows. The system was designed to maintain constant wall temperature boundary conditions. The measuring element is a thin-film heat flux gage made by sputter-coating gold on a substrate. A constant-temperature anemometer is used to maintain the thin-film gage at a specified temperature under fluctuating conditions. A separate temperature control system maintains the surrounding boundary at the gage temperature.

The system was calibrated for both steady and unsteady flows using a specially designed calibrator for local heat flux gages. The steady calibration was done with predominantly convective heat transfer. The unsteady calibration was achieved by adding oscillating radiant energy to the surface. Consequently, quantitative results can be obtained for both mean and fluctuating components of the heat transfer. The frequency response was good to 92 hertz. Sample results are presented for unsteady heat transfer caused by the vortex shedding from a cylinder in a steady crossflow. The shedding frequency was 82 hertz.

ACKNOWLEDGEMENTS

First and foremost, I would like to thank Dr. T. E. Diller for his guidance, insight and patience during his supervision of this thesis. I appreciate his constant support and genuine concern that he showed for this work.

I would like to thank the members of my advisory committee, Dr. T. E. Diller (Chairman), Dr. D. P. Telionis and Dr. A. Moutsoglou for giving of their time to provide input to this thesis project.

The support of this project as part of contract No. DE-A505-82ER 12022 under the direction of Dr. Oscar Manley from the Office of Basic Energy Research, Department of Energy, is gratefully acknowledged.

I would like to thank all the faculty and fellow graduate students who encouraged me and made my graduate studies enjoyable and memorable. I would like to thank Dr. Wood for teaching me the value of asking others for insight on engineering problems (ie. two heads are better than one). I also express thanks to Zelda, our bookkeeper, and the men in the shop, without whom all this would not have been possible.

I would especially like to thank my father, sister and grandparents for their constant support (financial and otherwise). I also thank my girl friend, Mary, and her mother for all the encouragement and providing a home-away-from-shack during the last year and a half. In conclusion, I pray that I will use the knowledge that I leave here with to glorify God and His son, the Lord Jesus Christ.

TABLE OF CONTENTS

LIST OF FIGURES

LIST OF TABLES

NOMENCLATURE

Symbol		Meaning
A	-	peak-to-peak amplitude of bridge voltage signal, volts
A_{film}	-	surface area of gage film, including copper contacts, m^2
A_{film}	-	surface area of calibration plate, m^2
Bi	-	Biot number, hx/k
D	-	cylinder diameter, m
E_{AC}	-	A.C. RMS component of bridge voltage, volts RMS
E_{br}	-	bridge voltage, volts
E_{DC}	-	D.C. component of bridge voltage, volts
E_{film}	-	voltage across gold film, volts
E_{htr}	-	A.C. RMS voltage across calibration plate heater
f	-	frequency, Hz
f_{cut}	-	cutoff frequency
h	-	heat transfer coefficient, $W/m^2\text{-}°C$
$\bar{h}$	-	time-averaged heat transfer coefficient, $W/m^2\text{-}°C$
h_{avg}	-	average heat transfer coefficient over calibration plate, $W/m^2\text{-}°C$
h_{gage}	-	heat transfer coefficient calculated from gage output, $W/m^2\text{-}°C$
h_r	-	radiation heat transfer coefficient, $W/m^2\text{-}°C$
h_{theo}	-	heat transfer coefficient determined from cylinder stagnation point correlation, $W/m^2\text{-}°C$
k	-	thermal conductivity of medium (air or solid), $W/m\text{-}°C$

Nu - Nusselt number, hD/k

P_{atm} - atmospheric pressure, in. Hg

P_{stag} - stagnation pressure, in. H_2O

PD - percent difference

Q_{back} - the portion of Q_{htr} which is lost through the back of the calibration plate, W

Q_{cond} - the conduction losses into the substrate due to temperature mismatch, W

Q_{film} - power dissipated in the gage gold film, W

Q_{htr} - power dissipated in calibration plate heater, W

Q_{side} - the portion of Q_{htr} which is lost through the balsa wood strip around the calibration plate, W

Q_{top} - the portion of the calibration plate power which is lost from the top surface, W

q_{film} - unit power dissipated in gage film, W/m^2

q_{rad} - unit power lost from gage to radiation, W/m^2

q_{gage} - unit power dissipated in gage film, W/m^2

R_{back} - thermal resistance through the back of the calibration plate, W/°C

R_{cable} - electrical resistance of the co-axial cable leading to the gage, ohms

R_{film} - electrical resistance of the gage film, ohms

R_{gal} - electrical resistance of the gage leads, ohms

R_{htr} - electrical resistance of the calibration plate heater, ohms

R_{oper} - gage operating resistance (electrical) set into IFA-100, ohms

R_{top} - thermal resistance through the top of the calibration plate, W/°C

Re - Reynolds number, VD/ν

rr - maximum rise rate of the bridge voltage, volts/sec

T_{film} - gage film temperature, °C

T_a - ambient temperature, for radiation loss calculations, °C

T_∞ - freestream temperature, °C

T_m - mean film temperature for calculating air properties, °C

T_p - average calibration plate temperature, °C

x - width of balsa wood strip, m

V_{htr} - A.C. RMS voltage across calibration plate heater, volts RMS

V - velocity, m/sec

$w_{A_{film}}$ - uncertainty of A_{film} measurement

$w_{E_{DC}}$ - uncertainty of E_{DC} measurement

$w_{E_{AC}}$ - uncertainty of E_{AC} measurement

$w_{h_{gage}}$ - uncertainty of h_{gage} calculation

$w_{P_{atm}}$ - uncertainty of P_{atm} measurement

$w_{P_{stag}}$ - uncertainty of P_{stag} measurement

$w_{Q_{cond}}$ - uncertainty of gage conduction losses due to 0.1°C mismatch

$w_{q_{film}}$ - uncertainty of q_{film} calculcations

$w_{R_{oper}}$ - uncertainty of R_{oper} measurement

$w_{R_{gal}}$ - uncertainty of R_{gal} measurement

$w_{R_{cable}}$ - uncertainty of R_{cable} measurement

$w_{T_{film}}$ - uncertainty of T_{film} measurement

$w_{T_{\infty}}$ - uncertainty of T_{∞} measurement

w_{β} - uncertainty of β, due to differences in test conditions

α - resistance-temperature coefficient

β - constant associated with cylinder stagnation point calibration (usually 0.955)

Δ - change in variable

ε_{film} - gage film emissivity

ε_{p} - calibration plate emissivity

ν - kinematic viscosity of air, m^2/sec

σ - Stefan-Boltzman constant, 5.67×10^{-8} W/m^2K

τ - characteristic response time, sec

1.0 INTRODUCTION

The object of this research is to develop an instrument which can transduce rapidly varying heat fluxes. Many different methods have been used to measure the time-averaged local convective heat transfer between a fluid and a heated surface. However, very little experimental information has been collected about the time-resolved heat transfer from a surface. Many flows that have been traditionally treated as steady actually have significant components of unsteadiness. Examples range from vortex shedding by cylinders in crossflow to the effect of rotor wakes on stator blades in turbomachinery to the growth of flow instabilities leading to turbulence to the bubble regime of fluidized beds. The impetus for this development is an ongoing investigation of the effects of flow pulsation on heat transfer over a cylinder situated in a crossflow. The understanding of the fundamental heat transfer mechanisms would be greatly aided by detailed time-resolved measurements of the heat transfer.

The gage developed for this research is constructed of a thin film of gold sputter-coated onto a substrate. A constant-temperature anemometer is used to maintain the thin-film gage at a specified temperature under fluctuating conditions. A small thermocouple is imbedded in the substrate immediately below the film. This is used to match the film temperature with the surrounding surface temperature so that a constant wall temperature boundary condition is maintained and conduction losses, due to temperature mismatch, are minimized. The heated film covers the

entire exposed side of the substrate. This configuration maintains the constant wall temperature boundary condition (i.e. does not disturb the thermal boundary layer development) so that representative local heat transfer measurements can be made. Also, losses into the substrate, due to convection from an unheated surface, are prevented.

A large portion of this research was involved with developing both steady and unsteady heat flux calibration methods for the gage. Two convective methods were developed for the time-averaged calibration. One method consisted of measuring the heat transfer from a guarded hot plate situated in an impinging jet flow and comparing the results to the output of the gage mounted in the plate operating at the same local conditions. The other method involved using the gage to measure the time-mean heat transfer at the front stagnation point on a cylinder situated in steady crossflow. The results were then compared to other time-mean experimental measurements at this point.

Two methods were also used to determine the frequency response of the gage. The first method was a standard electronic square wave test used with constant-temperature anemometers for estimating the frequency response of hot-wire and hot-film velocity probes. The other method, developed for this research, consisted of directing a chopped thermal radiation source at the gage, which created a square wave variation in the surface heat flux. The settling time due to this perturbation was used to determine the response.

Sample results are presented for unsteady heat transfer caused by the vortex shedding at a cylinder in Appendix B. Measurements were made in the laminar boundary layer region near the front stagnation point. These

results are presented as a demonstration of the potential of this type of gage.

2.0 LITERATURE REVIEW

One of the early methods for measuring local heat fluxes was the calorimeter or slug-type gage [1]. In this type of gage a metallic slug or plate is mounted in a 'cold' wall and the temperature of the slug is recorded versus time. The heat transfer can then be obtained by time differentiating the temperature-time history. A drawback of this instrument is that it is limited to short duration heat transfer measurements, since the slug will eventually tend towards the fluid temperature. Also, the response time is limited by the slug material properties (density, specific heat, conductivity).

A second type of convective heat transfer gage is the circular foil-type gage developed by R. Gardon [2] in the early 1950's for the measurement of radiative heat transfer. More recently it has also been used for convective heat transfer measurements [3,4]. This gage is constructed of a thin circular foil of constantan mounted on the end of a hollow copper tube. A small gage copper wire is then welded to the center of the constantan foil. This forms a thermocouple circuit which measures the temperature difference between the center and the edge of the foil. The temperature difference can be related to the heat transfer, depending on the heating condition (convective or radiative). The gage is mounted with the foil flush with the test surface. Although this gage can be used to measure unsteady heat transfer, the response is limited to less than 1 hertz by the thermal capacity of the constantan foil [5,6].

Other developments in measuring transient convective heat fluxes includes the work by R.J. Vidal [7] at Cornell Aeronautical Labs in the late 1950's. A gage was constructed of a thin film of highly conducting metal (platinum, gold, nickel) deposited on a low conductivity substrate, typically quartz. He utilized the resistance-temperature variation of certain metals to create a surface temperature sensor (the metallic film). The heat flux can be deduced from the temperature-time history by solving the one-dimensional non-homogeneous conduction equation for this situation. Use of this type of gage has found extensive use in turbine blade [8,9,10] and hypersonic shock tube testing [11,12] where response on the order of 1 msec is required. However, this type of gage is used exclusively for heat transfer to cold walls in highly transient environments (not steady heat transfer). Variations of this include passing a small current through the film, which generates a small, but significant, offset heat flux [12].

In order to continuously measure unsteady heat transfer, some investigators have used constant-temperature anemometer (CTA) control systems to supply power to gages constructed similar to the previously mentioned gage used to measure transient heat fluxes [13,14,15,16]. The anemometer maintains the gage film at a constant resistance (and hopefully constant temperature). The heat transfer from this type of gage is assumed to be the joule heating in the thin surface film, with some correction made for conduction losses into the substrate (usually large). These gages are flush mounted and are operated either at the temperature of the surrounding wall or with some overheat. They have been used for measuring continuous unsteady heat flux from cylinders in fluidized beds [14,15]

and the turbulent heat transfer fluctuations on the surface of a cylinder [13] and a sphere [16]. Since these gages are controlled by CTA circuits, they can be expected to have relatively high frequency responses. Here, limits on frequency response come from the thermal capacity of the metallic films and substrates and especially from protective films used for erosive environments [14].

This type of thin-film gage with constant-temperature anemometer control has also been used with a large overheat to measure shear stress [17,18]. Because the temperature of the film is much higher than the surrounding surface, the gage actually measures the thermal boundary layer that develops over the film strip itself. All of the surrounding surface is purposely adiabatic to localize the thermal boundary layer development to the heated strip on the gage. Conversely, heat flux measurements are usually desired at locations on an entire surface that is heated. The development of the thermal boundary layer over the surface is, therefore, a necessary part of the experiment. The difference, then, between a shear stress measurement and a heat flux measurement is the thermal boundary condition on the surface upstream of the gage [19].

In the previous work with thin-film heat flux gages the continuity of the constant wall temperature boundary condition has often not been maintained. In some cases a significant area around the heated film is left as adiabatic surface [14] or the gage is given an overheat [15]. Some gages have even been used with a non-uniform film width, which causes spatial variations in the film heat flux [15]. The unheated surface of the substrate around the film creates a larger effective heated area from which energy is dissipated. For this problem the losses into the

substrate vary with the frequency of the freestream fluctuations [17]. Only one gage, constructed by Boulos and Pei [13], had a film which covered the entire surface of the substrate. One of the other difficulties with these small gages is accounting for the conduction losses. The non-uniform temperature around the gage makes calibration difficult, and it usually has not been reported in detail [13-16].

The calibration of heat flux gages can be divided into steady and unsteady calibrations. One method of steady calibration, used to calibrate a Gardon-type gage, consisted of measuring the total heat transfer from a flat plate normal to an impinging jet flow [4]. The total heat transfer measured from a guarded hot plate was then used to calibrate the output voltage of the Gardon gage that was mounted in the flat plate. Some authors using CTA-controlled gages compared the gage heat transfer results over a cylinder in steady cross-flow to other experimental results [14,15]. The reported agreement for these cases was from 6 to 7 percent, with large corrections made for conduction losses. Instead of averaging over the whole cylinder, another possible method of calibration is to use the well-documented prediction for the stagnation point of a cylinder in an air crossflow [20]

$$Nu = 0.95\sqrt{Re}$$

where the Reynolds number and Nusselt number are based on the cylinder diameter.

The unsteady calibration can be divided into two parts: determining the frequency response and determining the amplitude roll-off. Methods

for determining the frequency response are not discussed in great detail in the cited literature for the CTA controlled gages. However, conversations with Figliola [21] revealed that he used a step change in heat transfer [a damp cloth being suddenly applied to the gage] to obtain a response time of his gage. Boulos and Pei [13] used the electronic sine wave test described by Nielson and Rasmussen [22] to determine the -3dB roll-off point. A classical method, reported by Bellhouse and Schultz [17] used a shaker plate to determine the frequency roll-off for skin friction gages. Perry [23] describes a technique for determining the response of a constant-current anemometer which consists of a chopped thermal radiation source to obtain a simulation of a square wave variation in free-stream temperature.

The principle methods used to test anemometer systems are those of imposing either a electronic sine wave or square wave on the hot film in the system. The sine wave test, a more involved test than the square wave test, is used when optimization of the anemometer compensation controls for a given velocity probe is needed. The square wave test is widely used for quick adjustment of the anemometer controls to near optimum response conditions. Both of these tests can be used to estimate the maximum frequency response of hot-wire and hot-film velocity probes. Phase and amplitude data are used to determine the frequency roll-off with the sine wave test, while the response time is determined from a characteristic shape of the transient bridge voltage for the square wave test. Freymuth and Fingerson [24] and Freymuth [25,26,27] discuss electronic sine and square wave testing of hot-wire and hot-film constant-temperature

anemometer systems. Descriptions of these tests are also listed in Perry [23] and Goldstein [28].

The determination of amplitude and phase changes due to frequency roll-off could made by comparison to theoretical results. Papers written by Ishigaki [29,30,31], Lighthill [32] and Gersten [33] discuss solutions to various types of quasi-steady heat transfer problems. A paper by Kim et al. [34] presents results of a numerical calculation of the heat transfer from a cylinder in cross flow with a periodic freestream velocity disturbance. However, creating an experiment to match theoretical results is a difficult task due to turbulence and the ability to accurately model or develop unsteady experimental flow conditions. Therefore, discrepancies in comparing theoretical results to experimental results could be due to gage response, inadequate theoretical modeling or errors in experimental flow matching.

3.0 EXPERIMENTAL APPARATUS

This section describes the gage developed and the equipment used to calibrate it for time-averaged heat transfer and to determine the frequency response. In the latter sections, the details of the experimental procedures are given along with the data reduction methods.

3.1 HEAT FLUX GAGE

The design and construction of this heat flux gage was defined by several requirements. First, the heat transfer gage is to be used in flows with a periodic free-stream disturbance of up to 40 Hz. So the gage response should be at least 100 Hz to be able to transduce the heat transfer (neglecting turbulence). Second, the heat transfer was to be from a hot wall to a cold gas, which limits the gage type. Third, the gage is to be mounted in a cylinder and used to measure local heat transfer, so for good resolution it should substend an angle of less than 5 degrees of arc. Also, the instrument needs to be installed in the cylinder without disturbing the fluid or thermal boundary layers.

The gage chosen for this research, similar to that of Boulos and Pei [13], was the hot film type, which is maintained at a constant temperature (resistance) by a constant-temperature anemometer (CTA) unit. The gage was constructed from a thin metallic film deposited on an insulating substrate. The metal for the film was chosen such that it has a large positive variation of resistance with temperature. When connected to the

anemometer, the gage becomes one leg of a bridge circuit (Figure 1). The CTA control circuitry operates to balance the bridge under fluctuating conditions by varying the bridge voltage with a high gain feedback control circuit. The power supplied to the gage is proportional to the square of the bridge voltage. When the bridge is balanced, the gage will be at the same resistance as the control resistance, which corresponds to the film operating temperature. Moreover, the resistance-temperature curve can be measured for the gage so that the desired operating condition can be obtained.

This gage is to be operated in a wall maintained, ideally, exactly at the gage operating temperature. In this situation an energy balance reveals that the only heat lost from the gage is through forced convection and radiation to the ambient. However, for forced convection the radiation losses will be small for small wall-ambient temperature differences. Also, the gage film (gold) has a low emmissivity which further reduces the radiation losses. However, if the film temperature is not matched to the wall temperature there will be significant conduction losses (see Appendix D).

The design used is shown in Figure 2. The gage is nominally 13 mm (0.5 in) long by 2.03 mm (0.080 in) wide by 1.6 mm (0.0625 in) thick. This size spans approximately 3 degrees of cylinder arc for the 6.03 cm dia test cylinder. It is constructed of a gold film which is sputter coated onto a substrate of printed circuit board. The gage is sputtered until a nominal resistance of 25 ohms is reached. The lead wires are brought to the surface through the substrate and soldered to copper contacts on the surface. The gold film is deposited onto the copper con-

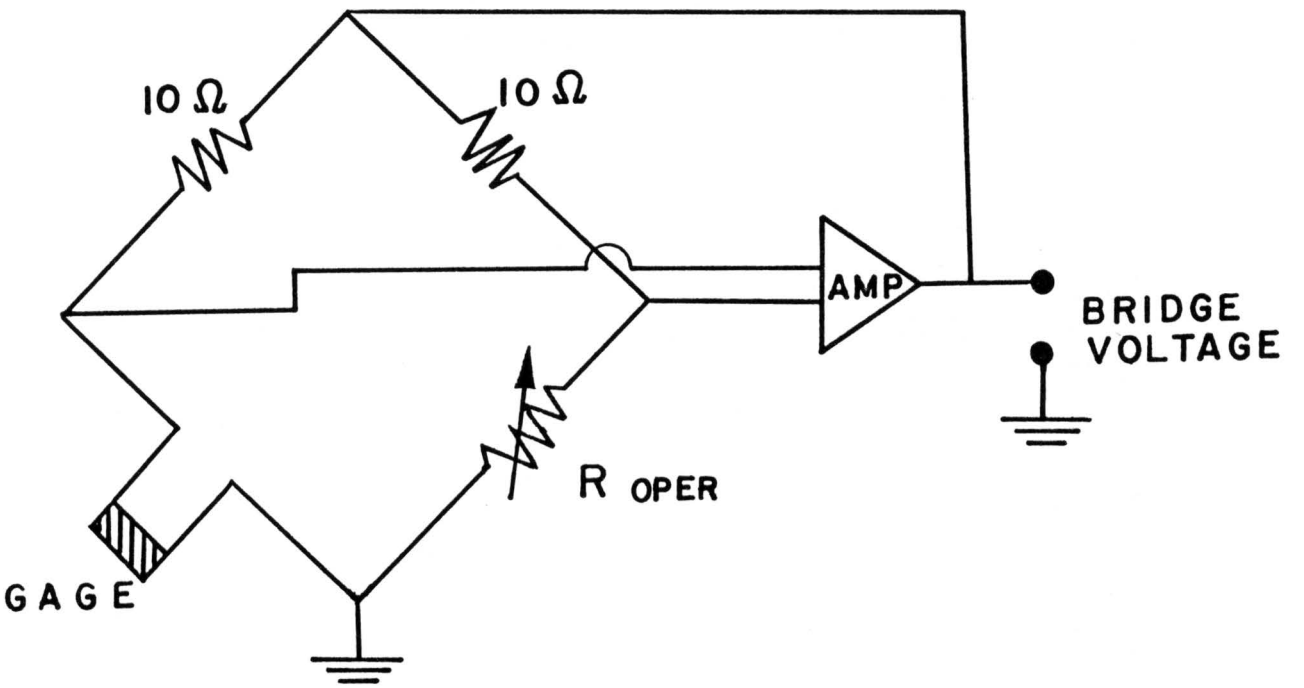

Figure 1. Bridge circuit schematic.

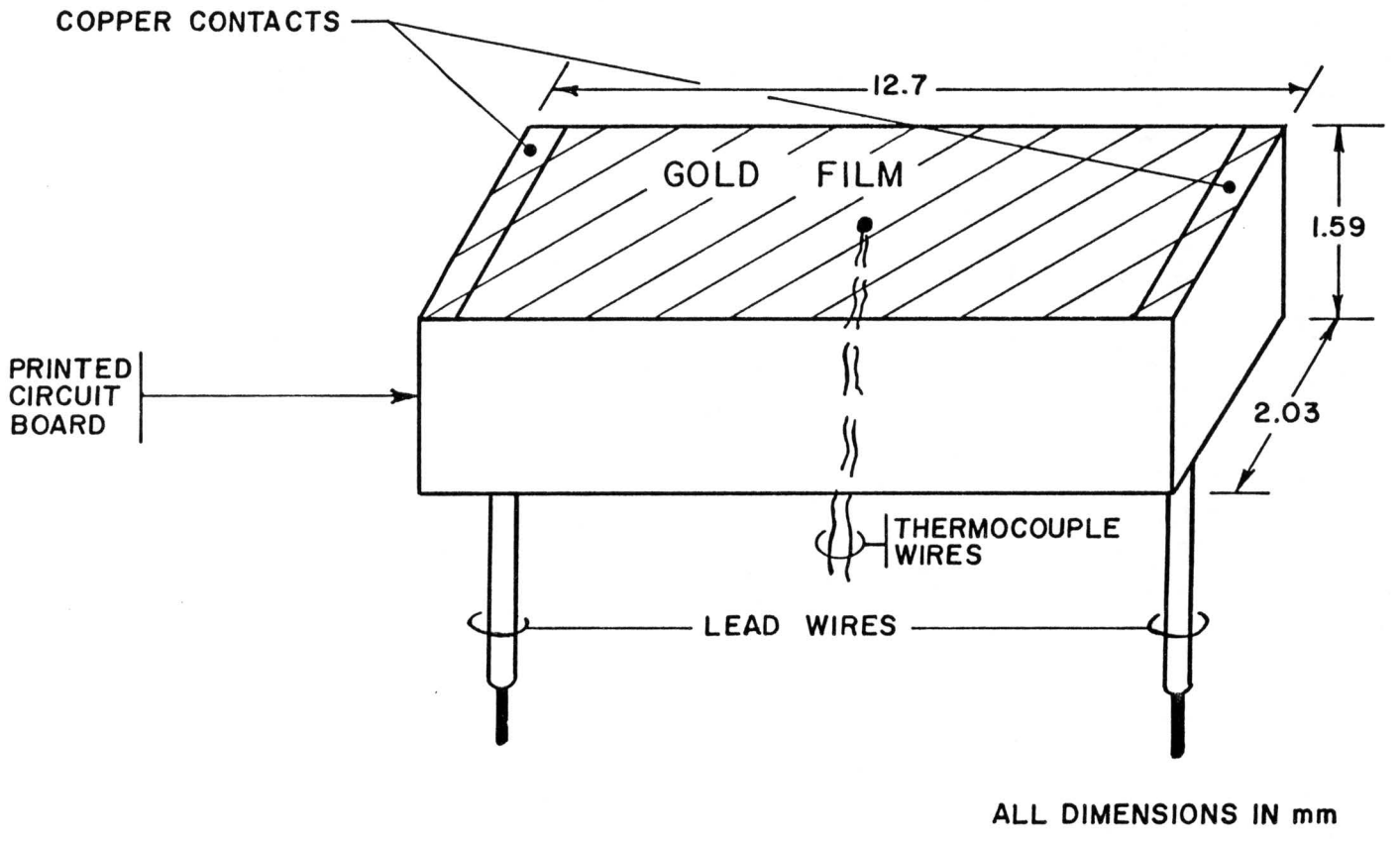

Figure 2. Thin-film heat flux gage.

tacts, which eliminates problems associated with connecting the lead wires to the film. Also, a thermocouple, with 0.076 mm (0.003 in.) diameter leads and a 0.25 mm (0.01 in.) diameter junction bead, is mounted in the center of the surface of the substrate, approximately 0.127 mm (0.005 in.) below the film. The thermocouple is used as an external monitor of the film temperature. The periphery of the gage is coated with library tape, .05 mm thick, to electrically isolate the gage from the cylinder. Details of the materials and construction of the gage are given in Appendix A.

3.2 IMPINGING FLOW CALIBRATION APPARATUS

The flat plate apparatus used for steady calibration of the heat flux gage is shown in Figure 3. It primarily consists of a blower-type small wind tunnel and a flat plate test stand. The apparatus is in the same equipment used by Borell [35], to calibrate a Gardon gage in a convective environment, except that the center plate was modified to accommodate the thin-film heat flux gage.

In operation, the wind tunnel generates a free jet which impinges on the flat plate, mounted normal to the jet. The free jet developed by the wind tunnel leaves the contraction section in a square cross sectional form (10.2 cm (4 in) by 10.2 cm (4 in)) with velocities of up to 60 m/sec. The settling chamber in the tunnel has two screens and a section of plastic straw flow straighteners to reduce turbulence and improve jet uniformity. The freestream turbulence at the plate location is approximately 2 percent.

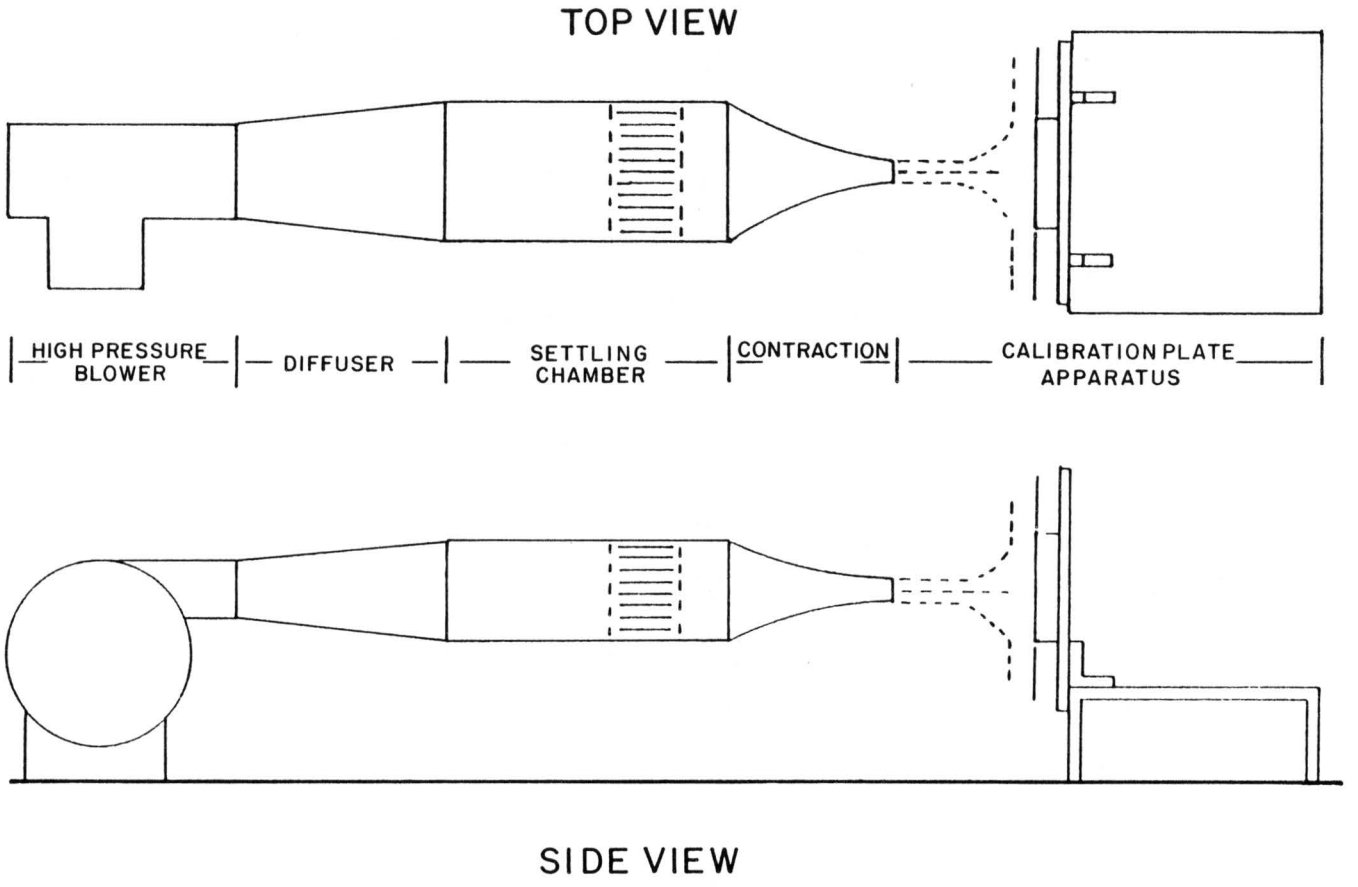

Figure 3. The impinging flow calibration stand (Fig. 16 from reference 35).

The flat plate test stand consists of a guarded calibration plate mounted in a plywood box, which in turn is slide mounted behind a stationary flow shield. The flow shield is 0.667 m square and has a 0.286m square hole cut in its center. The center hole allows the guarded calibration plate assembly to be traversed across the flow field without disturbing the flow. The calibration plate assembly has an apron shield affixed level with the calibration and guard plates, which ensures that the hole in the flow shield is always filled during a traverse.

The calibration plate, Figure 4, is constructed from an aluminum plate, 15.2 cm square by 1.27 cm thick. The plate is instrumented with fourteen 24 GA type T thermocouples and has a slot, 0.203 cm (0.08 in.) wide by 0.254 cm (0.1 in.) deep by 1.52 cm (0.6 in.) long, cut in the center to accommodate the heat flux gage. The slot has three 0.1 cm (0.040 in.) holes drilled, on 0.635 cm (0.25 in.) centers, for the gage leads. A 0.076 mm (.003 in.) diameter type T thermocouple was mounted through the center hole, behind the gage. This thermocouple was used as a monitor of the plate temperature near the gage. The center plate is edged with 0.476 cm wide balsa wood strips to reduce side losses. The calibration plate is surrounded by four guard plates, 5.1 cm by 15.2 cm by 1.27 cm thick. Each of the guard plates was instrumented with three 24 GA type T thermocouples, each positioned directly opposite one along the edge of the calibration plate.

The center plate and guard plates were heated with silicone rubber resistance heaters capable of 0.78 W/m^2. The power to each of the heaters was supplied by separate variable voltage autotransformers. The center plate was maintained isothermal to $\pm$ 1°C and the guard plates were main-

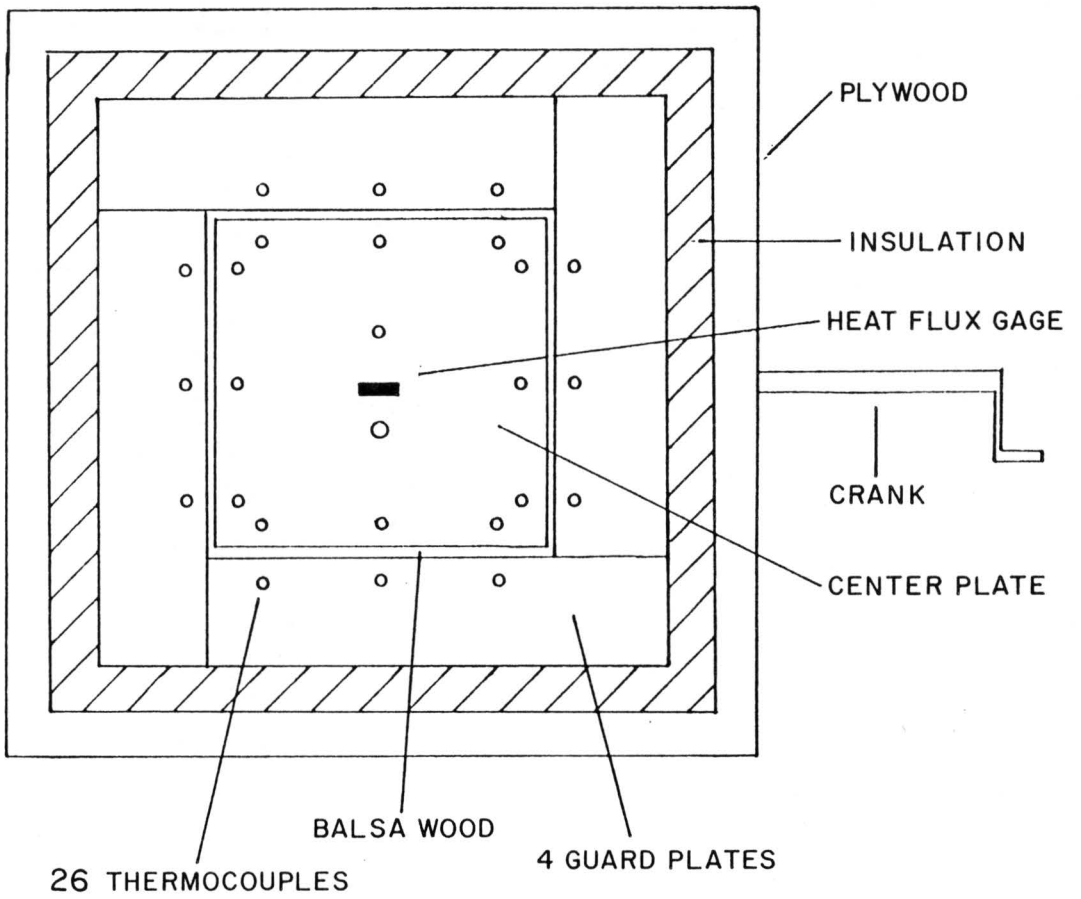

Figure 4. The calibration plate (Fig. 17 from reference 35).

tained to within ± 0.2°C of the center plate temperature. Although the side losses to the guard plates were negligble, the losses through the balsa wood to the surrounding air, through convection, were modeled and included in the heat transfer calculations. The losses through the back of the plate were minimized by various insulation layers and were also modeled and included in the heat transfer calculations (Figure 5). Further details on the construction and materials used in this apparatus are given by Borell [35].

3.2.1 IMPINGING FLOW CALIBRATION PROCEDURE

For the impinging flow calibration tests, the free jet tunnel was turned on and the power to the heaters was adjusted until the center and guard plates came to equal steady state temperatures. The center and guard plates temperatures along with the gage and freestream temperatures were read from a Doric 410A thermocouple readout, calibrated to ± 0.1°C. Also, the A.C. RMS voltage across the calibration plate heater and the heater resistance were recorded from a Hewlett-Packard 3468A digital volt meter.

The gage operating temperature was then adjusted until the thermocouple in the gage matched the thermocouple mounted behind the gage to within 0.1°C. Six randomly selected bridge voltages (three A.C. RMS and three D.C. voltages) were then recorded for processing the heat transfer data. Also, the probe cable and operating resistances were recorded from the IFA-100.

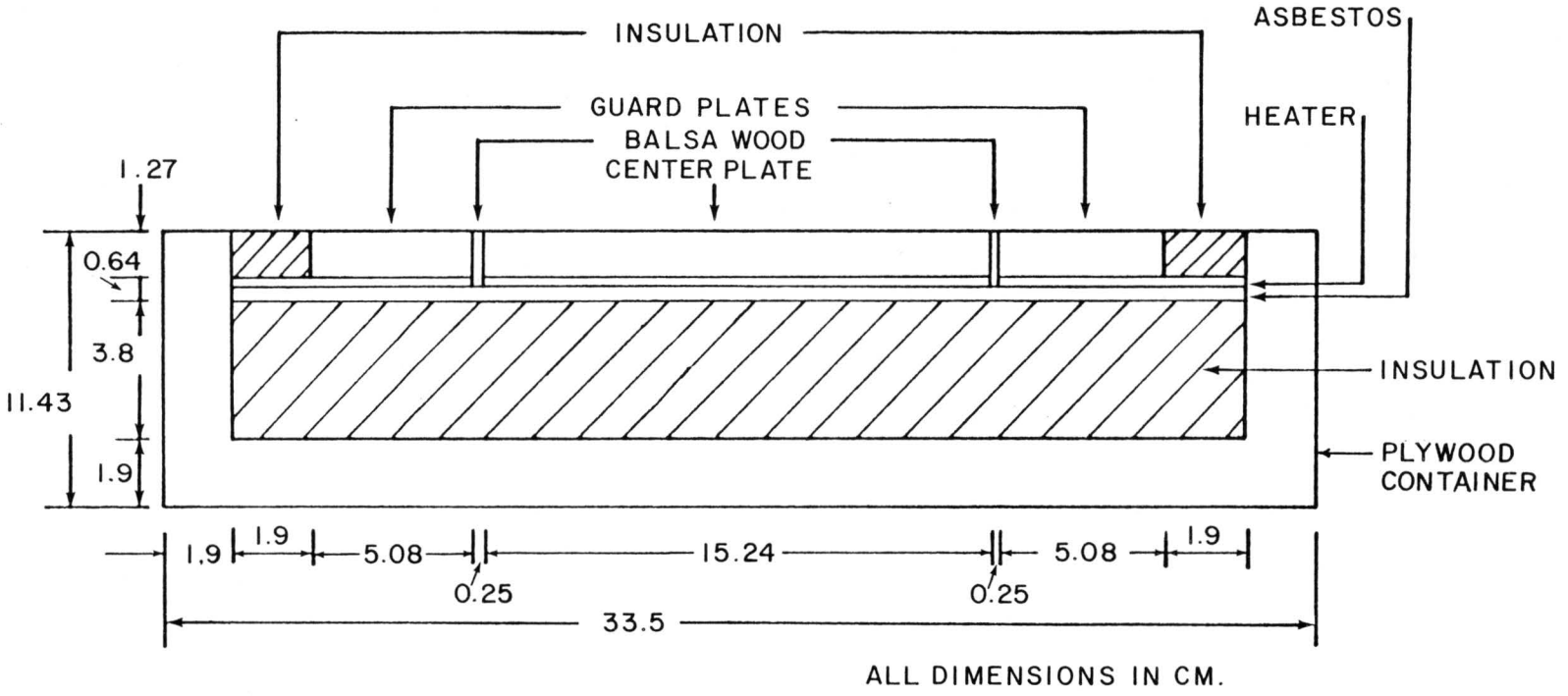

Figure 5. Cross-sectional view of the calibration plate (Fig. 18 from reference 35).

3.3 CYLINDER STAGNATION CALIBRATION APPARATUS

3.3.1 TEST CYLINDER

The test cylinder was constructed from a hollow aliminum cylinder with a 6.03 O.D., 0.55 cm thick and 36 cm long. The cylinder was split lengthwise for ease of installation of instrumentation. When assembled, the cylinder was held together by Plexiglas end pieces (see Figure 6). A pointer was attached to one end cap and a large protractor was fitted to the test section. The cylinder assembly was held in place in the tunnel test section by threaded aluminum pins, which also allowed the cylinder to rotate. The cylinder was heated by a 0.318 cm (1/8 in.) thick silicone rubber wire resistance heater capable of 0.78 W/m^2. The heater was held against the inside cylinder wall by a 4.13 cm (1-5/8 in.) O.D. piece of RUBBATEX pipe insulation. The hollow insulation tube allowed passage of the instrumentation lead wires down the axis of the cylinder and out the ends. The cylinder was instrumented with four 24 GA type T thermocouples. The thermocouples were soldered into a 0.318 cm (1/8 in.) O.D. brass tube, Figure 7, and press fit into holes drilled in the cylinder wall.

The heat flux gage is fitted into a slot milled in the center of one of the aluminum halves (see Figure 8). The slot is 0.191 cm wide by 0.254 cm deep by 1.52 cm (nom) long. The slot had 3 holes, 0.10 cm (0.040 in.) diameter and 0.635 cm (0.25 in.) apart on center, drilled through the cylinder. These holes allowed the gage leads and thermocouple wires to pass into the cylinder. The ends of the slot were rounded due to milling,

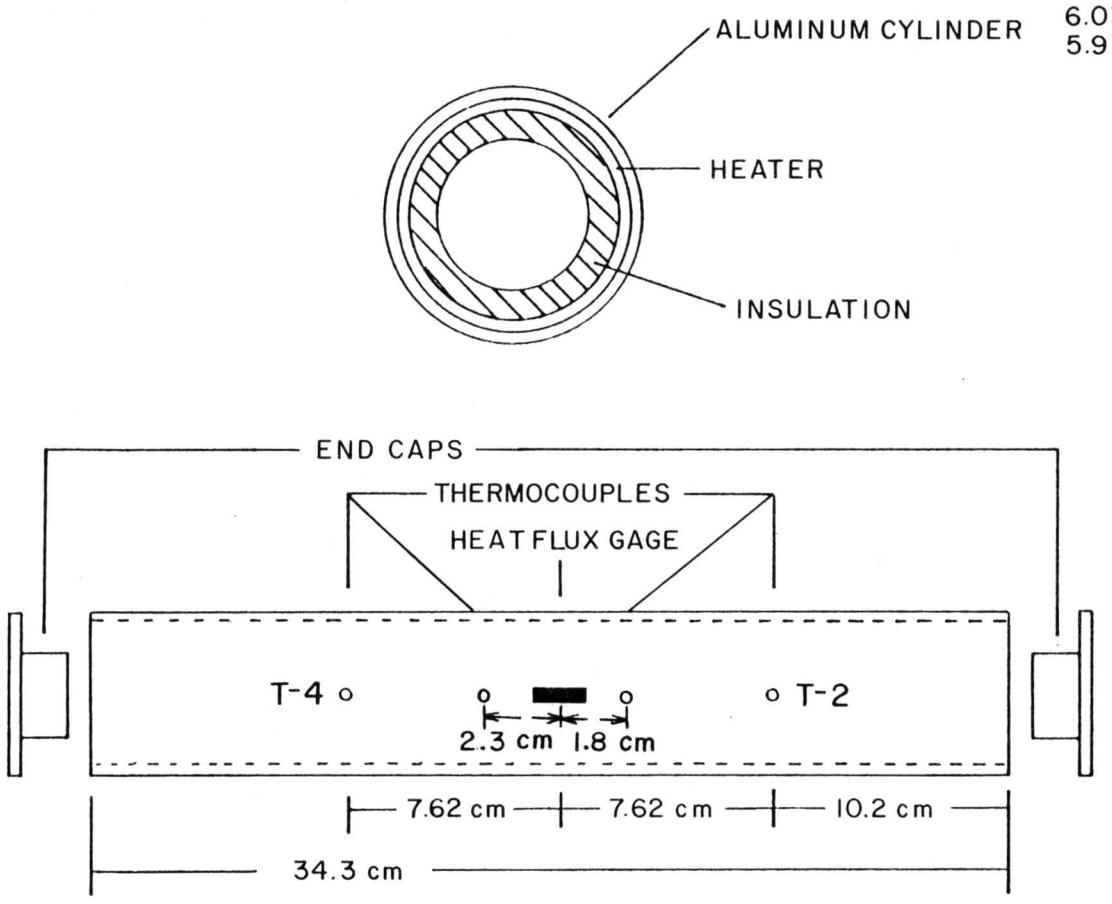

Figure 6. The cylinder used for stagnation point calibration (Fig. 4 from reference 35).

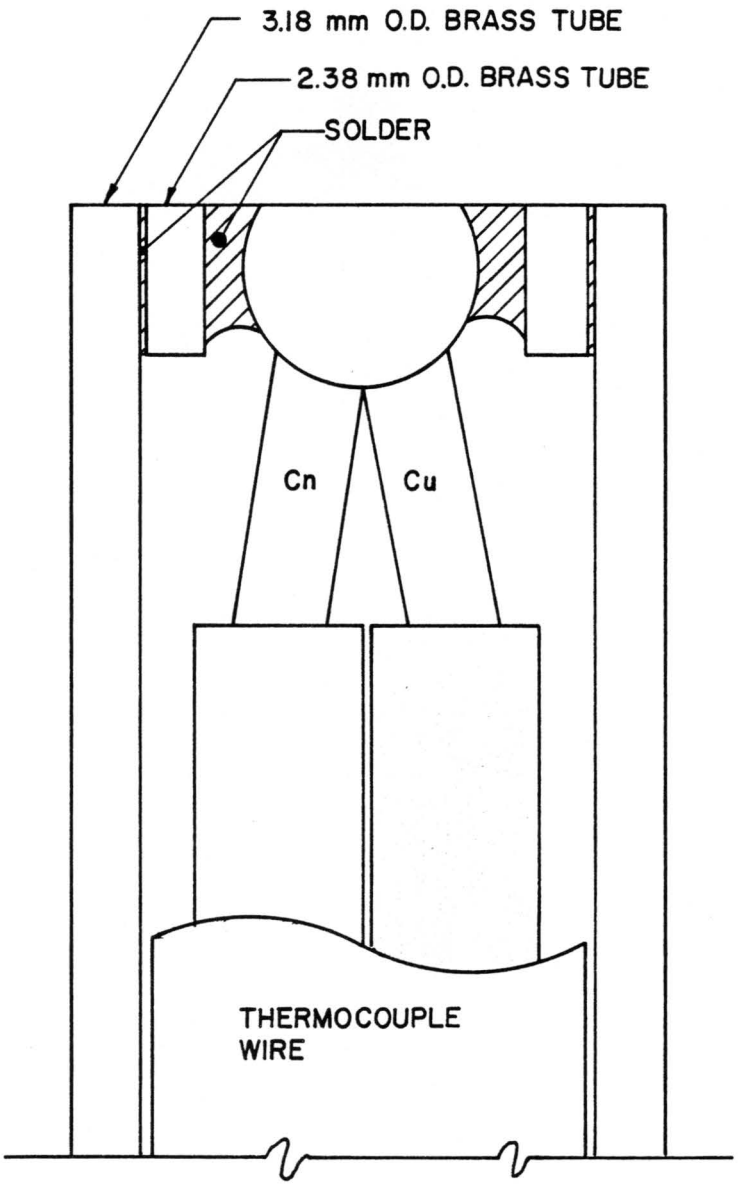

Figure 7. The Thermocouple plug.

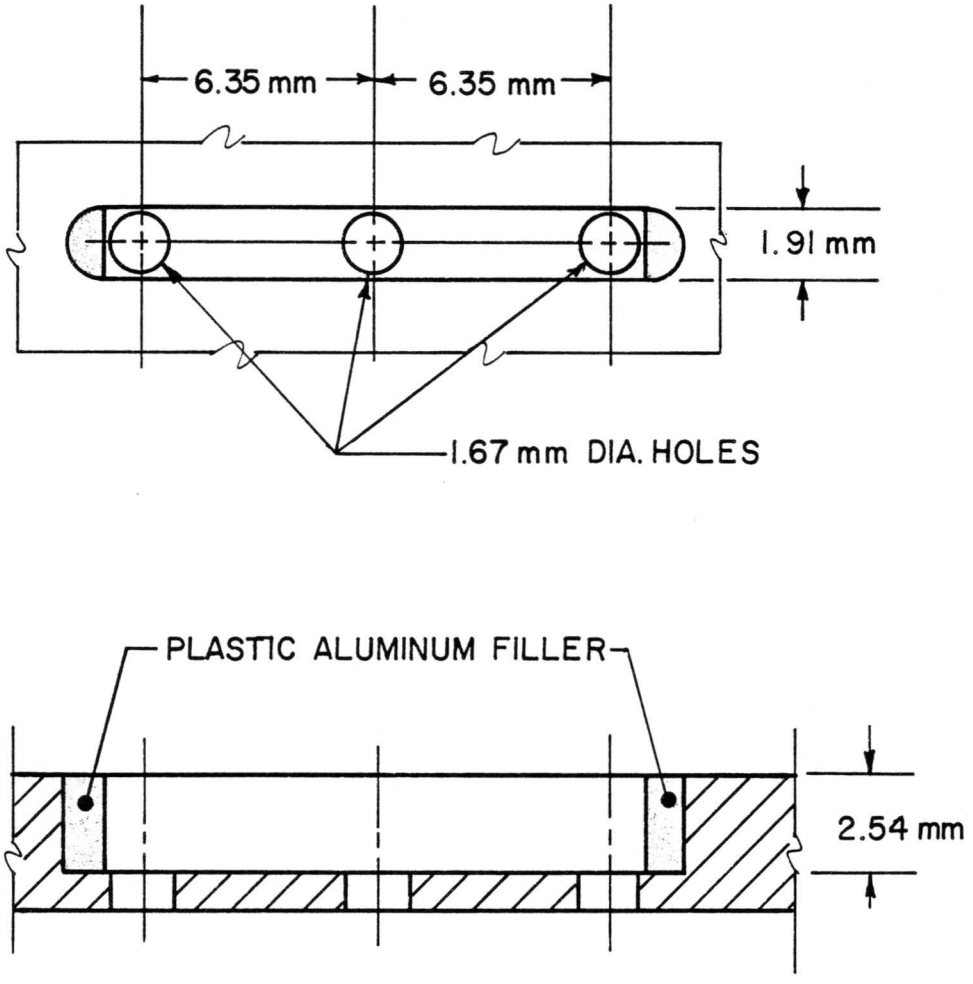

Figure 8. Slot for the heat flux gage.

but they were made square by filling with Dupont Plastic Aluminum. This is the same cylinder described and used by Borell [35], except for the modification for mounting the heat flux gage used in this research.

The temperature of the cylinder was controlled by a Eurotherm 810 temperature controller and a Eurotherm 831 Phase Angle Fired power supply. The controller is a three-term-type controller (proportional, integral, differential), which allowed the variation of the control parameters to optimize the response of the system. The terms for the controller were determined experimentally. The terms selected for this research maintained the local cylinder temperatures to $\pm$ 0.1°C, and the cylinder temperatures stabilized in about 10 minutes from a cold start. The 0.55 cm thick cylinder wall allowed good axial and circumferential conduction which aided in maintaining the cylinder temperature to $\pm$ 0.5°C in the center region. Also, the temperature gradient through the cylinder wall was negligible even at the maximum heat flux condition, as determined by a 1-D conduction analysis (0.1°C at 4500 W/m^2)

3.3.2 WIND TUNNEL

The wind tunnel used in this research was a low speed blower type capable of velocities of up to 22 m/sec (Figure 9). Since this tunnel has also been used for pulsating flow research [35], the shutters were locked in a horizontal position to minimize flow disturbances and maximize the flow rate. The tunnel has a contraction ratio of 6:1 and has a Plexiglas test section 1.24 m long with a cross section of 24.5 by 36 cm. The test section has 25 percent blockage with the 6.03 cm diameter cylinder used.

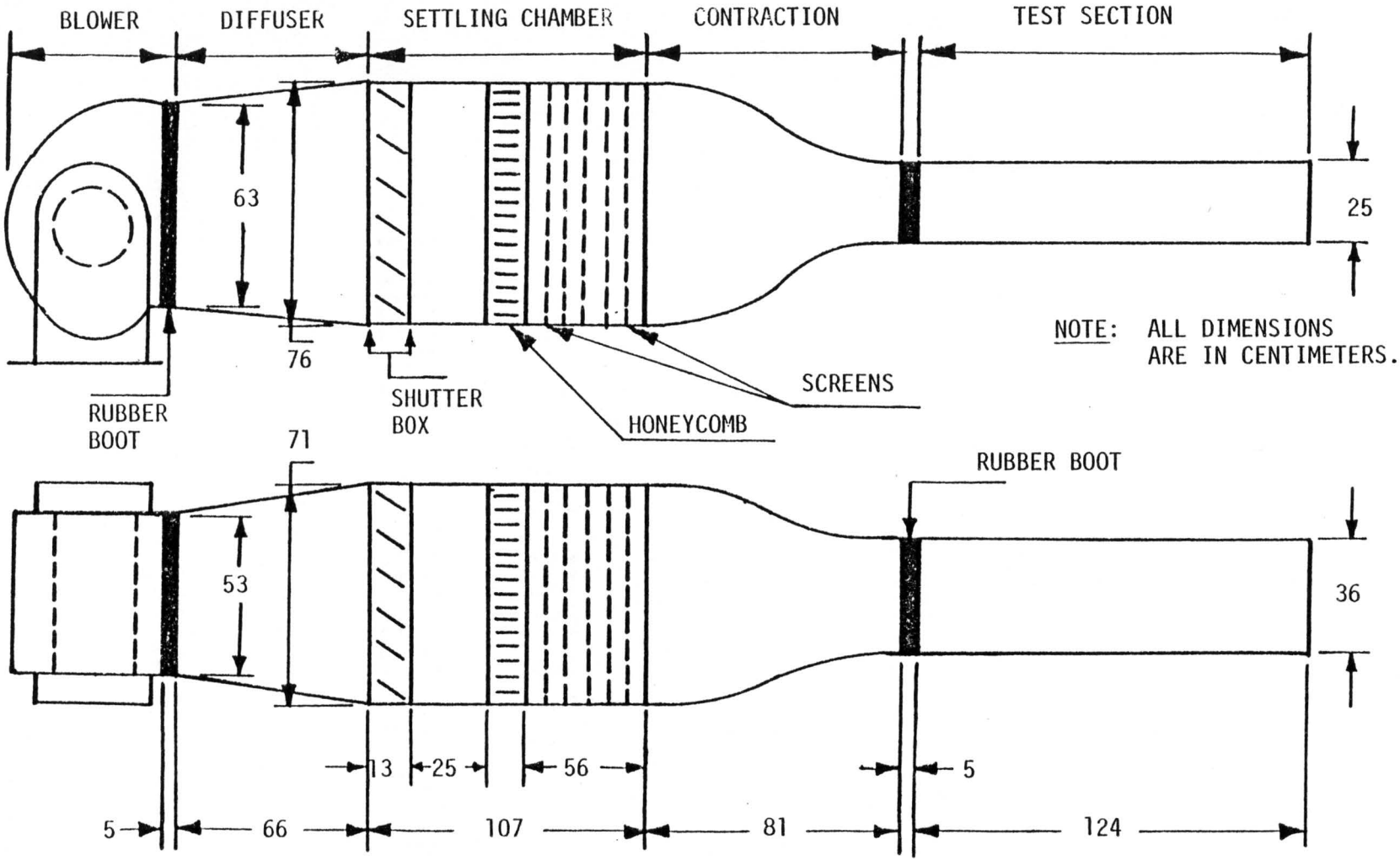

Figure 9. The wind tunnel (Fig. 3 from reference 35).

The turbulence intensity is 0.2 percent and the flow is uniform to ± 1.5 percent, outside of the the wall boundary layers [35]. The turbulence is controlled with a section of honeycomb and 5 screens located in the settling chamber.

3.3.3 CYLINDER STAGNATION CALIBRATION PROCEDURE

Prior to taking heat transfer data on the cylinder, the front stagnation point was located and used to properly align the cylinder. This point was located to ± 0.5 degrees by the existance of a rectified heat transfer signal due to zero net flow at the stagnation point (Meier et al.[36]). This phenomenon causes the heat transfer signal to have significant frequency content at twice the shedding frequency. This phenomena was monitored with a Hewlett-Packard 5420A Digital Signal Analyzer, a Fast Fourier Transform machine.

For each test, the tunnel velocity was adjusted and the cylinder, controlled by the Eurotherm 810 temperature controller, was allowed to come to the set point temperature. Then the freestream velocity and temperature were measured approximately 15 cm and 5 cm upstream from the cylinder through the top of the test section, respectively. The velocity was measured with a pitot tube and an inclined manometer, while the temperature was measured with a thermocouple, both inserted about 2 cm into the flow. The cylinder wall temperatures along with the freestream temperature were read from a Doric 410A thermocouple readout, calibrated to ± 0.1°C. During the tests the cylinder temperature was maintained about 35 to 40°C above the freestream temperature.

The gage operating resistance was then adjusted until the thermocouple temperature in the gage matched the nearest cylinder thermocouple temperature (T-2 in Figure 6). Then, as for the impinging flow calibration, three A.C. RMS and three D.C. bridge voltages were recorded from the Hewlett-Packard 3468A volt meter, along with the cable resistance and operating resistance.

3.4 ELECTRONIC SQUARE WAVE TEST APPARATUS

The electronic square wave test is used to obtain a step change in the system and monitor the response. Some typical pulse shapes in response to a square wave test are shown in Figure 10. Freymuth and Fingerson [24] report that excellent response to velocity steps, for hot wires, is achieved if the anemometer controls are adjusted to get one good "ring" (curve 3), without under shoot (curves 1 and 2) or oscillation (curve 4). Freymuth and Fingerson determined that the cut-off frequency, characterized by a -3dB roll-off point in the amplitude versus frequency plot, for cylindrical hot-film sensors and wedge-type gages could be calculated from:

$$f_{cut} = 1 / \tau \qquad (1)$$

where τ is defined as in Figure 11. Since the heat flux gage used in this research is similar to a hot-film velocity probe, the above definition for the cut-off frequency was adopted as an estimate of the frequency response of the gage. However, technical representatives from Thermo

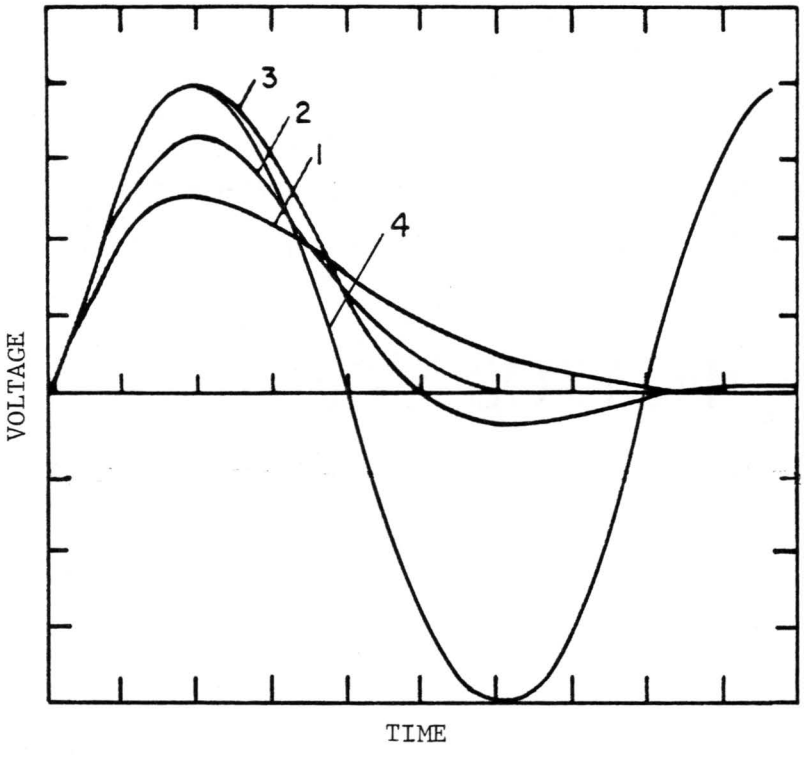

Figure 10. Pulse shapes in response to a square wave test (Fig. 3 from reference 24).

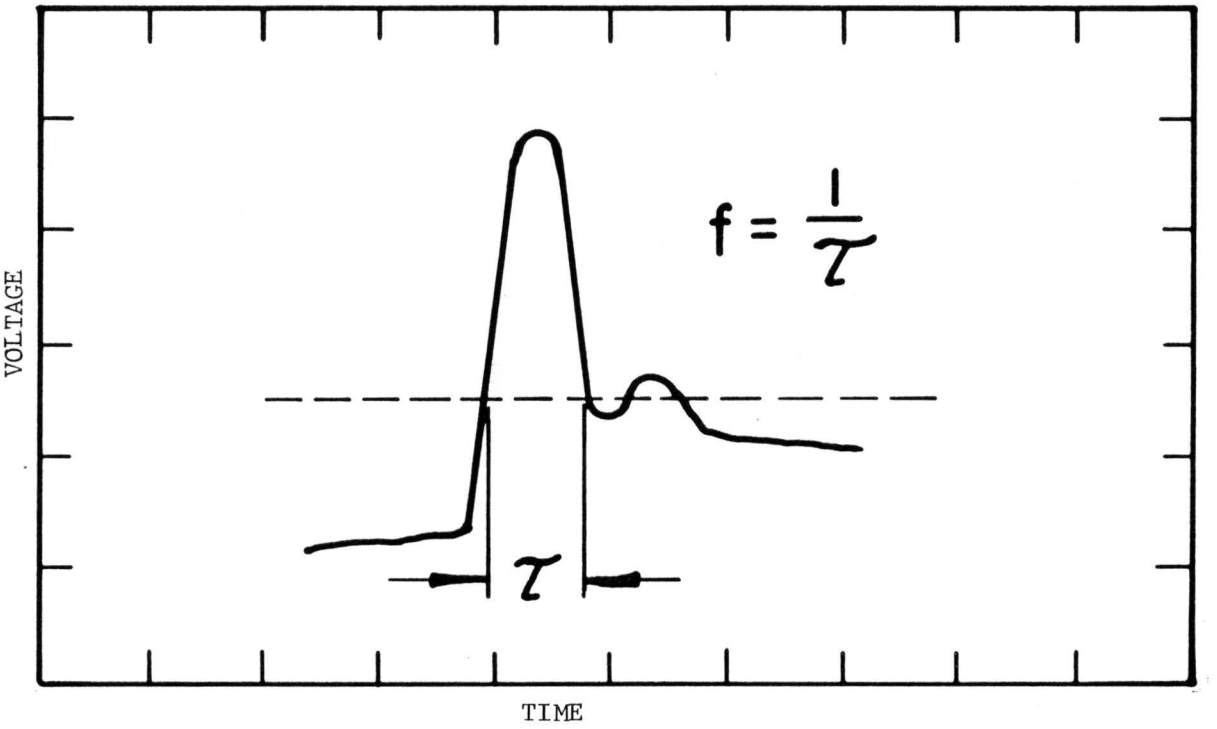

Figure 11. Square wave test frequency response estimate for film sensors (Fig. 8 from reference 24).

Systems Inc. (TSI) recommended a conservative approximation to the frequency response for specialty gages as:

$$f_{cut} = 0.1 / \tau \qquad (2)$$

or an order of magnitude less than what would be expected for a cylindrical hot film sensor. Although the square wave test gives a quick approximation of the frequency response, Freymuth and Fingerson [24] recommend using the sine wave test, to more accurately determine the frequency roll-off characteristics for cylindrical- and wedge-type hot-film sensors. A detailed description of the sine wave test is given in Nielson and Rasmussen [22].

The electronic square wave used to approximate the gage response time is built into the IFA-100 circuitry. The square wave generator is applied in parallel with the gage, Figure 12, which produces an alternating probe current. The amplitude and frequency of the square wave can be controlled with adjustments on the front of the anemometer unit. The gage was tested while in the flat plate calibration stand so that the results could be directly compared to the thermal square wave test results. For these tests the Eurotherm 810 temperature controller was used to control the center plate temperature.

3.4.1 ELECTRONIC SQUARE WAVE CALIBRATION PROCEDURE

For each electronic square wave test, the plate temperature was allowed to come to the set point temperature of the controller and the gage

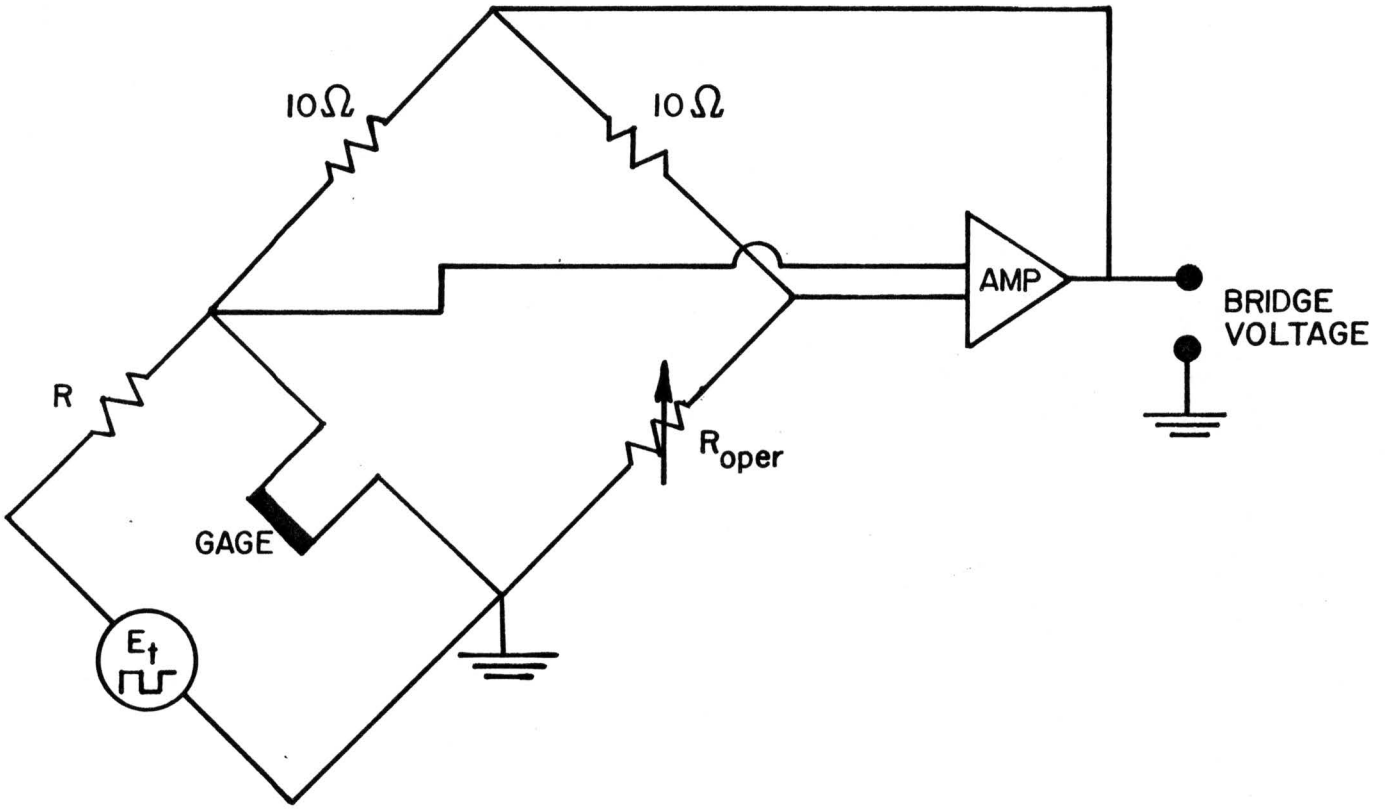

Figure 12. Bridge circuit with square wave generator in parallel with thin-film heat flux gage.

operating resistance was adjusted until the gage thermocouple matched the temperature of the thermocouple mounted behind the gage. The square wave signal was then activated and the amplitude adjusted for easy viewing on the oscilloscope. The bridge output was monitored on the oscilloscope while the bridge and cable compensation controls on the IFA-100 were adjusted to give a bridge voltage trace similar to that shown in Figure 11. Although the response time is a function of the flow velocity (heat transfer rate) the tests were run at one flow velocity since only a limited range of heat transfer coefficient could be calibrated on this test stand. Also, the electronic square wave would cause the IFA-100 to shutoff at low heat transfer levels.

For each test, the local plate temperature, the mean D.C. bridge voltage and the cable and operating resistances were recorded. In addition, the amplitude and frequency of the square wave were recorded from the oscilloscope along with the settling time, τ, and the bridge compensation value (from the IFA-100).

3.5 THERMAL SQUARE WAVE TEST APPARATUS

As for the electronic square wave test, the thermal square wave test was used to produce a step change in the heat transfer condition over the gage and monitor the system response. A top view of the test stand, Figure 13, shows the orientation of the calibration plate, free jet tunnel and the thermal radiation source. The apparatus was mounted approximately 15 cm from the gage in the flat plate calibration stand. The entire calibration plate assembly was rotated 90 degrees so that the gage length

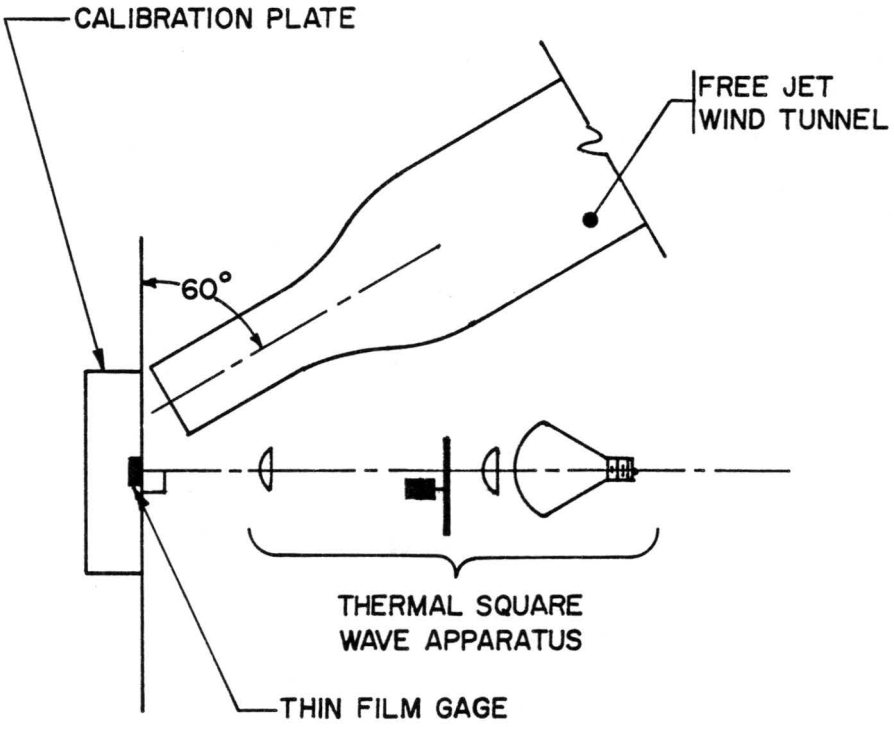

Figure 13. Alignment of the test stand for the thermal square wave test.

was perpendicular to the flow direction which provided a more uniform heat flux condition over the gage. This test was run on the calibration stand since the thermal radiation source could be easily directed at the gage while there was air flow over the gage.

The apparatus used for generating the chopped thermal radiation signal is shown in Figure 14. The thermal radiation source is provided by a 300 watt flood-lamp bulb with two plano-convex lenses used to focus the light. The distances of lens 2, lens 1 and the front of the flood lamp from the flat plate were 17.8 cm (7 in.), 49.5 cm (19.5 in.) and 51.4 cm (20.25 in.), respectively. The light was focused to a 2.54 cm (1.0 in.) diameter spot on the calibration plate, which was sufficiently large to fully illuminate the gage. The light was chopped by an aluminum splitter plate, Figure 15. The disk had two slots, 2.0 cm (0.8 in.) wide, each spanning 90 degrees of rotation. The chopper wheel was mounted in between the two lenses, which produced a sharp cut of the light signal. Two slots are used so that a square wave frequency twice that of the rotational frequency can be achieved with a dynamically balanced disk.

A small D.C. motor, powered by a Hewlettt-Packard 6200B D.C. power supply, was used to drive the splitter plate. The motor is capable of turning the splitter plate up to 3600 RPM, which corresponds to a maximim square wave frequency of 120 Hz. Each complete cycle of the wheel was sensed by a variable reluctance transducer, which was triggered by a small iron tab epoxied to the periphery of the wheel.

A sample result for the thermal square wave test is shown in Figure 16. The response time, τ, is defined as the time required for the gage to respond from one extreme heating condition and settle to the other

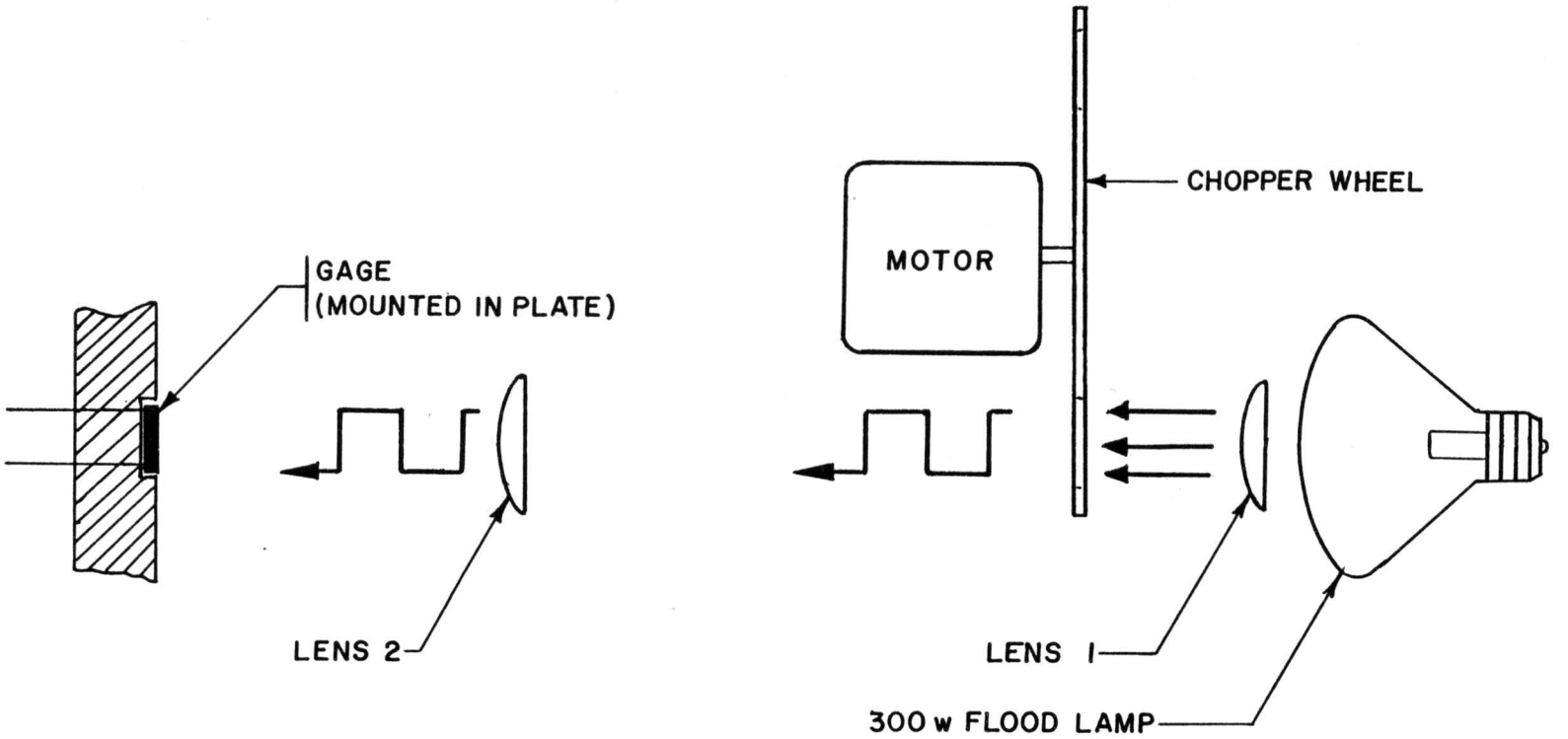

Figure 14. The thermal square wave apparatus for the response time calibration.

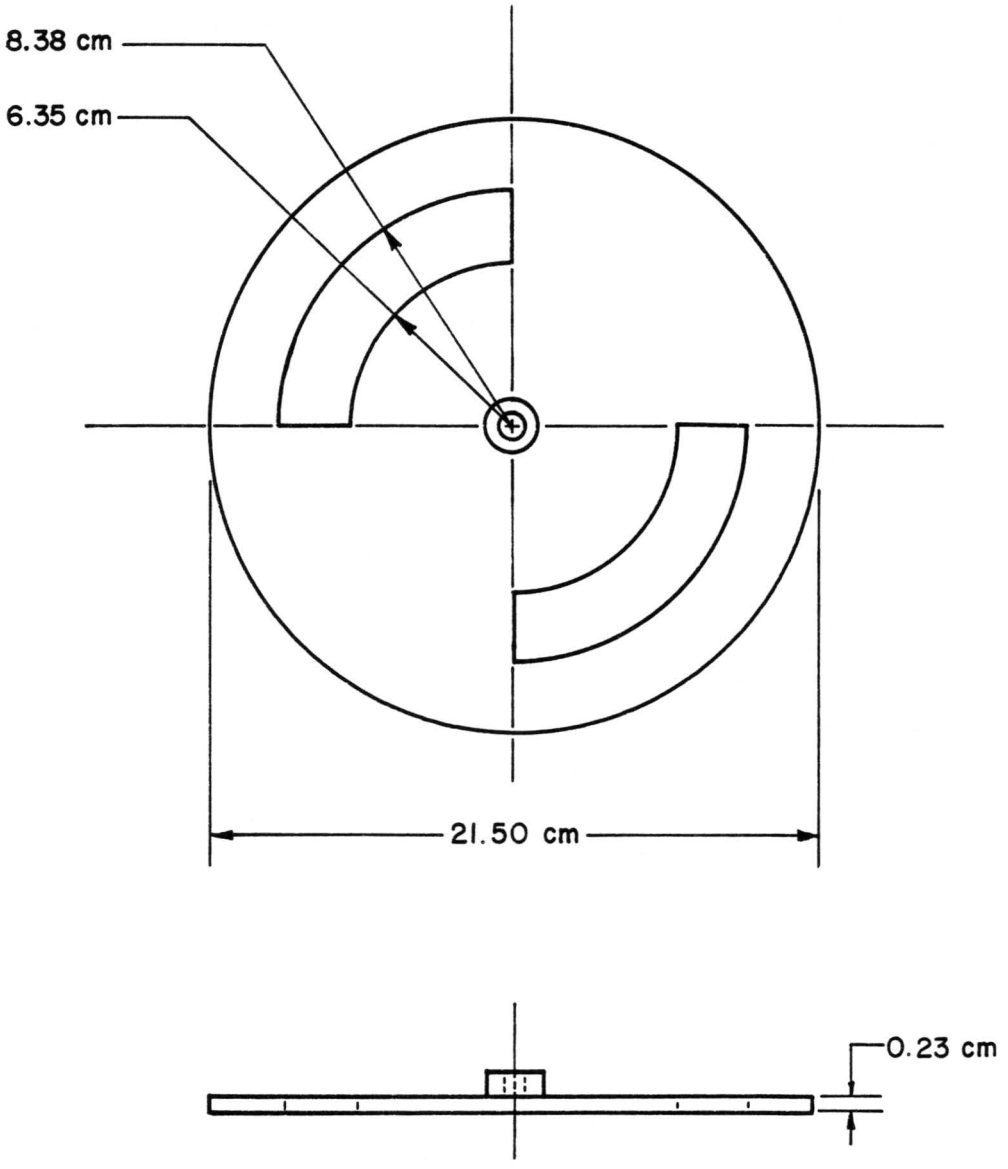

Figure 15. The chopper wheel.

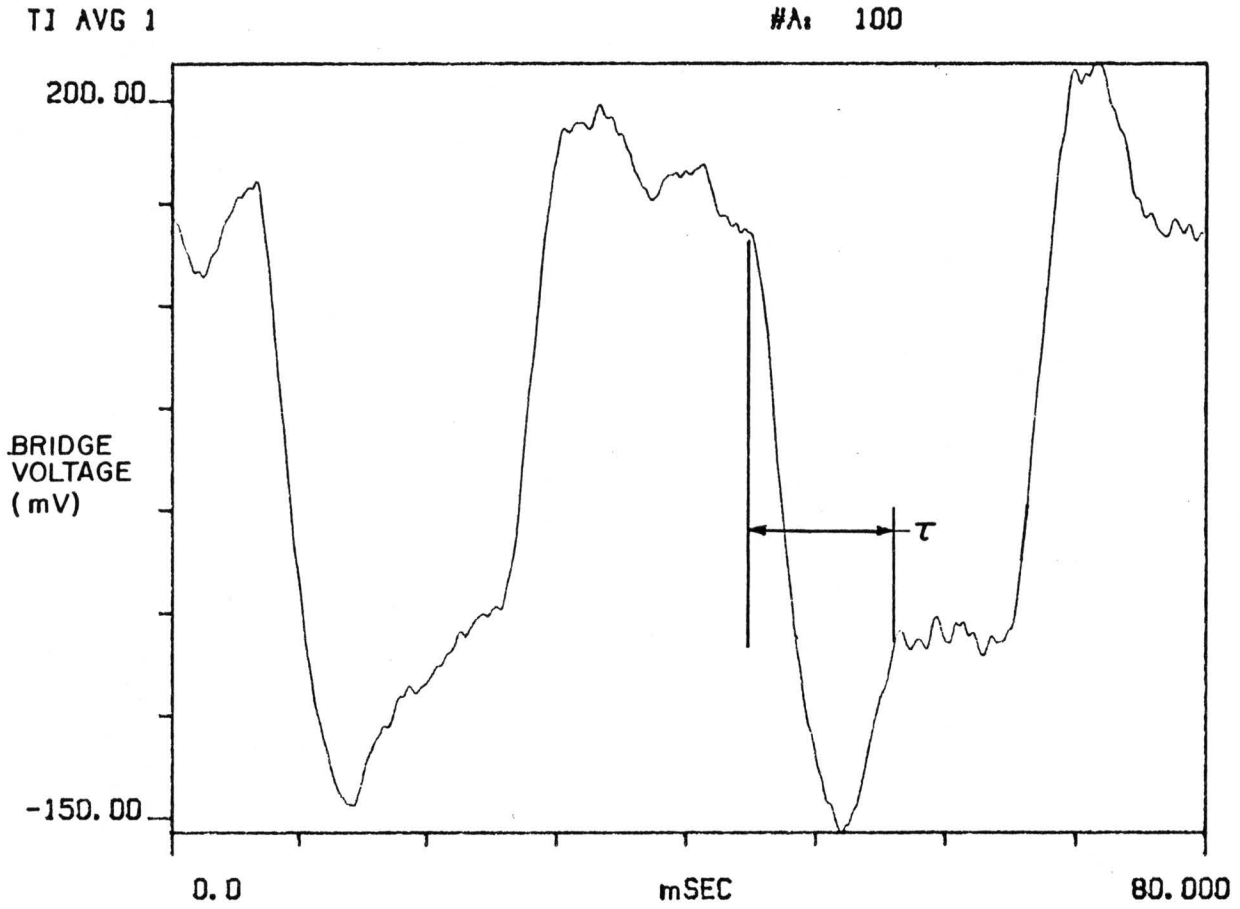

Figure 16. Typical thermal square-wave test result at low frequency.

extreme. The maximum frequency response is estimated from the response time as:

$$f = 1 / \tau. \qquad (3)$$

A better method of determining the (-3dB) cut-off frequency is to examine the response shape as that of a second order system.

3.5.1 THERMAL SQUARE WAVE CALIBRATION PROCEDURE

For each thermal square wave test, the small blower tunnel was activated and the plate temperature was controlled to a steady-state temperature of approximately 65°C. The gage was then activated and the operating resistance was adjusted until the gage thermocouple temperature matched the temperature of the thermocouple mounted behind the gage.

The first step in the calibration process was to determine the peak-to-peak amplitude of the thermal square wave. This was determined by alternately turning the thermal radiation source on and off while recording the bridge voltages. For each case, 5 A.C. and 5 D.C. bridge voltages were recorded along with the operating resistance, the gage temperature and the freestream temperature.

For the actual square wave tests, the mean D.C. bridge voltage was recorded along with the gage operating temperature for various chopper wheel rotational velocities. However, since there was significant freestream turbulence, the bridge voltage was ensemble-averaged with the Hewlett-Packard 5420A digital signal analyzer to obtain a clear time re-

cord. Like the electronic square wave test, the thermal square wave tests were run for only one flow velocity since the IFA-100 would shut off because of the large variations in bridge voltage caused by the thermal radiation source.

3.6 DATA REDUCTION

Since the power dissipated in the thin-film gage was used in all the tests, the first step in reducing the heat transfer data was to determine the power dissipated in the gage film through joule heating. Since the bridge voltage was recorded, the power dissipated in the film needs to be backed out from the the bridge circuit (Figure 17). On the gage leg of the bridge, there is the resistance of the cable leading to the gage leads, R_{cable}, the gage lead resistance, R_{gal}, and the resistance of the gold film, R_{film}. In the control resistance leg of the bridge, there is the gage operating resistance and the cable resistance, which is set internally in the IFA-100 by zeroing the cable resistance via a shorting wire. With this circuit, the operating resistance corresponds to the gage film resistance plus the gage lead resistance. Therefore, the voltage across the gage can be easily found from looking at the left half of the bridge circuit, assuming the bridge is balanced (Figure 18). From Figure 18, the voltage across the film, E_{film}, is given by:

$$E_{film} = E_{br} \frac{R_{film}}{R_{film} + R_{gal} + R_{cable}} \tag{4}$$

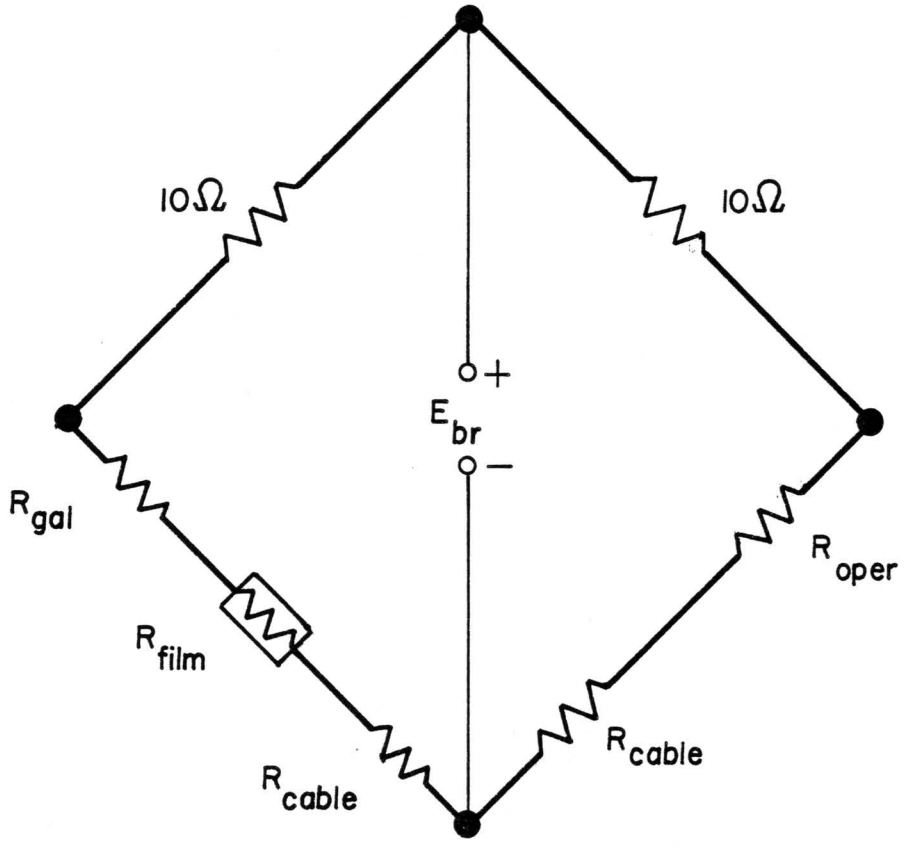

Figure 17. Constant-temperature anemometer bridge circuit schematic.

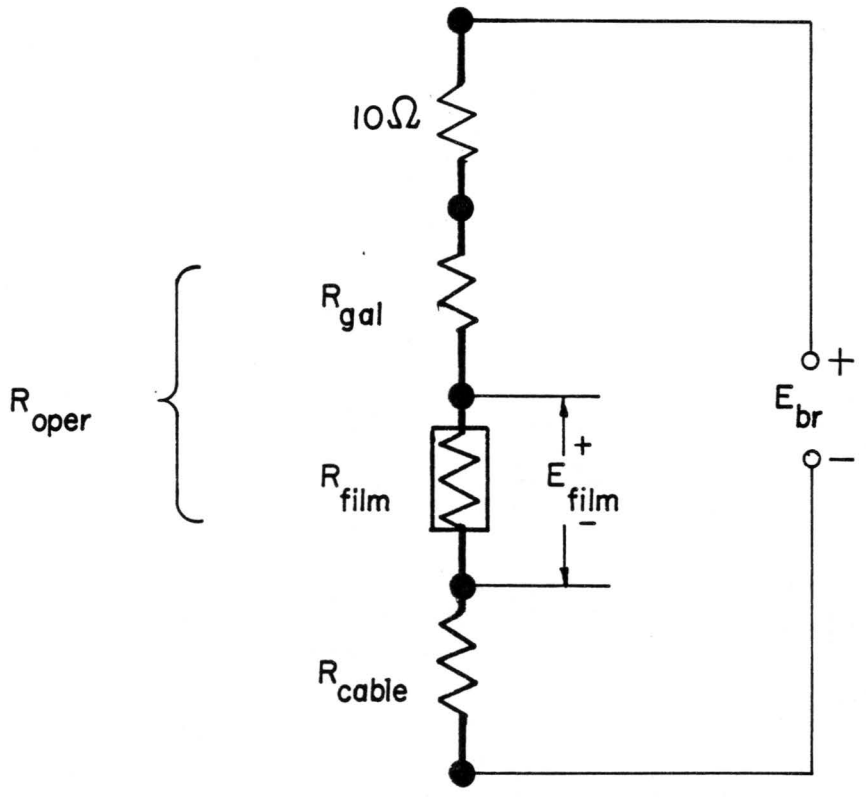

Figure 18. The gage side of the CTA bridge circuit.

The operating resistance is

$$R_{oper} = R_{film} + R_{gal} \tag{5}$$

which gives the film resistance as

$$R_{film} = R_{oper} - R_{gal}. \tag{6}$$

Therefore, Equation 4 can be written in the form:

$$E_{film} = E_{br} \frac{R_{oper} - R_{gal}}{R_{oper} + R_{cable}} \tag{7}$$

which is only in terms of experimental data. The gage lead resistance will be small and can be experimentally determined once for use in all calculations. The operating resistance and cable resistance are recorded from the IFA-100.

With the bridge voltage and the film resistance, the power dissipated in the film can be calculated from:

$$Q_{film} = E_{film}^2 / R_{film} \tag{8}$$

Using Equation 6 and 7, Equation 8 can be written in the form:

$$Q_{film} = E_{br}^2 \frac{(R_{oper} - R_{gal})}{(R_{oper} + R_{cable})^2} \tag{9}$$

and, with the area of the film, A_{film}, the unit power can be calculated:

$$q_{film} = Q_{film} / A_{film} \tag{10}$$

where q_{film} = unit power dissipated in the film (W/m^2)

Q_{film} = power dissipated in the film (W)

and A_{film} = film area, including copper contacts (m^2).

Also, with the free stream temperature, T_∞, and the gage film temperature, T_{film}, the local heat transfer coefficient can be calculated from:

$$h_{ga} = \frac{q_{film} - q_{rad}}{(T_{film} - T_\infty)} \tag{11}$$

where the radiative loss term, q_{rad}, is

$$q_{rad} = \varepsilon_{film} A_{film} \sigma (T_{film}^4 - T_a^4) \tag{12}$$

3.6.1 IMPINGING FLOW DATA

The calibration curve from the flat plate calibrator was determined. The total power supplied to the heater was calculated from the data from,

$$Q_{htr} = E_{htr}^2 / R_{htr} \tag{13}$$

Three heat flow paths were identified in the analysis: 1) through the calibration plate to the ambient by convection and radiation, 2) through the balsa wood surrounding the calibration plate to the ambient by convection and 3) through the back of the assembly to the ambient by natural convection. Corrections to the total power for losses through the back and the balsa wood to the ambient were applied. The recorded data was input to a computer data reduction program. The total heat transfer from the top surface of the calibration plate can be expressed as,

$$Q_{top} = h_{avg} A_{top}(T_P - T_\infty) + \sigma (\varepsilon_P A_P) (T_P^4 - T_a^4) \qquad (14)$$

where Q_{top} is defined as the power supplied to the heater less the back and side losses. The average plate temperature, T_p, was calculated from an average of the fourteen plate thermocouple temperatures. Since the side losses depend on the value of h_{avg}, the above equation needs to be solved iteratively for h_{avg}. The total power supplied to the heater was used as an initial estimate for Q_{top}, from which h_{avg} could be estimated. The side and back losses were determined and subtracted from the total power to calculate an updated value of Q_{top}. The iteration process was continued until the difference betweed successive values of h_{avg} was 0.0001 or less.

The back loss term was determined from a simplified 1-D analysis, Figure 19. The losses from the balsa wood through convection have been neglected for the calculation of the back losses, Q_{back}. Since the heat loss through the balsa wood was small, approximately 2 percent of Q_{top},

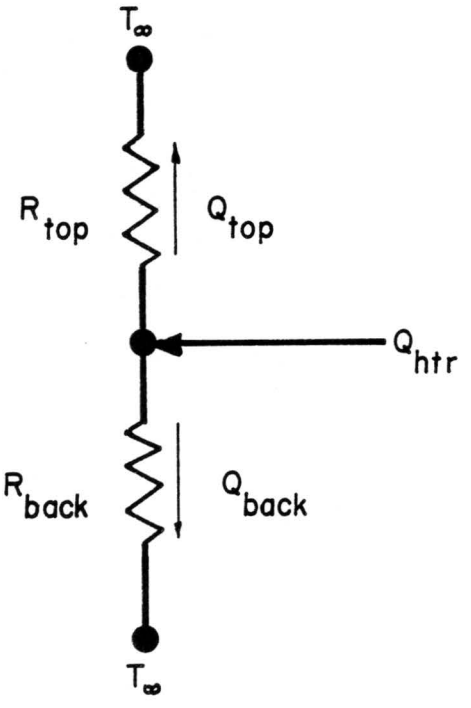

Figure 19. Simplified 1-D approximation used to determine the back losses.

this is a good approximation. The back losses can be found by noticing that Q_{top} and Q_{back} are parallel heat flow paths

$$\frac{Q_{back}}{Q_{htr}} = \frac{R_{top}}{R_{top} + R_{back}} . \tag{15}$$

All that needs to be determined are the resistance terms in equation (15). The plate resistance term can be expressed as:

$$R_{top} = \left(\frac{1}{kA}\right)_{plate\ calibration} + \frac{1}{(h_{avg} A + h_r A)} \tag{16}$$

Where the parallel radiative loss term has been included using a convective heat transfer coefficient analogy.

$$h_r = \varepsilon_p \sigma (T_p^4 - T_a^4)/(T_p - T_\infty)$$

The back resistance term can be expressed as (see Fig. 5)

$$R_{back} = \frac{1}{kA}_{asbestos} + \frac{1}{kA}_{insulation} + \frac{1}{kA}_{plywood} + \frac{1}{hA}_{\substack{natural \\ convection}} \tag{17}$$

$$R_{back} = \frac{.00635\ m}{(.58\ W/m\text{-}K)(.023\ m^2)} + \frac{.0381\ m}{(.043\ W/m\text{-}K)(.023\ m^2)} \tag{18}$$

$$\frac{.0191\ m}{(.12\ W/m\text{-}K)(.023\ m^2)} + \frac{1}{(10\ W/m^2\text{-}K)(.023\ m^2)}$$

$$R_{back} = 49.8 \text{ K/W} \tag{19}$$

This value of R_{back} has been calculated without considering air gaps.

The side losses were determined by solving the 2-D conduction problem, Figure 20, by the method of separation of variables [37]. The following assumptions were used: 1) constant plate temperature, 2) constant h over the balsa wood surface and 3) center plate temperature equal to the guard plate temperature. The solution, an infinite series, was solved with a computer. The heat loss per unit length of the balsa per difference between wall and freestream temperature was determined for a wide range of Biot numbers (Figure 21), which was used as input data for the data reduction computer code. The Biot number was defined as

$$Bi = \frac{h_{avg} x}{k} \tag{20}$$

where x = width of balsa wood (m)

and k = thermal conductivity of balsa wood (W/m-K).

3.6.2 CYLINDER STAGNATION POINT DATA

The calibration curve for the cylinder test was generated by comparison to the well-documented prediction for the Nusselt number at the stagnation point on a cylinder in crossflow [20],

$$Nu = 0.95\sqrt{Re} \tag{21}$$

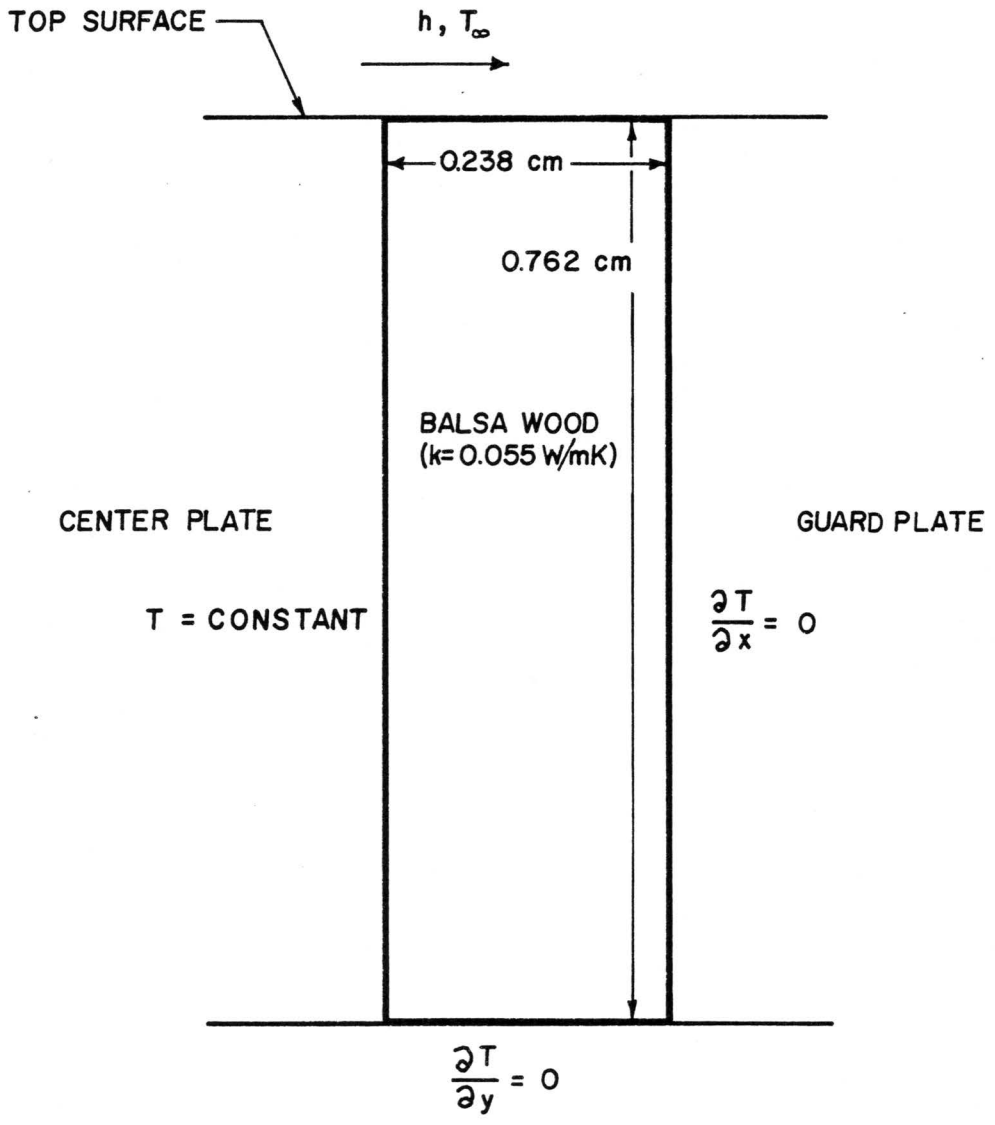

Figure 20. The 2-D slab analyzed to determine the side losses.

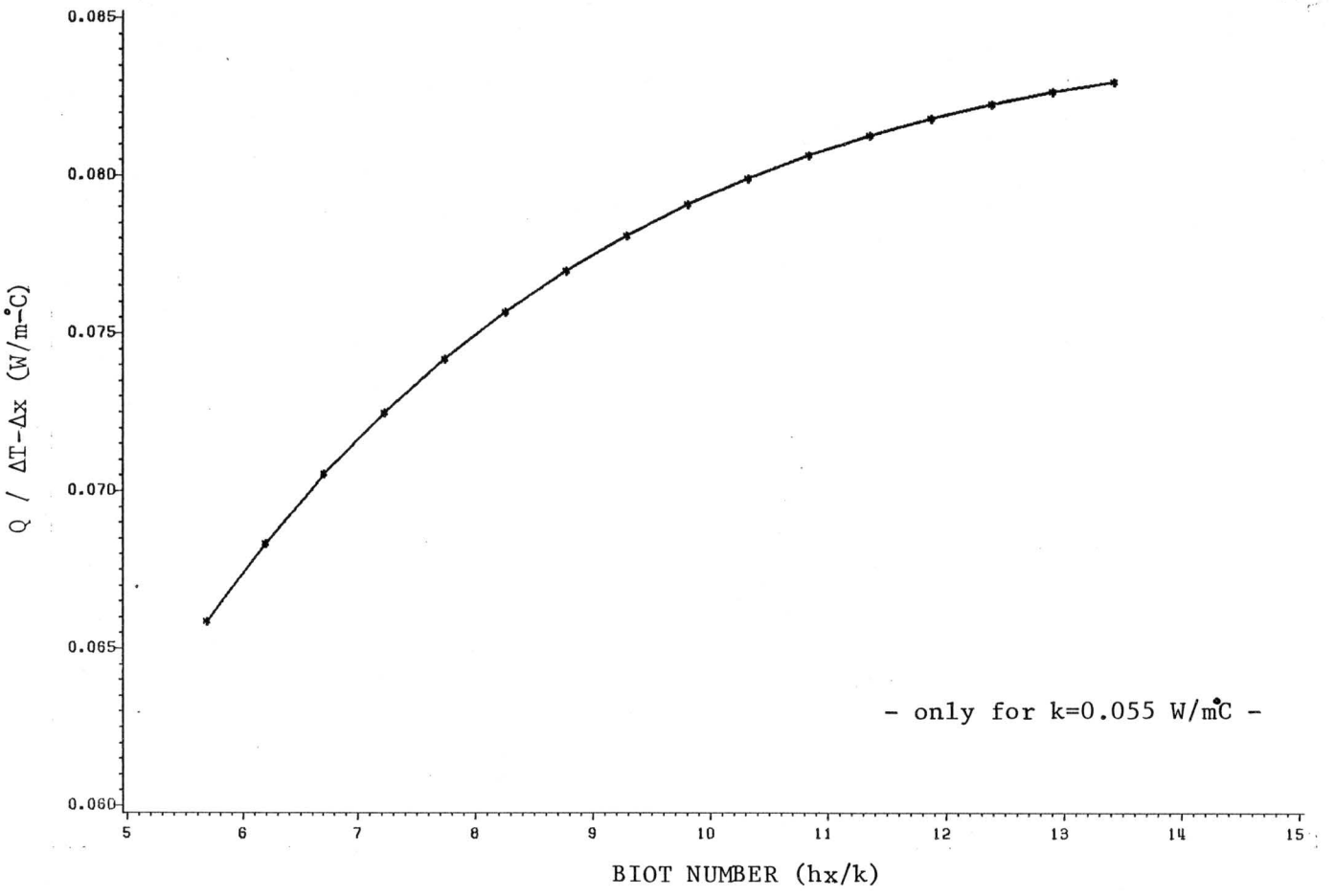

Figure 21. Plot of unit heat loss versus Biot nomber over range used (from reference 37).

Using the definitions for the Nusselt and Reynolds numbers, the heat transfer coefficient at the stagnation point can be expressed purely in terms of the measurable flow conditions,

$$h_{theo} = 0.95\ k\sqrt{\frac{V}{D\ \nu}} \tag{22}$$

This value was compared to the value of h_{gage}, determined from equation (11), to obtain a calibration curve. All the flow properties were taken at the mean air temperature,

$$T_m = \frac{T_{film} + T_\infty}{2} \tag{23}$$

The percent difference of the gage output compared to both the impinging flow and the stagnation point calibration is defined as

$$PD = \frac{(h_{ga} - h)}{h} \tag{24}$$

where h corresponds to the calculated standard h in each of the calibration methods.

3.6.3 SQUARE WAVE DATA

The response time, τ, for each of the electronic and thermal square wave tests was used to calculate the cut-off frequency as defined from equations (2) and (3), respectively. The peak-to-peak amplitudes along with the amplitude between the settled portions of the curves (if avail-

able) were recorded from the ensemble-averaged time records for the thermal square wave tests. Also, the frequency of each square wave was determined from the period for each of the electronic and thermal square wave tests.

4.0 RESULTS

All of the steady and unsteady calibration tests were run with a wall temperature of approximately 65°C. This temperature gave a temperature difference between the wall and the air of 35 to 45°C and allowed sufficient power to be dissipated in the thin-film gage for the constant-temperature anemometer to operate continuously over a range of heat transfer coefficients. For both steady calibration tests, the upper limit of the heat transfer coefficient was determined by the maximum tunnel velocities, while the lower limit was determined by the IFA-100 which would automatically shut off at the lower heat flux levels. Different gages were used for the impinging flow calibration and the cylinder stagnation calibration. In addition, two different gages were used in the cylinder stagnation calibration apparatus.

One of the questions about the gage operation was the match between the temperature determined from the gage thermocouple and the temperature from the operating resistance. Other researchers used resistance-temperature calibrations to set the gage operating temperature. However, in this research it was found that the probe resistance varies slightly during each test. A change of only 0.02 ohms in the resistance corresponds to a 1°C change in temperature. The resistance drift was seen as a change in the thermocouple temperature and a shift of up to 0.2 ohms in the resistance-temperature curve between the beginning and end of a test. Immediately after a resistance-temperature calibration the gage showed a temperature match to within $\pm$ 0.1°C between the gage

thermocouple and corresponding resistance, except when the boundary temperature was not matched with the gage. Therefore, when the boundary was matched to the gage temperature, the gage thermocouple was used as a direct measurement of the film temperature. Further details of this are given in Appendix C.

4.1 IMPINGING FLOW CALIBRATION

The results for the impinging flow calibration tests are given in Figures 22 and 23. A plot of the heat transfer coefficient determined from the gage output is plotted versus the calibration plate heat transfer coefficient in Figure 22. The uncertainty for the heat transfer coefficient determined from the gage output is $\pm$ 7 W/m^2-C and the uncertainty on the plate heat transfer coefficient is $\pm$ 1.5 percent. The dotted line is a linear regression fitted through the data, while the solid diagonal line represents a prefect one-to-one match between the gage and the calibration plate. The heat transfer coefficient calculated from the gage output is consistiently higher than that measured by the plate. The calibration range is from 80 to 113 W/m^2-C. The free jet had freestream turbulence levels of approximately 2 percent, measured with a cylindrical hot film velocity probe. This caused up to 10 percent fluctuations in the heat transfer signal. These large peak fluctuations caused the IFA-100 to automatically shut off at the lower heat transfer levels (3000 W/m^2).

The percent difference of the heat transfer coefficient determined from the thin-film gage output is plotted versus the plate heat transfer

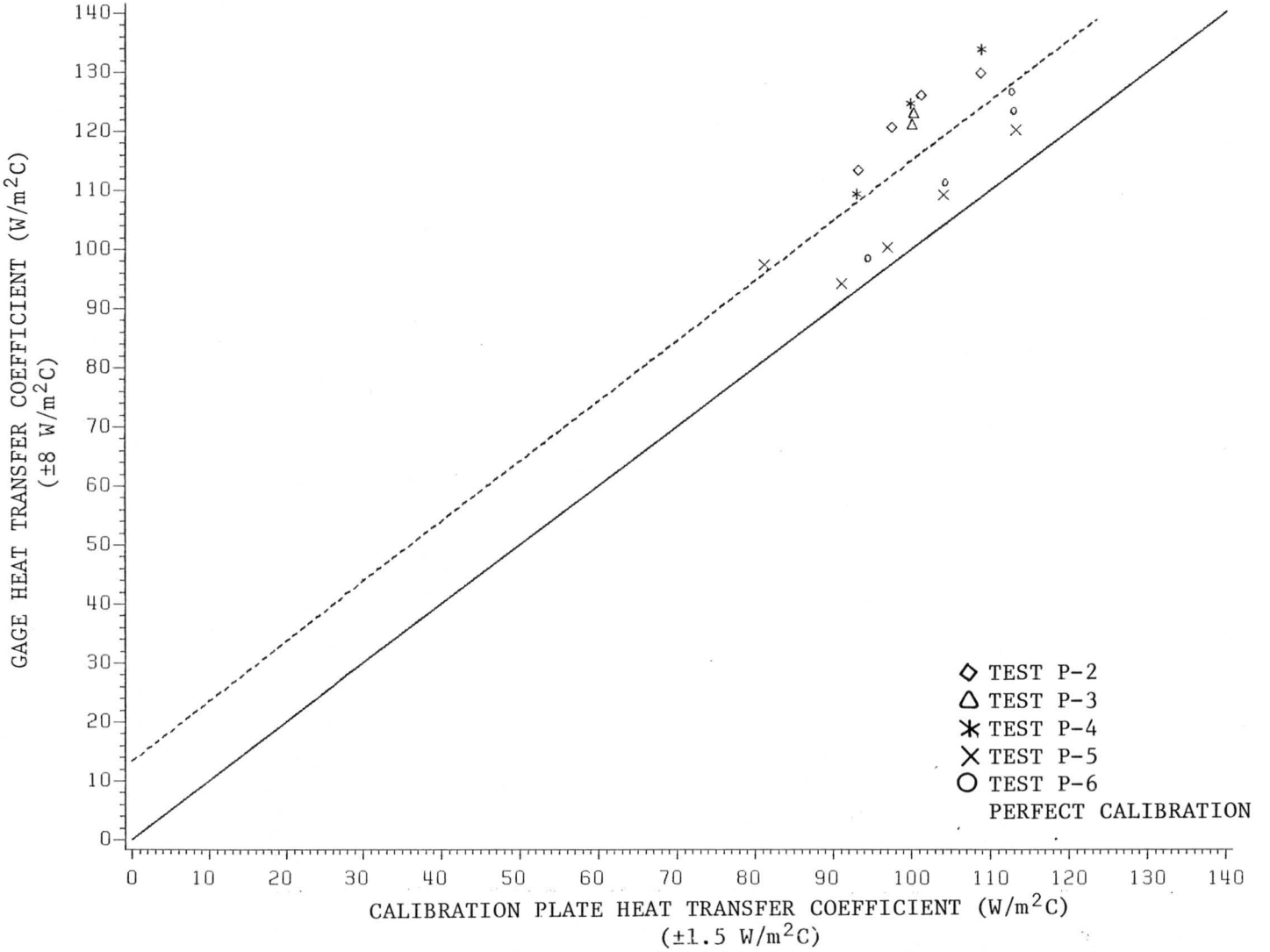

Figure 22. Impinging flow calibration data for the thin-film gage.

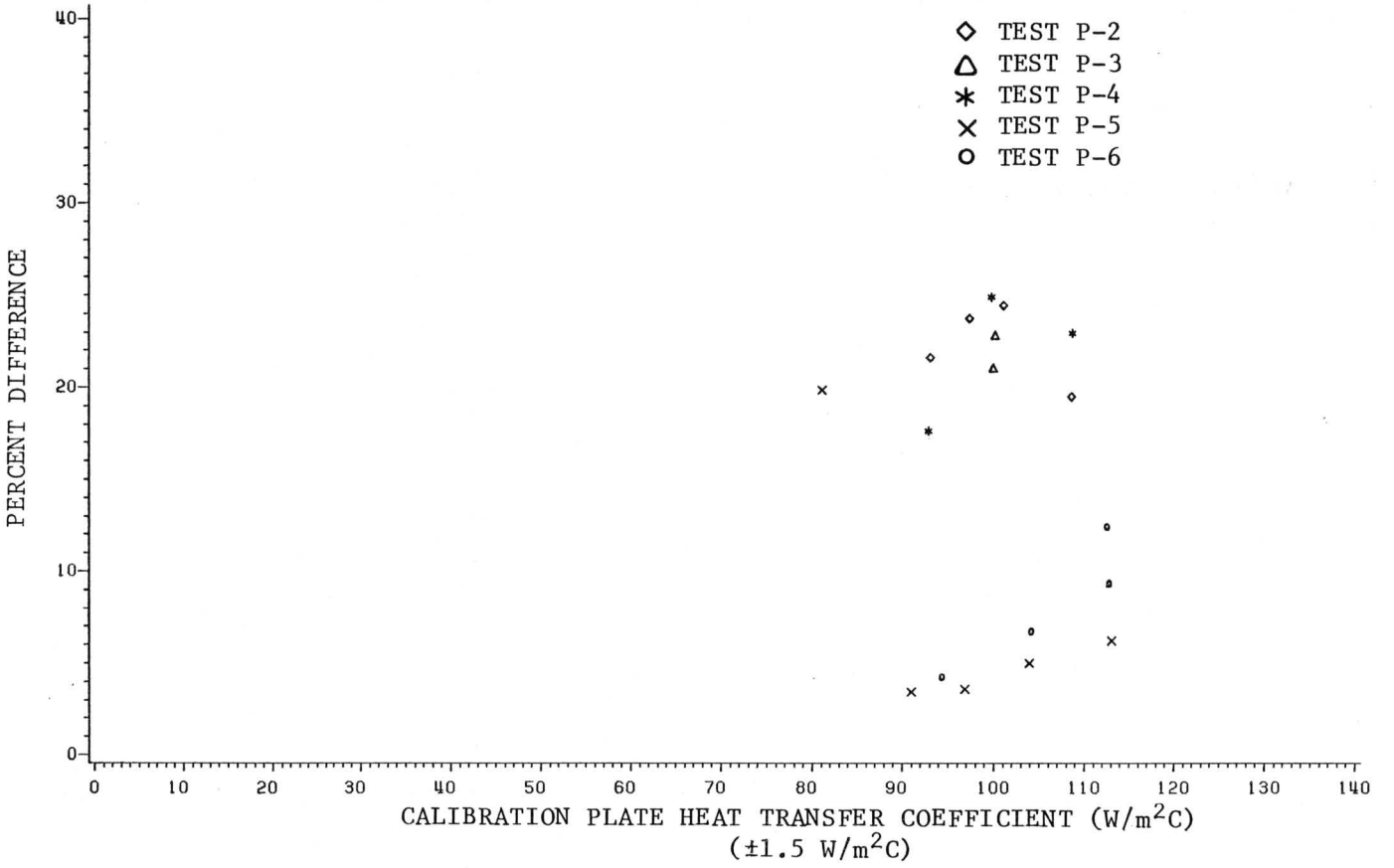

Figure 23. Percent difference of the gage heat transfer coefficient for the impinging flow calibration data.

coefficient in Figure 23. The error ranges from 5 to 25 percent for the five sets of data taken. In the most recent tests, P-5 and P-6, the thermocouples in the center region were recalibrated and extreme care was taken to match the gage temperature to that of the thermocouple mounted behind it. The temperatures in the center region were uniform to within $\pm$ 0.1°C during these tests. These two tests have the lowest errors of the tests run. At the lowest heat transfer rate in test P-5, the IFA-100 would not operate continuously due to the freestream turbulence. The data for this point was taken by repeatedly turning the IFA-100 on, waiting for the bridge voltage to stabilize and recording data until it shut off. This is likely the reason for the high value of error at this data point.

4.2 CYLINDER STAGNATION RESULTS

The results for the cylinder stagnation point calibrations are shown in Figures 24 and 25. The heat transfer coefficient determined from the gage output is plotted against the predicted stagnation point value. The uncertainty on the gage heat transfer coefficient is $\pm$ 7 W/m^2-C and the uncertainty on the correlation for the heat transfer coefficient at the stagnation point is $\pm$ 3 W/m^2-C. Tests C-3 and C-4 were conducted with the gage thermocouple temperature matched to the average of the thermocouple temperatures on either side of the gage. The average temperature difference between these two thermocouples was 0.3°C. Test C-8 was run with a different gage than the other tests, but seems to follow the other calibration curves. All tests show that the thin-film gage consistently overpredicts the stagnation point heat transfer coefficient.

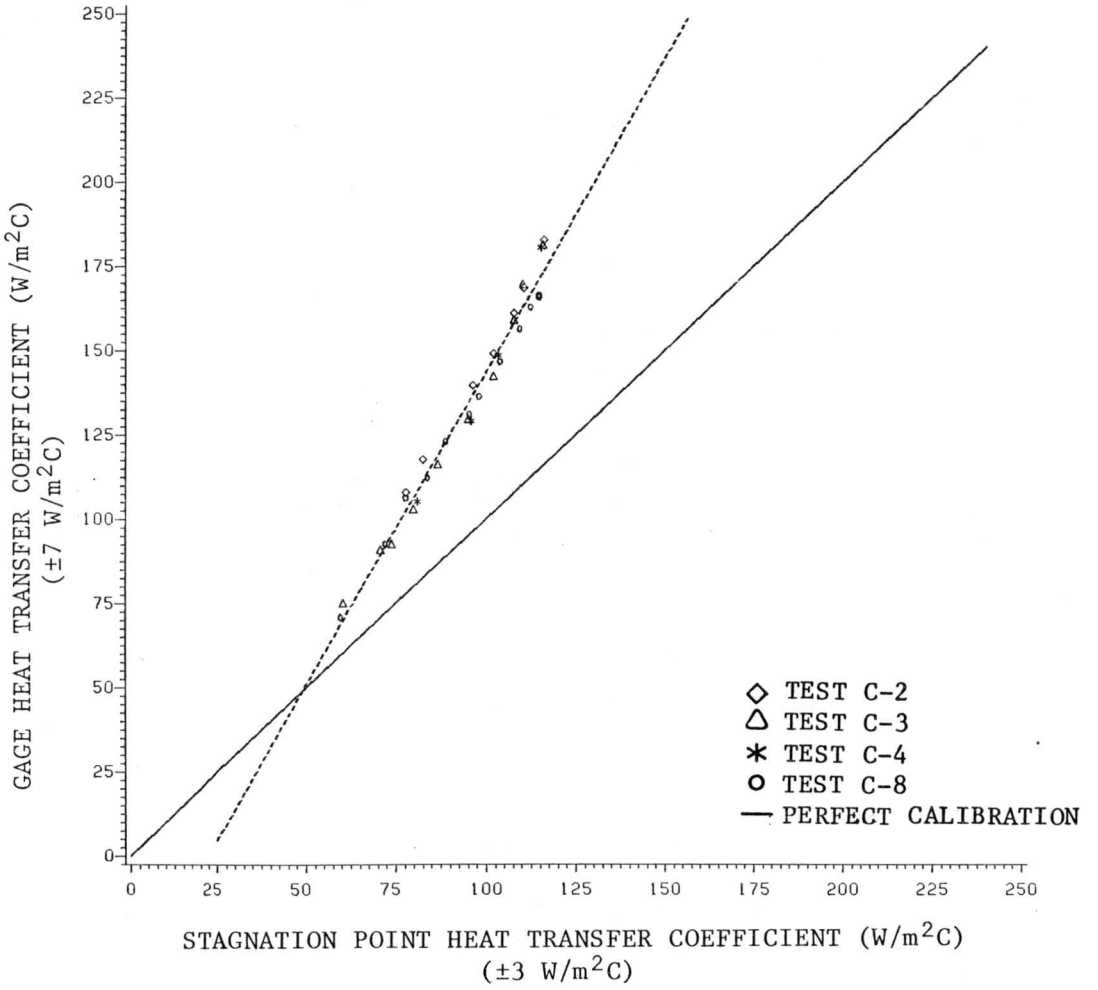

Figure 24. The cylinder stagnation point calibration data for the thin-film gage.

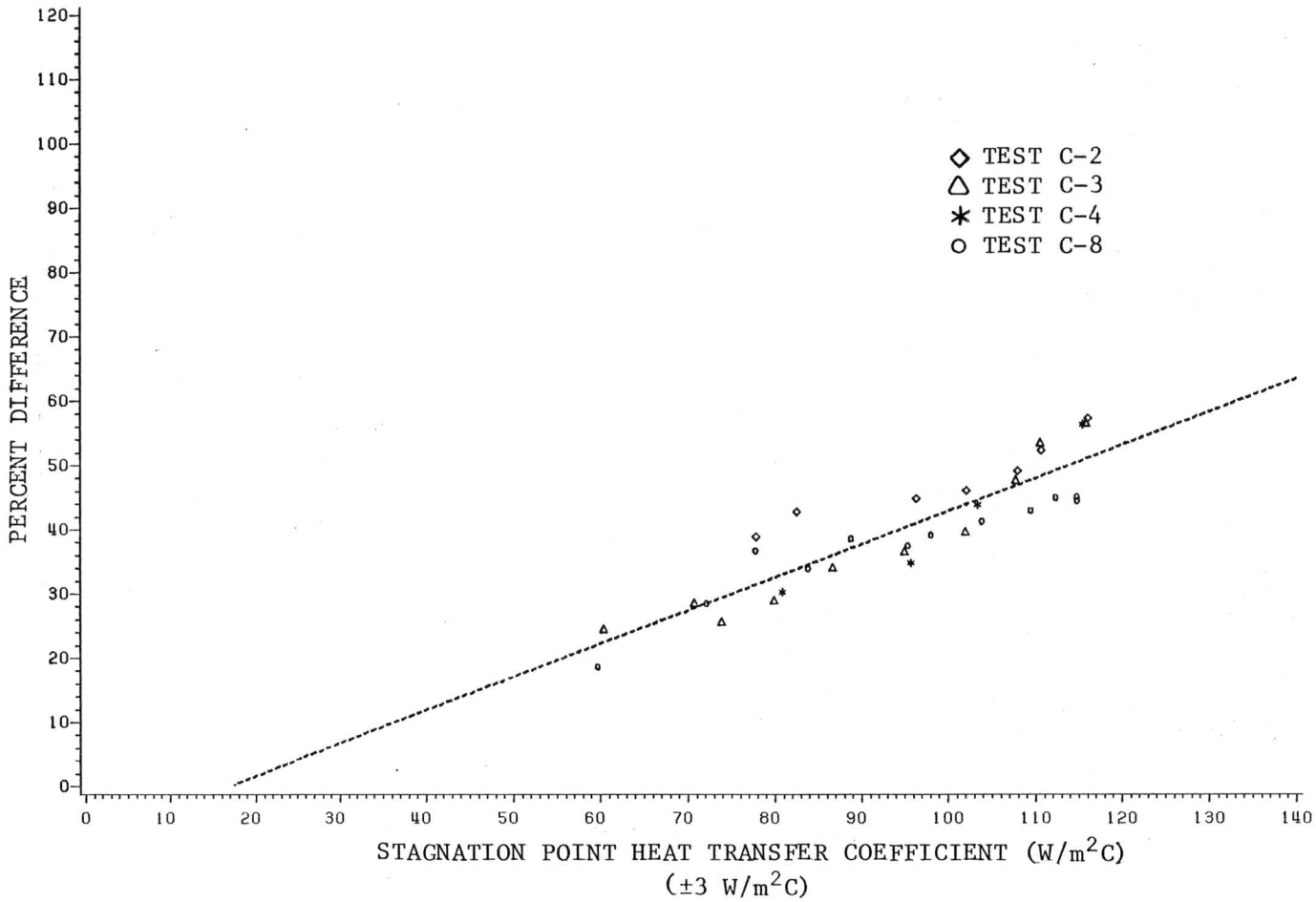

Figure 25. Percent difference of the gage heat transfer coefficient for the cylinder stagnation point calibration data.

The calibration range is from 60 to 115 w/m^2-C. The lower freestream turbulence levels in the wind tunnel allowed operation at lower heat flux levels than for the impinging flow calibrator (2300 W/m^2 versus 3000 W/m^2).

The percent difference is plotted against the heat transfer coefficient calculated at the stagnation point in Figure 25. The error ranged from 21 to 61 percent, with a marked trend of decreasing error for decreasing heat flux levels. In test C-3, the temperature difference between the two nearest thermocouples, at the same angular position as the gage, dropped from 0.5°C to 0.1°C when the heat flux condition was varied from maximum to minimum, respectively. This effect was also seen in the other tests, but test C-3 was run with the widest range of heat flux conditions.

Figures 26 and 27 are plots of the same data as in Figures 24 and 25, except that two more tests have been included for comparison purposes. Test C-1 shows data for the case when the gage temperature was approximately 0.6°C higher than the nearest thermocouple temperature and test C-6 was run with the gage temperature about 2.0°C higher than the nearest thermocouple temperature. These two test results overpredict the heat transfer coefficient more than the other cases.

4.3 ELECTRONIC SQUARE WAVE RESULTS

The results for the electronic square wave tests are given in Table 1. Because of the high frequencies involved, no equipment was available which was capable of accurately recording the signal directly. Therefore,

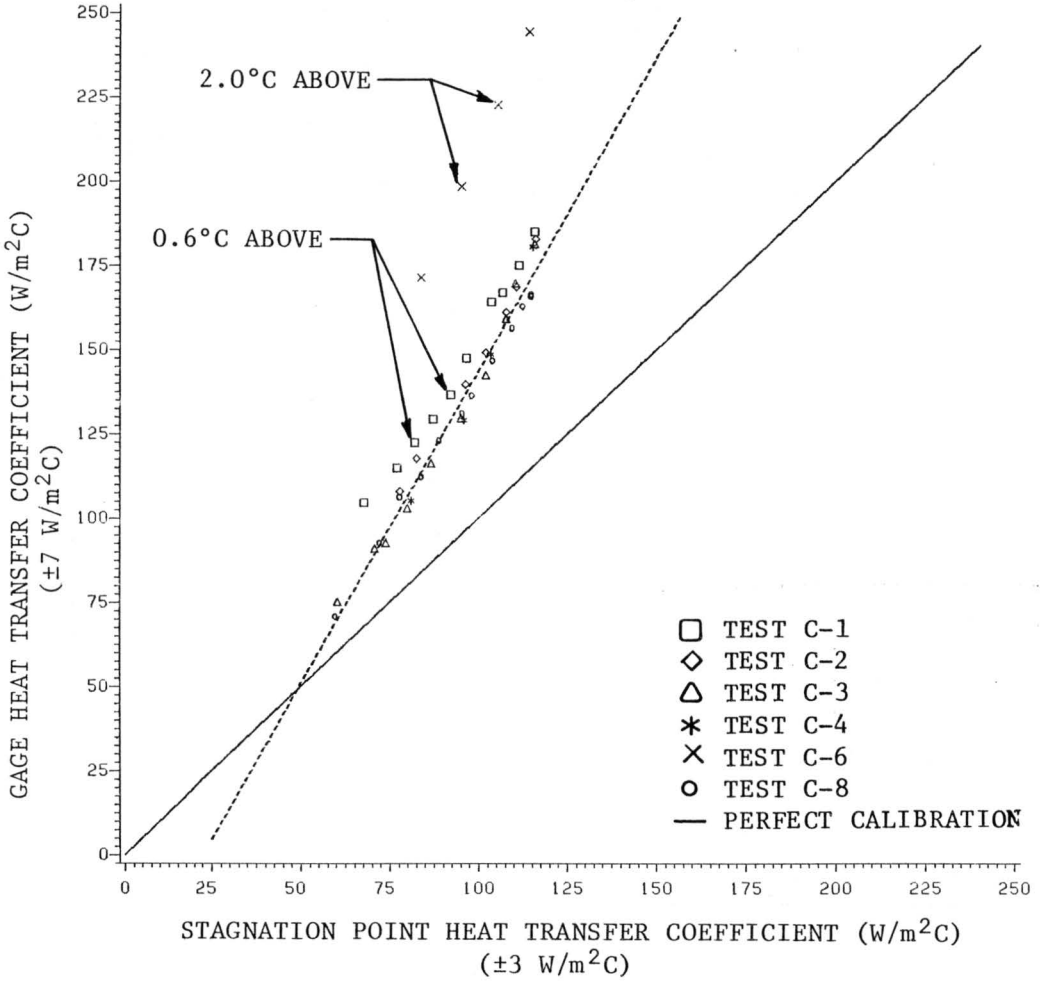

Figure 26. Cylinder stagnation point calibration data, including overheat cases (C-1 and C-6).

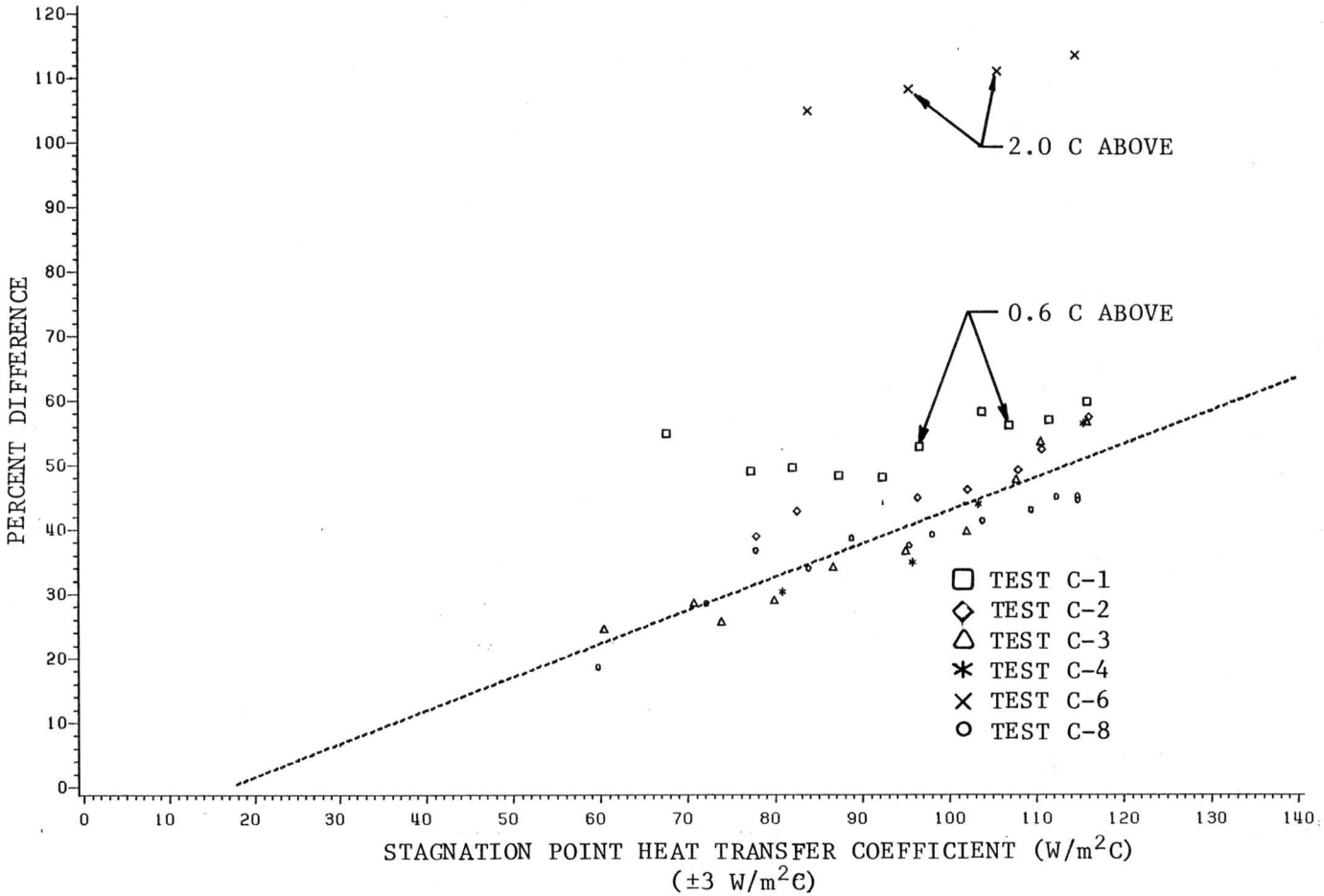

Figure 27. Percent difference in gage heat transfer coefficient for the cylinder stagnation point data, including overheat cases (C-1 and C-6).

Table 1. Electronic square wave test results.

SQUARE WAVE FREQUENCY (Hz)	τ (sec)	Cut-Off Frequency (from equation (2)) (Hz)
2,200	20×10^{-6}	5,000
6,900	15×10^{-6}	6,600

the signal was observed on an oscilloscope. The peak-to-peak amplitude of the square wave was set to about 0.15 volts which corresponds to approximately that of the thermal square wave amplitude. The cut-off frequency is conservatively estimated to be about 5 to 6.6 kHz.

4.4 THERMAL SQUARE WAVE RESULTS

The thermal square wave test was run at various square wave frequencies so that the thin-film gage response could be better investigated. The ensemble-averaged bridge output voltage is shown in Figures 28 through 33 for square wave frequencies between 26 and 120 Hz. The peak-to-peak amplitude of the thermal square wave was 0.18 volts, which was determined from the on-off test.

A distinct overshoot is seen for the 25 Hz case (Figure 28). The period of the overshoot, τ, was 0.011 sec which corresponds to a cut-off frequency of approximately 91 Hz. The peak-to-peak amplitude of the thermal square wave can be seen between the settled portions of the curve, after the overshoot, as shown in Figure 28. The peak-to-peak amplitudes, including overshoot, measured from the curves were all approximately 0.33 volts, except at 100 and 120 Hz where it is less. The peak-to-peak amplitude of the bridge voltage, as recorded in Figures 28 - 33, is plotted against the square wave frequency in Figure 34. The shape of the 25 Hz case (Figure 28) is approximately square, except for the overshoot. However, the shape of the curves tends towards that of a triangular wave as the frequency is increased towards 120 Hz. The maximum rise rate of

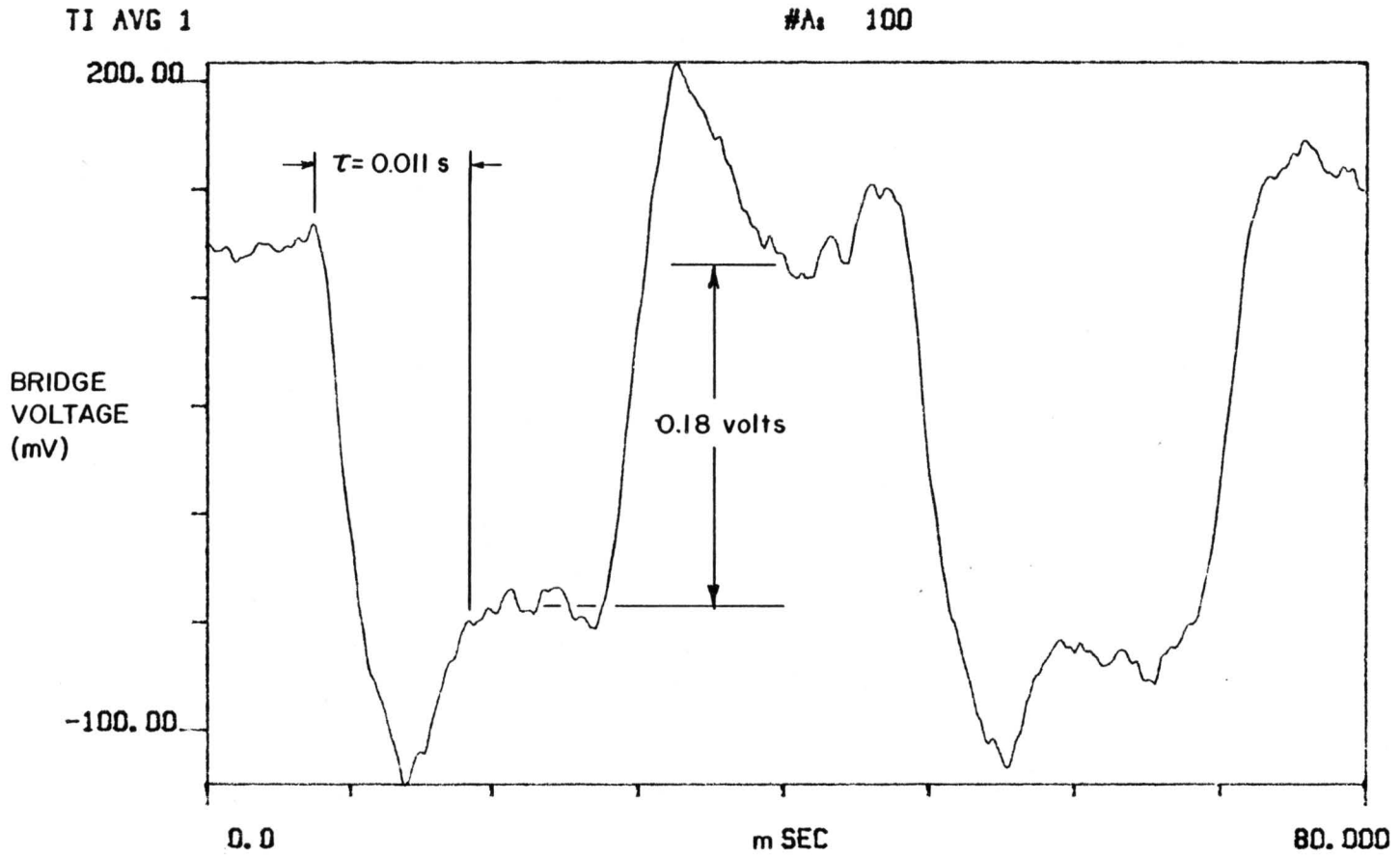

Figure 28. Thermal square wave test results at 25 Hz.

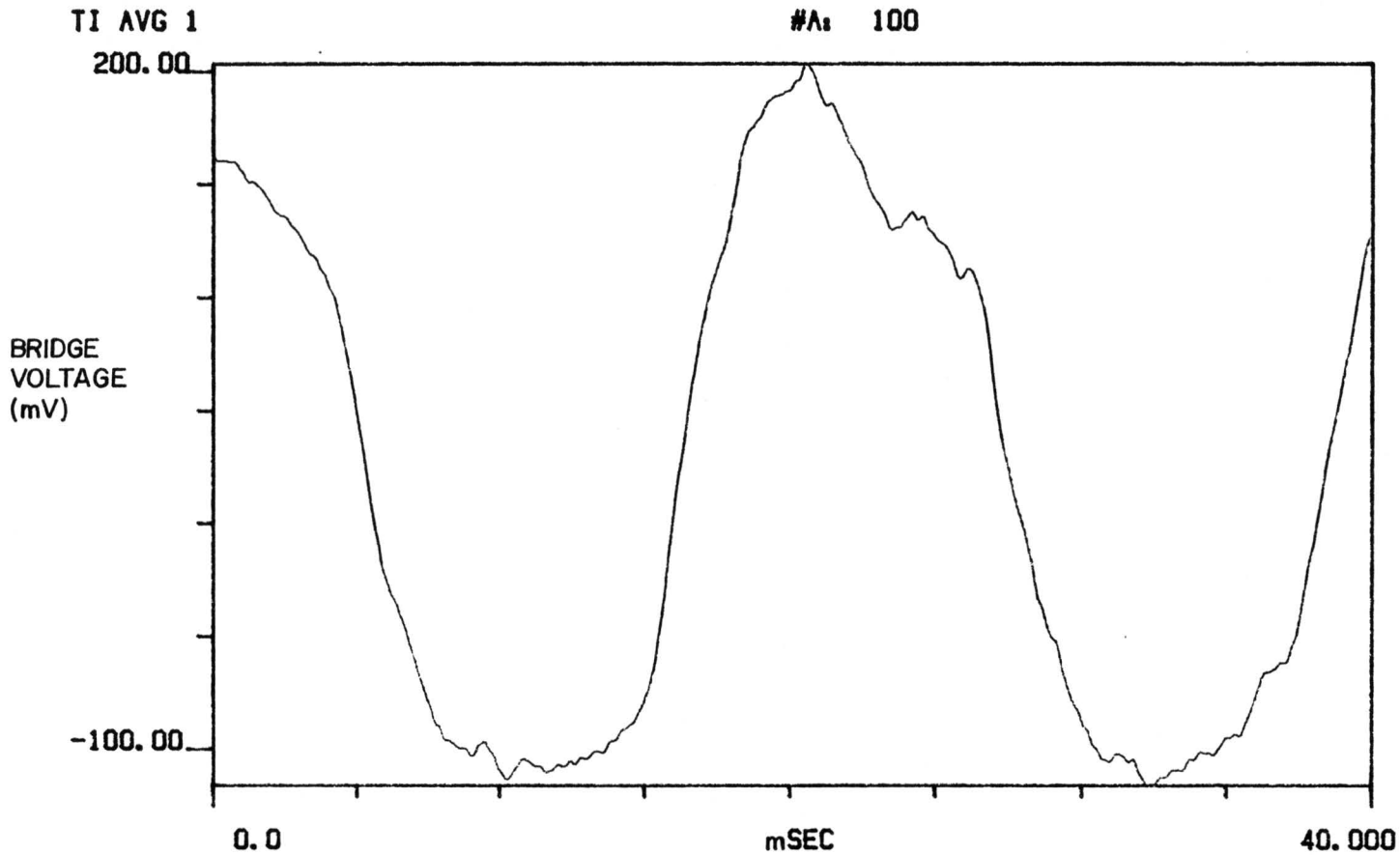

Figure 29. Thermal square wave test results at 45 Hz.

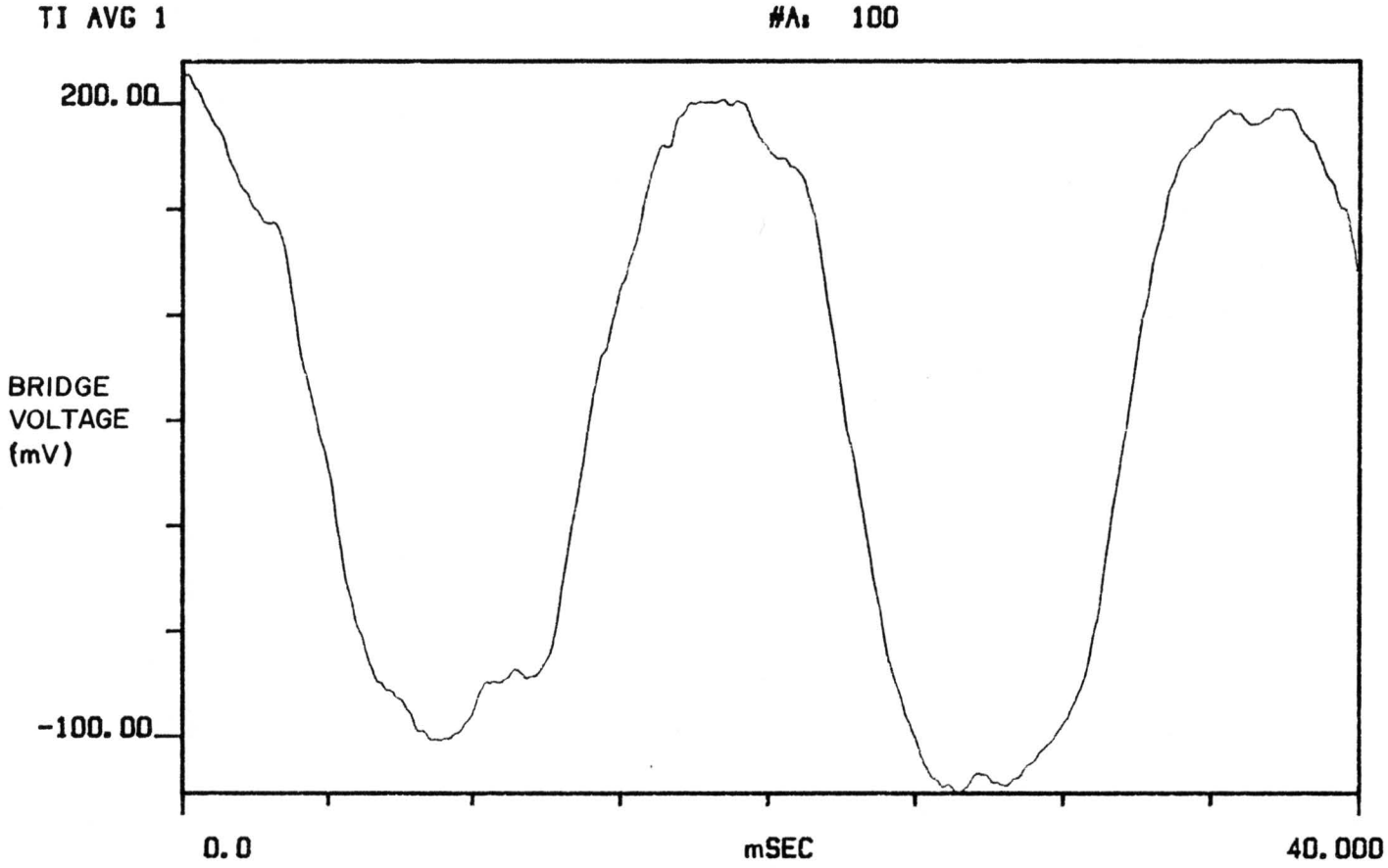

Figure 30. Thermal square wave test results at 55 Hz.

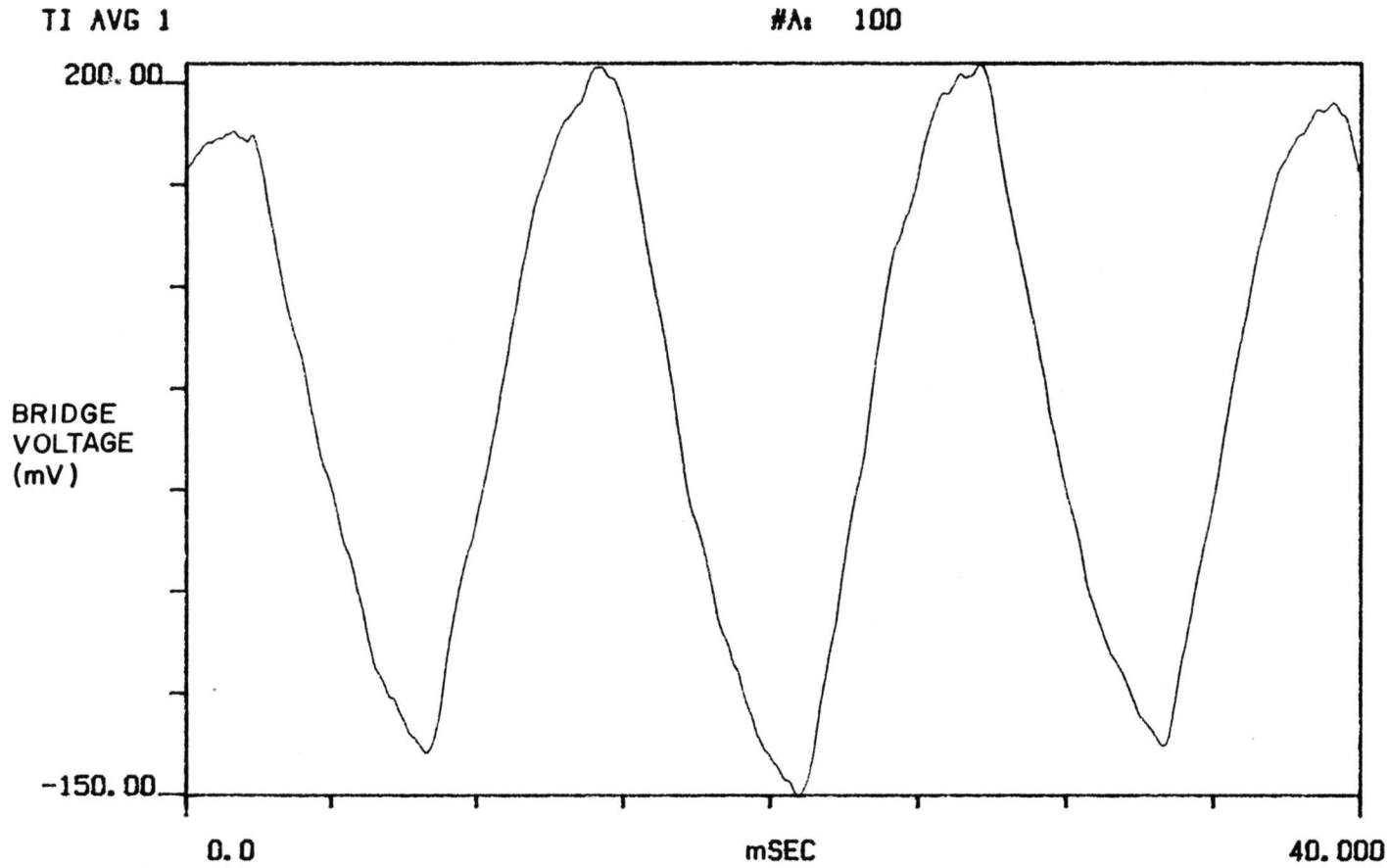

Figure 31. Thermal square wave test results at 78 Hz.

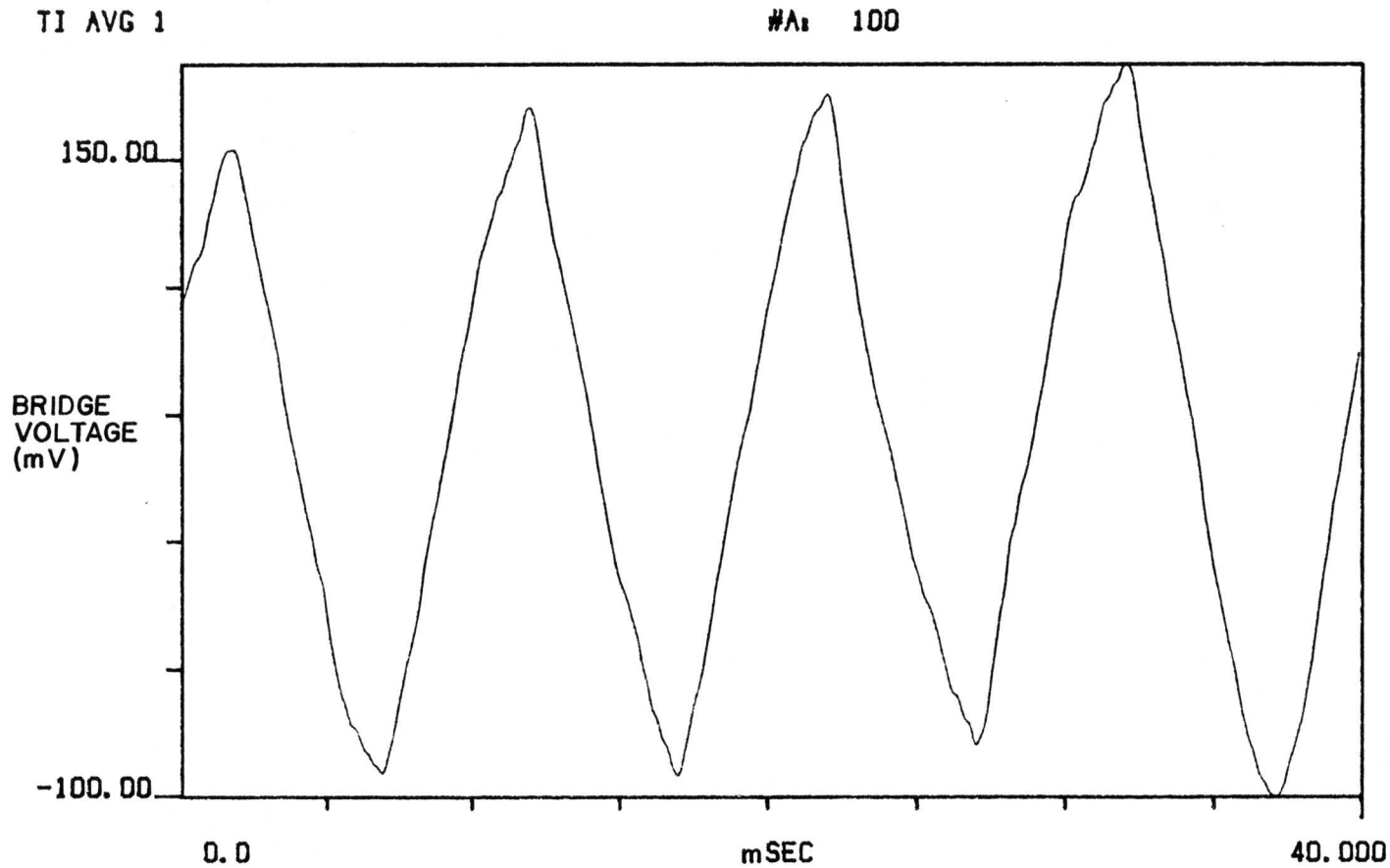

Figure 32. Thermal square wave test results at 100. Hz.

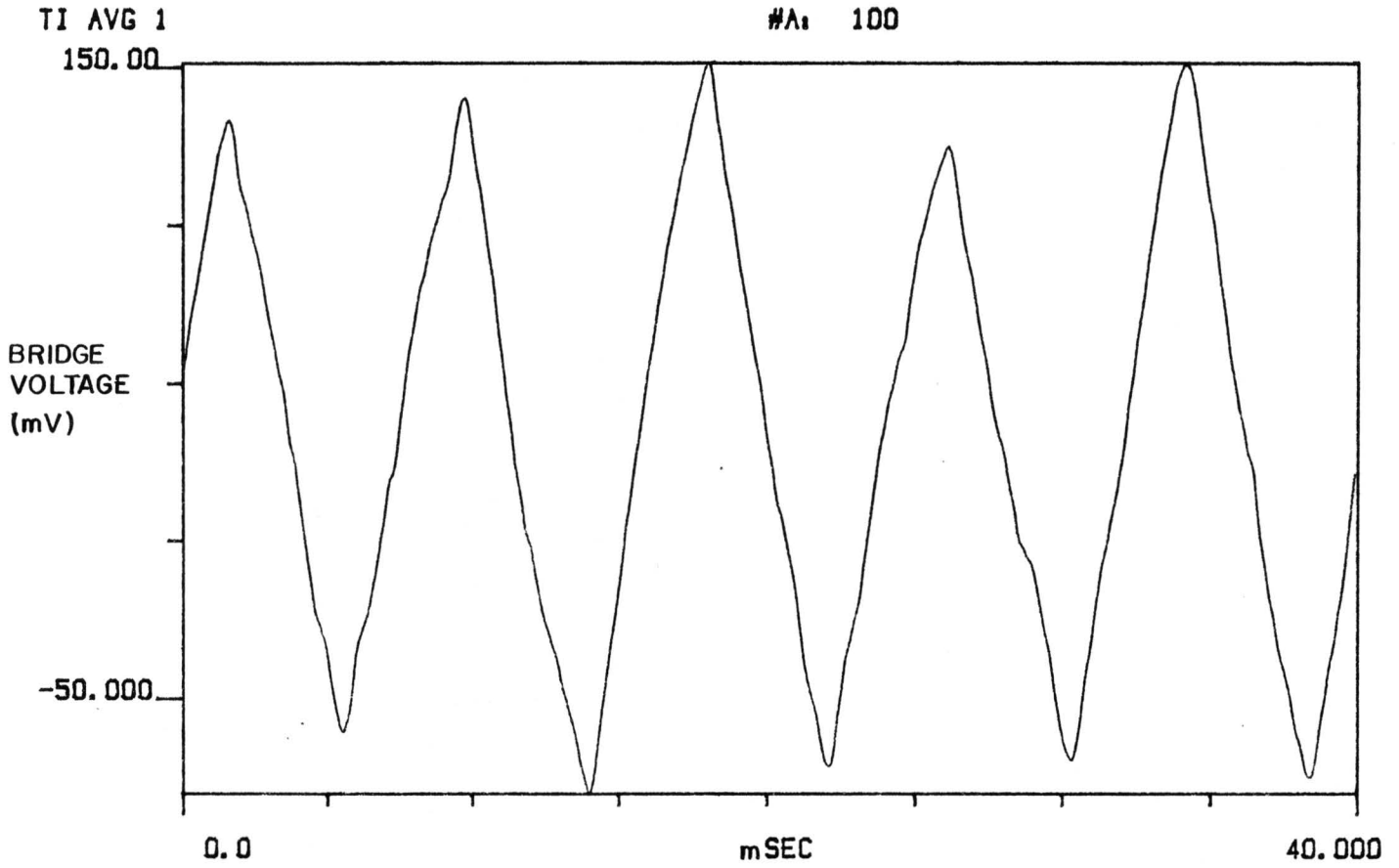

Figure 33. Thermal square wave test results at 120 Hz.

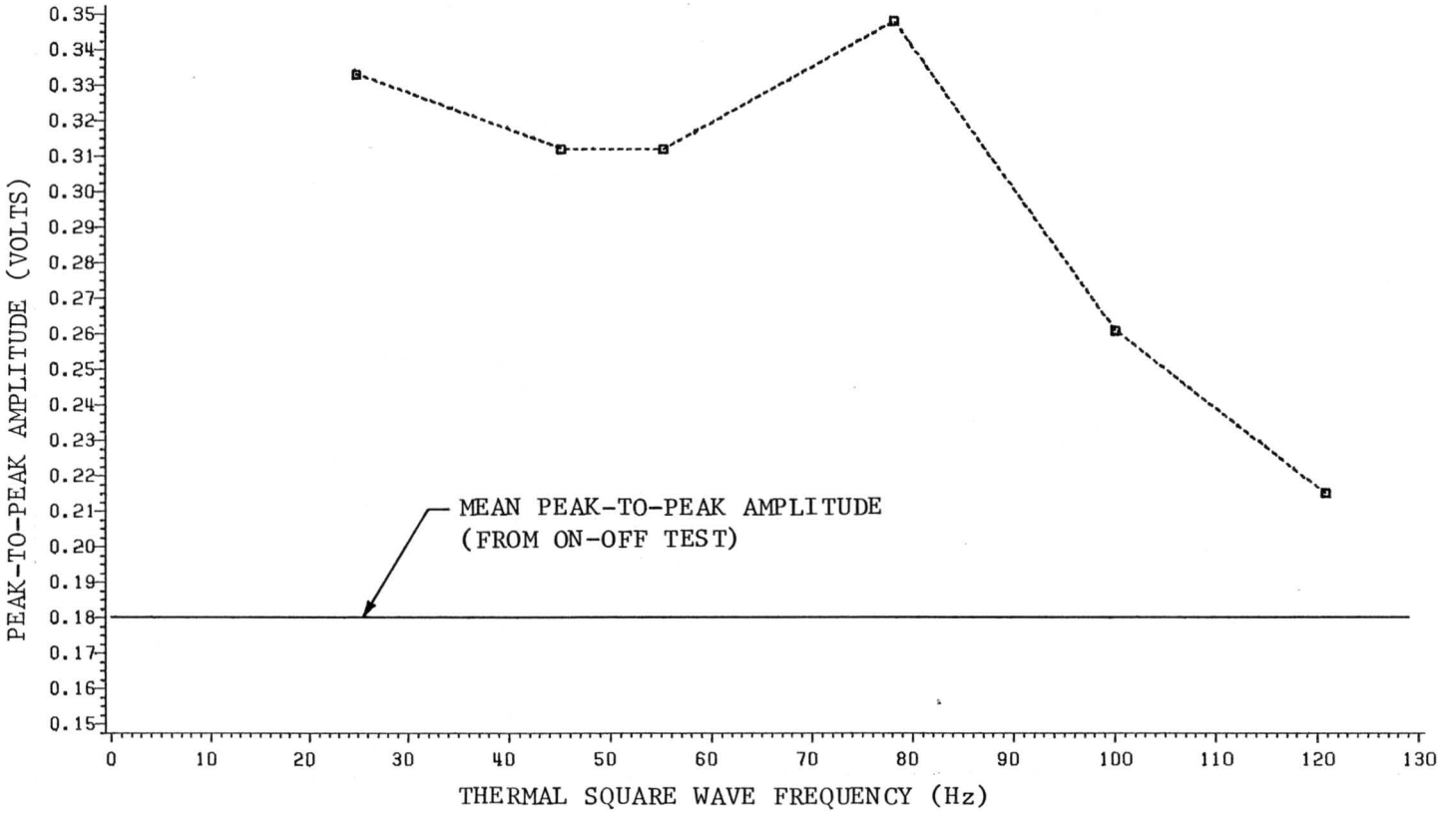

Figure 34. Plot of the peak-to-peak bridge voltage versus the square wave test frequency.

the bridge voltage, determined from the slope of the triangular wave form, is approximately 60 volts/sec.

5.0 DISCUSSION OF RESULTS

The primary objective of this investigation is to measure rapidly varying heat fluxes while maintaining a constant wall temperature boundary condition. However, because of the geometry of the gage, the uniform joule heating in the gold film actually maintains a constant heat flux boundary condition. This will very closely simulate a constant temperature boundary condition as long as there is not a significant variation of heat transfer coefficient across the width of the gage. The gage used in this research only spans 3 degrees of cylinder arc and the operation is therefore assumed to be constant temperature. An example of a flow in which the operation would not be constant temperature across the sensing film is near a standing shock wave.

5.1 STEADY CALIBRATION

The time-averaged calibration results (Figures 22 and 24) show a difference between the two calibration methods used. This presents a problem if the gage is calibrated in one apparatus and transfered to another for actual heat transfer measurements. However, when two different gages were calibrated in the cylinder stagnation point calibration apparatus, the results were very nearly the same (tests C-2 through C-4 versus test C-8). Both gages used were constructed using the same methods, so it would appear that there is not a significant variation between calibrations for different gages. Therefore, it will be assumed that the gage

used in the impinging flow calibrator would give the same results seen for the cylinder stagnation point calibrator if it were used as such.

There are several conditions that could cause changes in either the slope or the position of the cylinder calibration curve. The possible reasons are given below.

REASON FOR PARALLEL SHIFT IN CALIBRATION CURVE

- Constant temperature mismatch between gage and boundary

REASONS FOR CHANGE IN SLOPE OF CALIBRATION CURVE

- Varying temperature mismatch with heating condition
- Incorrect gage area
- Incorrect operating resistance

The constant temperature mismatch condition will shift the slope because the conduction loss term will be constant over all heating conditions. The incorrect gage area and operating resistance will change the slope since they are multiplying factors in determining the heat transfer coefficient. However, of these possible reasons the varying temperature mismatch with heating condition appears to be the most likely.

Therefore, the difference between the calibration results can be explained in terms of temperature matching between the thin-film gage operating temperature and the surrounding material. Between the two time-averaged calibration methods, the impinging flow calibration apparatus has the most temperature instrumentation and as a result, the boundary temperature near the gage was known to $\pm$ 0.1°C. The impinging

flow calibration data also had a smaller scatter than the cylinder stagnation point calibration data. The linear regression line fitted through the calibration data (Figure 22) is nearly parallel to the one-to-one line and is offset by an average of 10 W/m^2-C.

The two tests on the impinging flow calibrator with the lowest error (tests P-5 and P-6) were the tests to which the most attention was paid to temperature matching. In these tests, the thermocouples were calibrated prior to the tests and extreme care was taken to match the gage temperature to the temperature of the thermocouple mounted behind it. The one point in test P-5 which deviates from the low error levels is the point at the lowest heat flux level. At this point the IFA-100 would not operate continuously. The data was taken during the time the CTA was running and, consequently, the gage substrate temperature may have been at a lower temperature than its steady state temperature. This would cause power losses into the substrate and increase the error, as seen in Figure 25.

Contrasting the impinging flow results are the results from the cylinder stagnation point calibration. These tests had higher error than the impinging flow calibration, but also had less temperature instrumentation. The nearest thermocouples were 7.62 cm down the axis of the cylinder and there was an average of a 0.3°C difference between these two thermocouples (at the same angular position as the gage). The trend of decreasing error with decreasing heat transfer rate, Figure 25, could be due to heat energy being allowed to conduct more uniformly around the cylinder at lower heat transfer rates, thereby making the temperatures more uniform. To support this, the temperature data from test C-6 shows

that the average temperature difference between the two thermocouples, adjacent to the gage, drops from 0.5°C at the maximum heat flux condition to 0.1°C at the minimum condition. Therefore, if the local boundary temperature is better matched to the gage temperature, the losses into the substrate can be reduced which will reduce the error. When the gage temperature was operated above the cylinder temperature, tests C-1 and C-6, it was seen that there was increased error for increased gage overheat. The increased error is due to significant gage power being lost into the substrate through conduction. There will also be increased losses (secondary) to the air stream through convection because of the increased temperature difference and changes in the thermal boundary layer due to the effects of the gage deviating from the isothermal boundary condition.

A 2-D finite difference program was used to estimate the conduction losses due to temperature mismatch. The analysis showed conduction losses equivalent to a 4 W/m^2-C shift in the gage heat transfer coefficient due to a 0.1°C mismatch. Also, the analysis predicted the offset in heat transfer coefficient of 60 W/m^2-C between tests C-1 and C-6 to within 10 percent of the offset. Tests C-1 and C-6 were run with the gage temperature 0.7°C and 2.0°C above the cylinder temperature, respectively. Therefore, even with a $\pm$ 0.1°C match in temperatures there can still be a 5 percent error in the measurement of the mean heat transfer coefficient due to conduction losses. It may be practical to use this gage to measure the A.C. component of the heat transfer signal while the mean signal is measured with a more accurate time-mean gage. The details of the above analysis are given in Appendix D.

5.2 UNSTEADY CALIBRATION

The results of the direct thermal square wave calibration gave a frequency response an order of magnitude less than the conservative estimate from the standard electronic test. This difference is apparently because of the inherent differences between the two tests. The electronic test actually introduces an alternating probe current which instantly and uniformly changes the power dissipated in the film through joule heating. However, the thermal square wave imposes a square wave variation in the surface heat flux boundary condition and the effects of the change in heat flux must be conducted into the film. This condition more closely simulates the variations experienced during actual usage of the gage and is considered a much better test. Therefore, the frequency response is conservatively estimated to be that found from the thermal square wave test, 91 Hz.

The thermal square wave tests reveal that the thin-film gage measurement system can follow heat flux variations corresponding to a maximum bridge voltage rise rate, rr, of 60 volts/sec. The sections of Figs. 29-34 when the gage is responding from one extreme in heat flux condition to another are approximately linear (except for overshoot). Therefore, the curve shape becomes triangular at the higher frequencies since the system has not yet fully responded to one step when another step is encountered. If the frequency is increased beyond the value where the triangular wave first forms, the amplitude of the triangular wave will decrease since the system will be able to respond to less and less before the next step is encountered. This phenomenon is used to explain the

amplitude roll-off for the 100 Hz and 120 Hz cases (Figure 35) but the peak-to-peak amplitude is still higher than the amplitude determined from the on-off test. Although the data shows some variation of the rise rate, the peak-to-peak amplitude of the triangular wave can be estimated from the frequency of the thermal square wave as

$$A = rr / 2 f \tag{19}$$

where A = peak-to-peak amplitude of the triangular wave (volts)

rr = maximum rise rate of system (volts/sec)

f = frequency of thermal square wave (Hz).

5.3 OVERALL INTERPRETATION OF CALIBRATION RESULTS

The overall application of the calibration curves needs to be considered when actual unsteady test data is to be reduced. The calibration curves can be used one of two ways to reduce experimental data: 1) determine the mean and fluctuating components through the calibration curves or 2) use the calibration curve to determine the mean value and calculate the fluctuating components directly from the fluctuating power levels. Due to the steep slope of the cylinder stagnation calibration results, there could be significant differences in the magnitude of the unsteady components depending on how the data is reduced.

It appears from the impinging flow data, especially for tests P-5 and P-6, that when the gage film temperature is matched to the surrounding

boundary temperature that the heat transfer rates reduced from the gage output match those of the calibrator. The good agreement seen for the impinging flow calibration is most likely due to the region around the gage being isothermal, while the cylinder stagnation calibration yields worse results probably due to the uncertainty of the boundary temperature near the gage. This, of course, assumes similar operation between the gages used in the different calibration methods. Therefore, to reduce actual test data on the cylinder, the calibration curve generated from the cylinder stagnation calibration should be used to determine the mean heat transfer values while the fluctuating component should be calculated from the actual power fluctuations.

6.0 CONCLUSIONS AND RECOMMENDATIONS

The following conclusions can be drawn from the present development of the thin-film heat flux gage:

1) The system is a good method for measuring fluctuating heat fluxes up to 90 hertz.
2) Temperature matching is crucial to maintaining low error levels in measuring mean and fluctuating heat transfer.
3) Use the thin-film gage to measure fluctuating heat transfer in conjunction with a gage to measure mean heat flux levels.
4) The system developed was used to measure the effect of vortex shedding on cylinder heat transfer with shedding at 82 hertz.

The following recommendations are made for future development and experimental work with this system:

1) Resolve the problems associated with the constant-temperature anemometer system shutting off at low heat flux levels or in high turbulence flows. Improve the range of operation.
2) Resolve the errors seen in the cylinder stagnation point calibration data.
3) Use more temperature instrumentation on the cylinder so that temperature matching between the gage film and the cylinder is ensured.

LIST OF REFERENCES

1. Doeblin, Ernest O., Measurements Systems Application and Design, McGraw-Hill, Inc., 1975.

2. Gardon, R., "An Instrument for the Direct Measurement of Intense Thermal Radiation," Review of Scientific Instruments, Vol. 24, No. 5, May 1953.

3. Gardon, R.,"A Transducer for the Measurement of Heat Flow Rate," Journal of Heat Transfer, Trans. ASME, Series C, Vol. 82, 1960, pp. 396-398.

4. Borell, G. J., and Diller, T. E., "A Convection Calibration Method for Local Heat Flux Gages," ASME Paper No. 84-HT-45.

5. Keltner, N. R., and Wildin, M. W., "Transient Response of Circular Foil Heat Flux Gages to Radiative Heat Fluxes," Review of Scientific Instruments, Vol. 46, 1975, pp. 1161-1166.

6. Kim, B. K., Borell, G. J., Diller, T. E., Cramer, M. S., and Telionis, D. P., "Pulsating Flow and Heat Transfer Over a Circular Cylinder," in Proceedings of the Symposium on Nonlinear Problems in Energy , DOE CONF-830413, 1983, pp. 96-101.

7. Vidal, R. J., "Model Instrumentation Techniques for Heat Transfer Measurements in a Hypersonic Shock Tunnel," Cornell Aeronautical Laboratory Report No. AD-917-A-1, February 1956.

8. Dunn, M. G.,and Stoddard, F. J., "Measurement of Heat Transfer Rate to a Gas Turbine Stator," Journal of Engineering for Power, Vol. 101, April 1979, pp. 275-280.

9. Kercher, D. M., and Sheer, R. J. Jr., "Short Duration Heat Transfer Studies at High Free-Stream Temperatures," Transactions of the ASME, Vol. 105, January 1983, pp. 156-166.

10. Consigny, H., and Richards, B. E., "Short Duration Measurements of Heat-Transfer Rate to a Gas Turbine Rotor Blade," Transactions of the ASME, Vol. 104, July 1982, pp. 542-551.

11. Schultz, D. L., and Jones, T. V., "Heat-Transfer Measurements in Short Duration Hypersonic Facilities," AGARDograph Vol. 165, 1973.

12. Tsou, F. K., Chien, S. J., and Ko, S. Y., "Measurements of Heat Transfer Rates Using a Transient Technique," ASME Paper No. 83-HT-87, 1983.

13. Boulos, M. I., and Pei, D. C. T., "Dynamics of Heat Transfer From Cylinders in a Turbulent Air Stream," International Journal of Heat and Mass Transfer, Vol. 17, 1974, pp. 767-783.

14. Suarez, E., and Figliola, R. S., "Instantaneous Azimuthal Heat Transfer Coefficients from a Horizontal Cylinder to a Mixed Particle Size Air-Fluidized Bed," ASME Paper No. 83-HT-93, 1983.

15. Fitzgerald, T. J. and Catipovic, N. M., and Jovanovic, G. N., "Instrumented Cylinder for Studying Heat Transfer to Immersed Tubes in Fluidized Beds," Industrial Engineering Chemistry Fundamentals, Vol. 20, 1981, pp. 82-88.

16. Hayward, G. L., and Pei, D. C. T., "Local Heat Transfer from a Single Sphere to a Turbulent Air Stream," International Journal of Heat and Mass Transfer, Vol. 21, 1978, pp. 35-41.

17. Bellhouse, B. J., and Schultz, D. L., "The Measurement of Fluctuating Skin Friction in Air with Heated Thin-Film Gauges," Journal of Fluid Mechanics, Vol. 32, part 4, 1968, pp. 675-680.

18. Ramaprain, B.R., and Tu, S. W., "Calibration of a Heat Flux Gage for Skin Friction Measurement," J. Fluids Engng., Trans. ASME, Vol. 105, 1983, pp. 455-457. TA349 J6

19. Van Heiningen, A. R. P., Mujumdar, A. S., and Douglas, W. J. M., "On the Use of Hot Film and Cold Film Sensors for Skin Friction and Heat Transfer Measurements in Impingement Flows," Letters in Heat and Mass Transfer, Vol. 3, 1976, pp. 523-528. QC 319.8 L47

20. Kraabel, J. S., McKillop, A. A. and Baughn, J. W. "Heat Transfer to Air from a Yawed Cylinder," International Journal of Heat and Mass Transfer, Vol. 25, 1982, pp. 409-418.

21. Figliola, R. S., Personal Communication, January 11, 1984.

22. Nielsen, P. E., and Rasmussen, C. G., "Measurement of Amplitude and Phase Characteristics," DISA Information, No. 4, pp. 17-23, 1966.

23. Perry, A. E., Hot-Wire Anemometry, Clarendon Press Oxford, 1982.

24. Freymuth, P., and Fingerson, L. M., "Electronic Testing of Frequency Response for Thermal Anemometers," TSI Publication, 8 pages.

25. Freymuth, P., "Theory of Frequency Optimization for Hot-Film Anemometers," Journal of Physics E. Scientific Instruments, Vol. 11, 1978, pp. 177-179.

26. Freymuth, P., "Frequency Response and Electronic Testing for Constant-Temperature Hot-Wire Anemometers," Journal of Physics E Scientific Instruments, Vol. 10, 1977, pp. 705-709.

27. Freymuth, P., "Further Investigation of the Nonlinear Theory for Constant-Temperature Hot-Wire Anemometers," Journal of Physics E Scientific Instruments, Vol. 10, 1977, pp. 710-713.

28. Goldstein, Richard J., "Fluid Mechanics Measurements," Hemisphere Publishing Corporation, 1983.

29. Ishigaki, H., "Heat Transfer in a Periodic Boundary Layer Near a Two- Dimensional Stagnation Point," Journal of Fluid Mechanics, Vol. 56, part 4, 1972, pp. 619-627.

30. Ishigaki, H., "The Effect of Oscillation on Flat Plate Heat Transfer," Journal of Fluid Mechanics, Vol. 47, part 3, 1971, pp. 537-546.

31. Ishigaki, H., "Periodic Boundary Layer Near a Two-Dimensional Stagnation Point," Journal of Fluid Mechanics, Vol. 43, part 3, 1970, pp. 477- 486.

32. Lighthill, M. J., "The Response of Laminar Skin Friction and Heat Transfer to Fluctuations in the Stream Velocity," Proceedings Royal Society A, Vol. 224, 1954, pp. 1-23.

33. Gersten, K., "Heat Transfer in Laminar Boundary Layers with Oscillating Outer Flow," AGARDograph, Vol. 97, part 1, 1965, pp. 423-475.

34. Kim, B. K., VandenBrink, D. J., Cramer, M. S., and Telionis, D. P., "Unsteady Heat Convection Over Circular Cylinders," ASME Paper No. 84-HT-100.

35. Borell, G. J., "Heat Transfer From a Circular Cylinder in a Pulsating Crossflow," M.S. Thesis, VPI&SU, 1983.

36. Meier, H. U., Kreplin, H. P. and Fang, L. W., "Experimental Study of Two- and Three-Dimensional Boundary Layer Separation," International Union of Theoretical and Applied Mechanics, Symposium Toulouse, France, May 5-8, 1981, pp. 87-99.

37. VandenBerghe, T. M., to be submitted, J. Heat Transf., Trans. ASME.

38. Kaufman, E., "Instantaneous Temperature Sensor," Instruments and Control Systems, Vol. 11, 1968, pp. 89-90.

39. Lion, K. S., Instrumentation in Scientific Research, McGraw-Hill Book Company, New York, 1959.

40. Hayat, M. A., Introduction to Biological Scanning Electron Microscopy, University Park Press, Baltimore, Maryland, 1978.

41. Kline, S. J., and McClintock, F. A., "Describing Uncertainties in Single-sample Experiments," Mech. Eng.,p. 3, January, 1953.

42. Holman, J. P., Heat Transfer, Fourth Edition, McGraw-Hill Book Company, 1976.

APPENDIX A. GAGE CONSTRUCTION

This appendix describes the common methods for depositing metallic films and the types of substrate materials commonly used to deposit films on. The details of the gage construction procedure are given in the last section.

A.1 METAL FILM

The principal property of the metals to be used for the film material is that they must have a positive variation of resistance with temperature (resistance-temperature coefficient, α). The resistance-temperature coefficient should also be large so that the film temperature can be more easily resolved. The reason that a positive α is required is simply that the CTA control circuitry is designed for it. A table of common temperature resistance coefficients, α, are given below in Table 2. Of these metals, platinum is used exclusively in the literature cited for CTA controlled gages and for most transient gages.

There are three popular methods for depositing metallic films on surfaces: painting, vapor depositing and sputter-coating. The painting or printed circuit technique has found wide use in the construction of the transient-type and CTA controlled gages using platinum films. The printed circuit paints are composed of organic platinum and gold or silver compounds with binders and reducing agents. The paint is either penned (narrow films) or silk screened (lagrer areas) onto the surface to be

Table 2. Resistance-temperature coefficients at room temperature, 1/C

MATERIAL	α (1/C) from Vidal(7)	α (1/C) from Lion(39)
Aluminum	0.00403	0.0045
Carbon	-	-0.0007
Copper	0.00392	0.0043
Electrolytes	-	-0.02 to -0.09
Gold	0.00340	0.004
Iron (alloy)	-	0.002 to 0.006
Lead	-	0.0042
Manganin	-	+-0.00002
Mercury	-	0.00099
Nickel	0.00540	0.0067
Platinum	0.00301	0.00392
Rhodium	0.00430	-
Semiconductor (thermistors)	-	-0.068 to +0.14
Silver	0.00380	0.0041
Tungsten	-	0.0048

coated. The film is then cured at elevated temperatures to reduce the metallic oxides to pure metal and to remove the binders and other volatiles. Typically, a glass substrate coated with a platinum paint is heated to 1250 F for approximately 20 min and then cooled [7,38]. It is reported that lead wires can be soldered to the film with ordinary soft solder. One drawback of this method is that the minimum film thickness is controlled by the paint composition. Also, the film can be non-uniform in thickness. These printed circuit paints can be obtained from either Englehard Industries of Iselin, New Jersey or the Hanovia Chemical and Manufacturing Company of East Newark, New Jersey. For further details on procedures or materials used in this technique refer to Vidal [7], Schultz and Jones [11], or Kaufman [38].

The vapor depositing technique has found wide use in coating specimens for scanning electron microscopy. It consists of evaporating a metal under a hard vacuum (approximately 1.E-05 torr) with the piece to be coated located near the vapor source. The vapor source usually consists of a tungsten basket, in which the metal to be vaporized is heated, or of a small filament of that metal. Current is passed through the basket or filament causing the metal to heat up and evaporate. The vapor diffuses throughout the evacuated chamber and condenses to form a thin film on the workpiece. This method is used with a variety of metals in electron microscopy and is reported to give good uniform thickness [39]. The film thickness can be controlled by the quantity of evaporated metal and the distance of the workpiece from the vapor source. More details of this technique are given in the book by Hayat [39].

The final method for depositing metallic films is the sputter-coating technique. This technique is widely used in industrial thin film technology and scanning electron microscopy. Sputtering occurs when a target material (such as gold) is ionized by a strong electrical potential. Commercially available units consist of a two-electrode configuration with the piece to be coated placed on the anode (see Figure 35). The cathode is the target, with the anode held at some large positive potential (.8 to 2 kV typically [39]). The target is ionized and the ions travel down towards the specimen, at the anode. The sputtered atoms form a coating on the workpiece. This sputtering process is done at low vacuums of about 1.E-02 torr, which causes the sputtered atoms to undergo many collisions before they condense on the specimen. This gives a uniform coating even on very rough surfaces. The details of this process are given in the book by Hayat [39]. This process is reported to give a very uniform and repeatable coating. The film thickness is controlled by the amount of time the specimen is coated and by the magnitude of the current through the electrodes. The thickness can be determined by various equations [39] and certain sputter coaters have optional thickness sensors. Its wide use in electron microscopy makes it available on many university campuses. Also, there is a variety of target materials available (gold, platinum,nickel,etc.). The availability and uniform thickness provided by this method prompted its use on the project. However, the purchasing cost of a platinum cathode precluded the use of platinum films. Therefore, gold was chosen since a cathode was available for a per run cost.

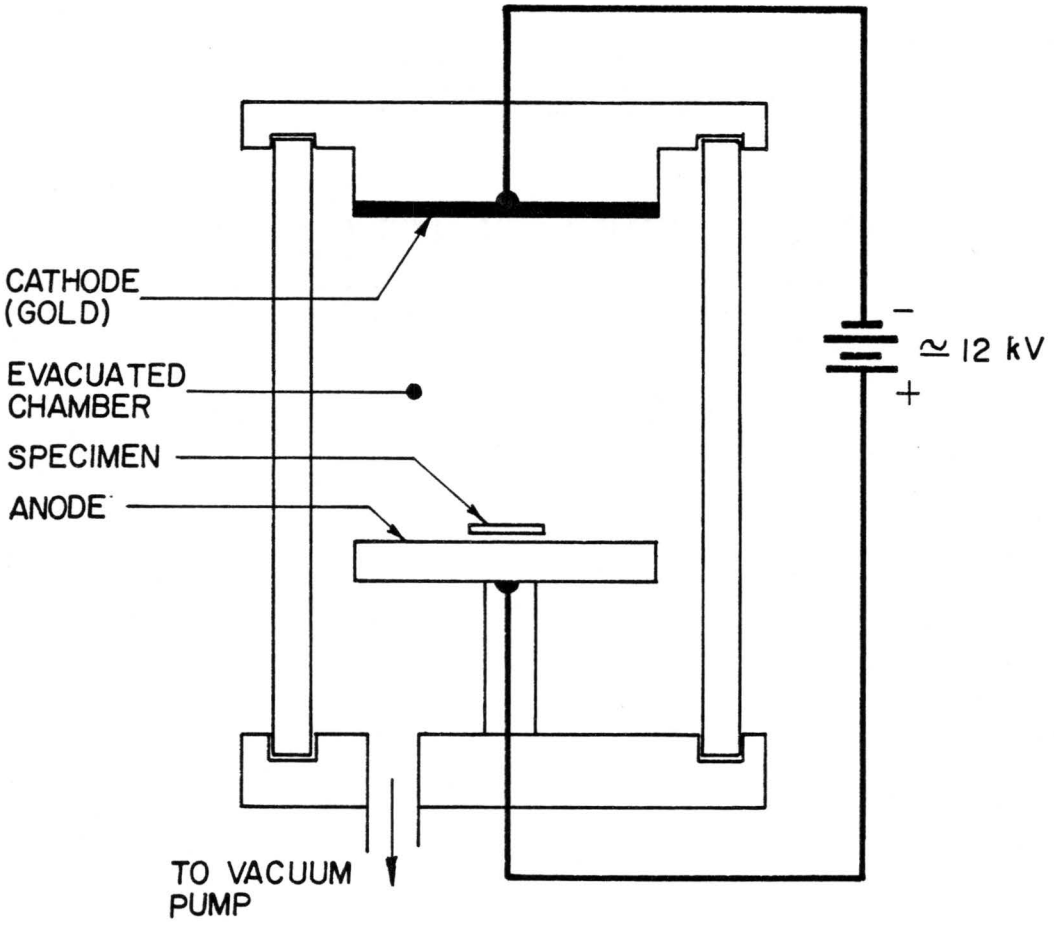

Figure 35. Schematic of sputter-coater.

A.2 SUBSTRATE

The substrate for the metallic film should be made from a thermal and electrical insulating material. The properties associated with an insulating material help electrically insulate the film from the surrounding material, usually metal, while also reducing conduction losses. Also, insulators reduce the problems associated with thermal feed-back caused by small film temperature fluctuations. Most researchers use glass substrates, but experience on this research showed that connection of the lead wires to the film is difficult to do without damaging the film. The methods that were used to attach leads in the cited literature were soldering or using conducting paint as an adhesive. The substrate used in this project was double copper clad G-10 fiberglass printed circuit board, which has comparable insulating properties to that of glass and superior machining properties. The machining properties allowed small diameter holes, for the lead wires and the thermocouple, to be drilled through the substrate. Also, the copper cladding provides a good contact surface on which to deposit the film and to solder lead wires.

A.3 CONSTRUCTION PROCEDURE

The gage construction begins with cutting 1- or 2-ounce double copper clad printed circuit board into blanks. The blanks are 1.91 cm (0.75 in.) long by approximately 0.203 cm (0.080 in. wide). The three 0.038 cm (0.015 in.) holes for the lead wires and the thermocouple are drilled on 0635 cm (0.25 in.) centers. Figure 36 shows a drawing of a completed

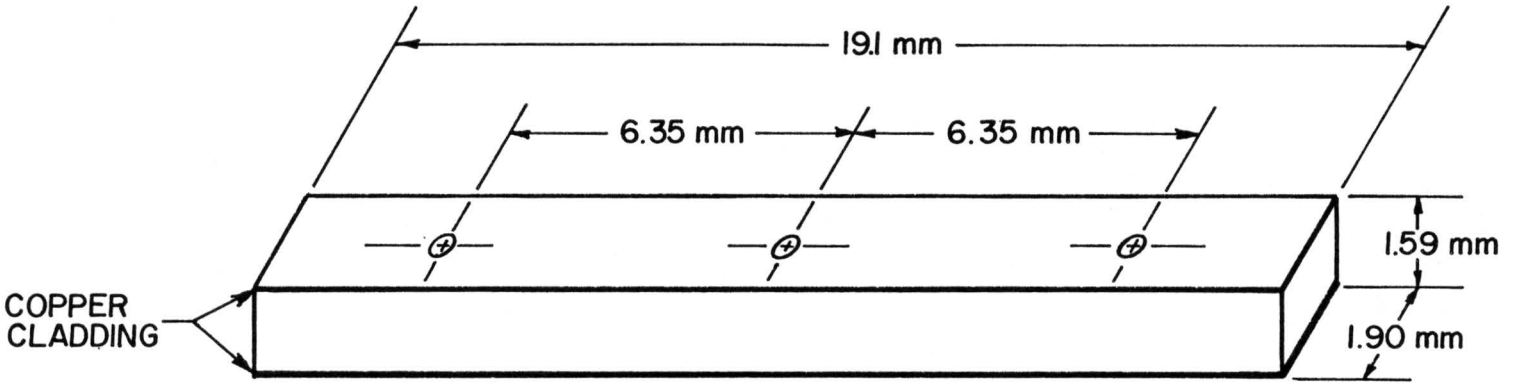

Figure 36. Completed gage blank.

blank. Final finishing of the width is done by careful sanding with 400 grit and 600 grit emery paper.

Next, the lead wires are soldered to the copper on the back and front sides of the blank. The wires are soldered to the back surface for strength since only enough solder for good electrical contact will remain on the front side. Either 28 or 30 GA teflon coated copper wire gives good strength and low lead resistance. Tinned and silvered copper wires were used, but the tinned 30 GA wires tended to be brittle. Care should be taken at this point to not get too much solder on the front surface, since any excess needs to be removed. Finally, the soldering should be done with all of the copper intact (before etching), since the small copper strips left after etching will debond from the fiberglass board from the heat of soldering.

The solder on the front surface is next filed as flat as possible without damaging the copper or the substrate. The excess solder is removed by careful sanding with 600 grit emery paper until the surface is flat.

The next step is to etch away all the copper, except for the contact strips on the front and the copper immediately around the solder on the back surface. The copper is etched with a commercially available $FeCl_3$ solution. Masking of the copper regions to be kept should be done with enamel paint. Although there are special felt-tip pens available to mark copper areas to be kept, the ink does not protect reliably the solder around the lead wires at the front surface. While using such pens in early tests, the solder around the lead wires of several gages was etched away, which resulted in electrical discontinuity between the leads and

copper contact strips. Also, care should be taken to paint the exposed copper on the lead wires extending from the back surface to protect them from being etched. The etching is done with a solution of 31.47% $FeCl_3$ with 68.53% H_2O, and a specific gravity of 1.304, in a plastic or glass cup. The gage is immersed in the solution and agitated for about 2.5 to 3 minutes (until all excess copper is removed). The enamel paint was then removed with acetone. During etching, the copper contact can get under-cut an shown in Figure 37. This edge should be burnished with a rounded object to remove the ledge. The failure of several gages was attributed to this phenomenon.

At this point the ends of the substrate were filed off square until the copper contact strips are about 0.127 cm (0.05 in.) wide or less. Care should be taken not to file into the lead wires in the substrate.

Next, the gage thermocouple is installed. The thermocouple is made from 0.076 mm (0.003 in.) diameter copper and constantan wire, covered with 0.076 mm (0.003 in.) thick teflon insulation. The junction was made with an argon purge thermocouple welder. Welding the small diameter wire took some practice, but eventually a bead of less than 0.038 cm (0.015 in.) was consistently achieved. The junction is made as shown in Figure 38 to facilitate the installation process. The thermocouple was cemented into the gage center hole with 5-minute epoxy. The thermocouple was positioned as close to the surface as possible while still maintaining a thin layer of epoxy over the thermocouple. The layer of epoxy is necessary to maintain electrical isolation between the thermocouple and the film to be deposited. After the epoxy cures, the excess epoxy on the front surface is carefully sanded away with 600 grit emery paper. A check

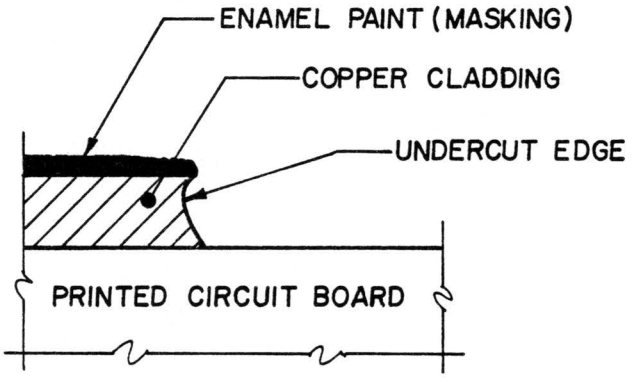

(a)

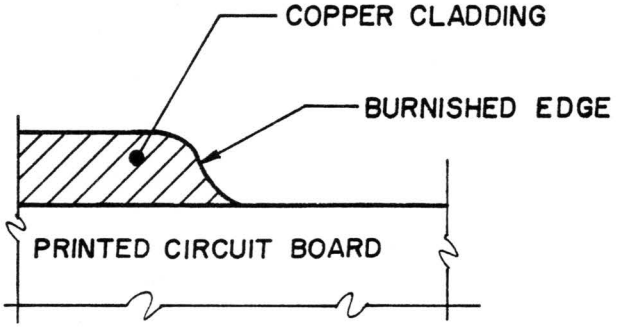

(b)

Figure 37. Detail of copper contact strip (a) after etching and (b) after burnishing to remove undercut edge.

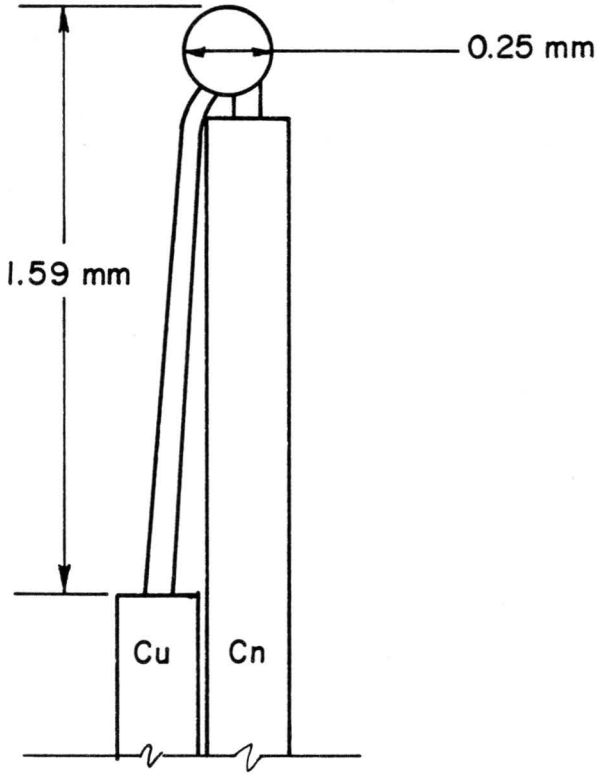

Figure 38. Detail of thermocouple construction.

should be made at this point to ensure that there is still a layer of epoxy covering the thermocouple. This was done by examining the front surface with a surface microscope. If there is still doubt, an electrical continuity check can be done with a sharp conducting probe.

Next, the gold film is deposited. The gage is first cleaned with acetone in a sonic cleaner to remove any oils or dirt on the front surface. After drying, the sides of the gage are masked with tape and the lead wires are wound together and protected from being sputtered by slide glass. Slide glass should be used since it does not outgas. If a material such as cardboard is used, the outgassing will prevent the sputter coater from reaching the vacuum required to operate. The sputtering was done with a SPI model 12121 sputter coater located at the Veterinary School Ultrastructure Research Lab. The gage was sputtered until a gage resistance of 20 to 30 ohms is achieved. Typically, the sputter coater was run for 3 minutes and 40 seconds at 35 milliamperes.

Finally, any exposed wire is coated with enamel paint to prevent it from shorting with the cylinder. The sides of the gage were covered with library tape, 0.05 mm thick, to give a better fit in the cylinder and to help electrically isolate it. The gage is installed by carefully pressing it into the slot machined in the cylinder wall. The very ends of the copper contacts should be used for this purpose. The gage is positioned so that it is flush with the cylinder surface.

Care should be taken when first operating the gage, since the nominal resistance will change. This change can result in gage burnout, especially at high overheats, since the CTA maintains the film at the initial operating resistance. Personal experience showed that the resistance

always decreases. The best explanation for this is that the gold is deposited as a dust and current flow through the film causes the dust to collapse, locally, and become more like a film. Gages used in this research were run for about 2 hours before data was taken.

APPENDIX B. APPLICATION TO CYLINDER HEAT TRANSFER

As a demonstration of its potential, the gage was used to measure unsteady heat transfer from a cylinder in a steady crossflow. The free-stream turbulence level of the wind tunnel was less than 0.5 percent and the Reynolds number was 77,000. The unsteadiness of the flow around the cylinder was due to the natural vortex shedding in the wake of the cylinder. This alternate shedding of vortices in the wake causes the front stagnation point to oscillate several degrees. The frequency of this oscillation is characterized by the Strouhal number, which has a value of approximately 0.2 for a wide range of Reynolds numbers.

Data was taken in the laminar attached boundary layer region at 0, 2, and 10 degrees from the front stagnation point. The gage operation was limited to angles of less than 50 degress from stagnation. The region beyond 50 degrees from stagnation through separation is a low heat flux area with low mean power levels being required by the gage. The IFA-100 would sense the unsteadiness in the heat transfer and interpret it as an oscillation condition (large amplitude fluctuation relative to the mean) in the control circuitry and shut off the system. The development personnel at TSI are investigating possible modifications to the anemometer control circuitry which would allow the system to operate under these conditions.

The gage output for the measurement locations is shown in Figs. 39 - 41. These are the actual time records of the A.C. component of the bridge voltage. The peak-to-peak amplitude of each heat transfer signal has been

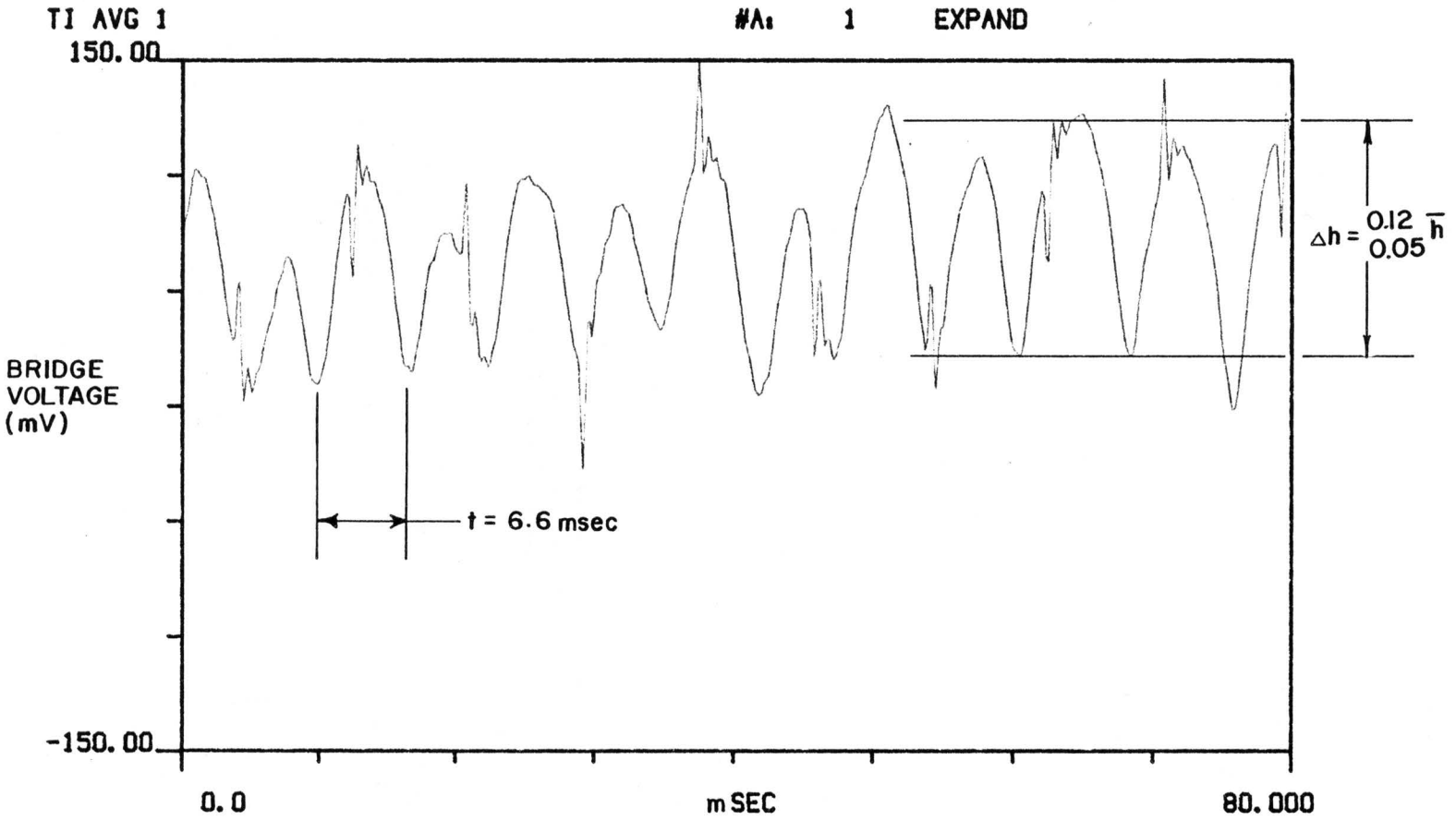

Figure 39. Cylinder results at 0°.

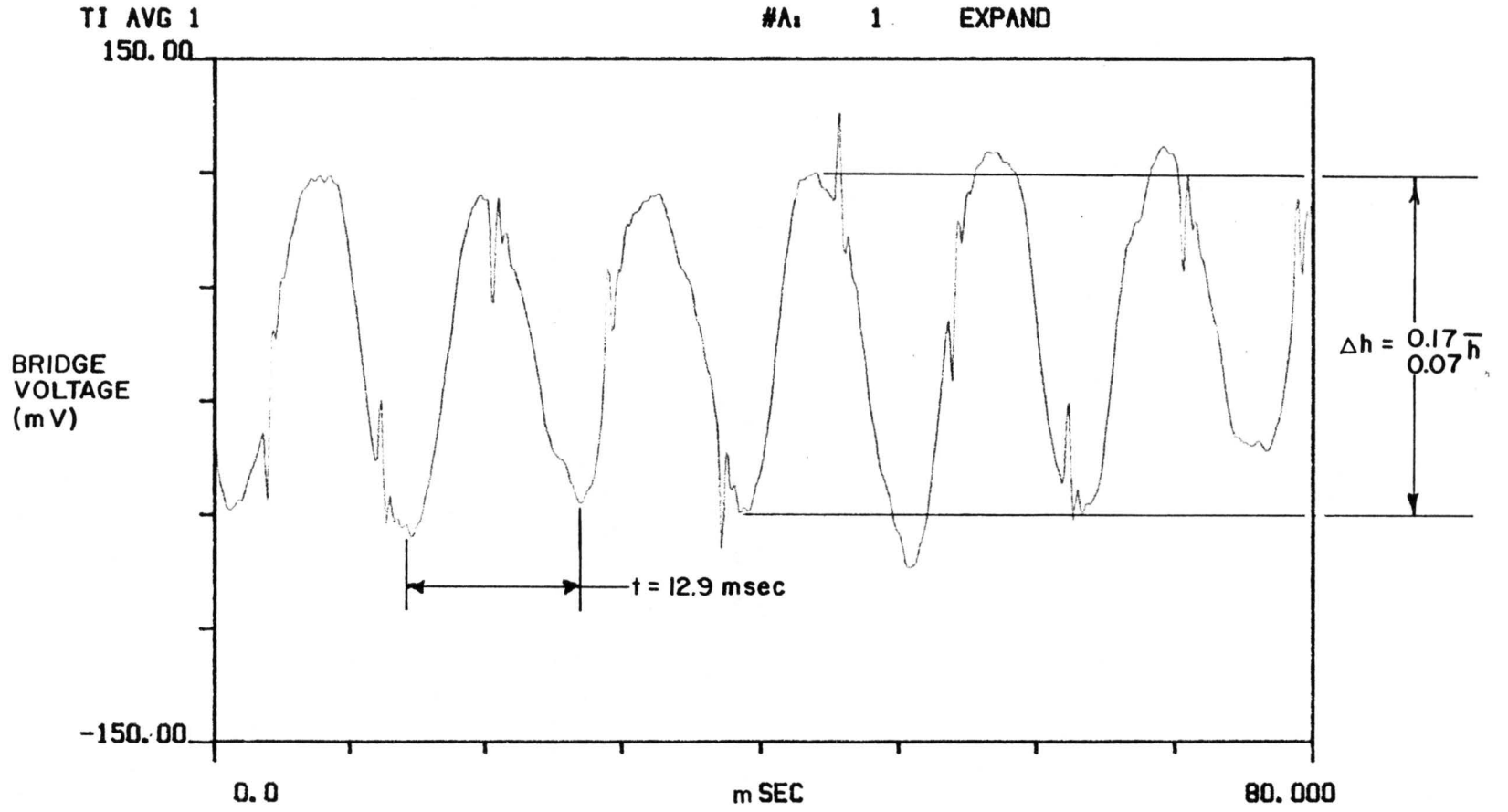

Figure 40. Cylinder results at 2°.

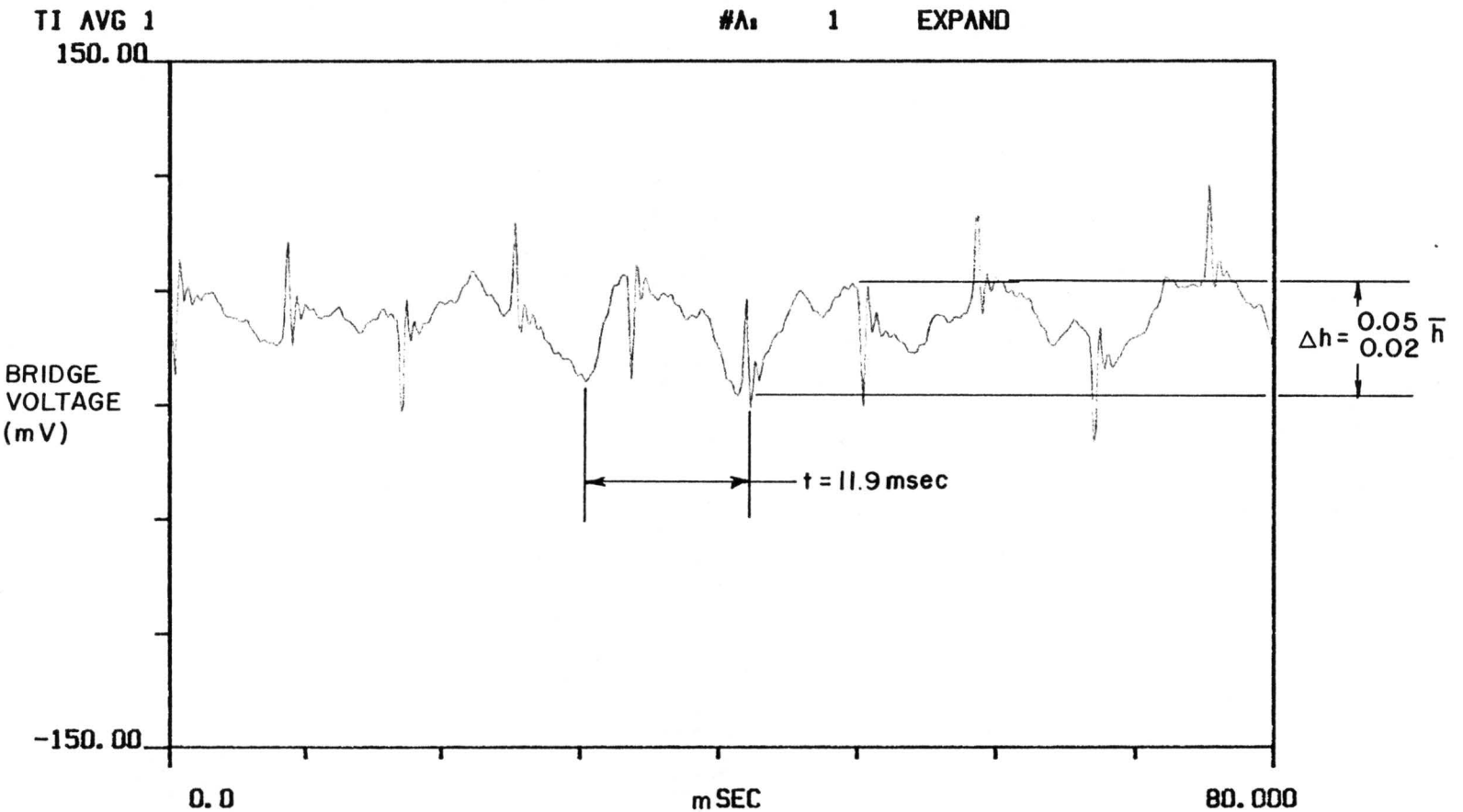

Figure 41. Cylinder results at 10°.

reduced two ways and is shown on each figure. The larger number is reduced from the amplitude of the power fluctuations and the smaller number is reduced from the calibration curve taken prior to the test. The following discussion is based on the amplitudes reduced from the calibration curve. Also, to insure that the fluctuations actually were due to the vortex shedding, a splitter plate was also installed immediately behind the cylinder for comparison for each of the tests. The results are shown in Figure 42 for the 2 degree case.

The only information in the cylinder data with the splitter plate is 60 cycle noise with some turbulence superimposed. The spiking in these plots is caused by the cylinder heater power source, which is phase angle fired. The data for the cylinder without the splitter plate plainly shows the effect of the vortex shedding on the local instantaneous heat transfer. At the front stagnation point (Figure 39) the signal shows that the fluctuations are at twice the shedding frequency compared to the signal at 2 degrees (Figure 40). This is due to the heat transfer signal being rectified because of the zero net flow at the front stagnation point. This phenomenon has been recorded in skin friction measurements by Meier et al. [36].

The peak-to-peak amplitude of the heat transfer signal at 2 degrees from stagnation (Figure 40) is approximately 7 percent of the mean signal. The amplitude shown at 0 degrees is only 5 percent, but this actually corresponds to 10 percent, an even larger peak-to peak signal than the 2 degree case. The lower portion to these curves has just been flipped (or rectified) at the stagnation point. Since the gage spans about 3 degrees on the cylinder, 2 degrees is about the maximum resolution possible. At

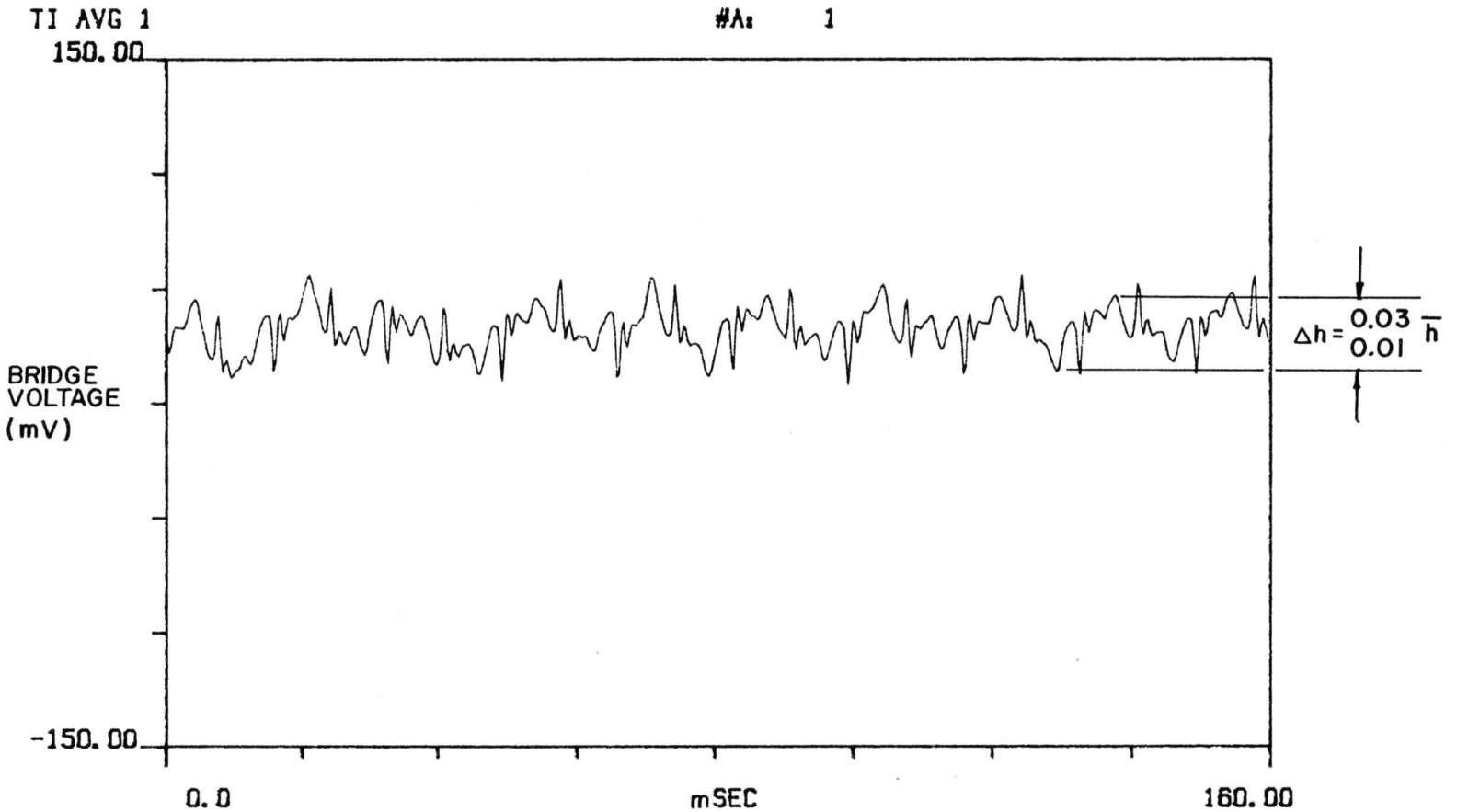

Figure 42. Cylinder results at 2°, with splitter plate.

10 degrees from stagnation (Figure 41) the fluctuating amplitude has dropped to about 2 percent. Such a sharp drop in amplitude was not recorded in the skin friction measurements of Meier et al. [36]. No comparable heat transfer measurements were found in the literature.

APPENDIX C. RESISTANCE-TEMPERATURE CALIBRATION

Previous researchers using the heated thin-film gages set the operating temperature of the film through resistance-temperature calibration curves[13,14]. This was required since there was no method available for directly measuring the film temperature during operation due to either the small size of the film or the hardness of the substrate prohibiting temperature instrumentation from being installed. In this research, however, the size of the film and the machinability of the substrate allowed a small diameter thermocouple to be installed immediately under the gold film as a secondary measurement of the film temperature. When resistance-temperature curves were used to set the operating temperature of the gage, two problems were encountered: 1) shifts in the curve due to contact resistances when the gage was calibrated remotely and 2) shifts in the resistance-temperature curve during operation. Since a 0.02 ohm shift in the gage resistance corresponds to a 1°C change in the film temperature, these problems were addressed.

At first, the resistance-temperature curves were generated remotely in a constant-temperature bath. Although this gives very accurate results, when the gage is reconnected with the constant-temperature anemometer the electrical contact resistances shift the resistance-temperature curve an unknown amount. The action taken to resolve this problem was to develop an in situ temperature calibration method. The ohm-meter internal to the IFA-100 was used for all resistance measurements, so that the resistance values would be the same in cali-

bration as in operation. The impinging flow calibration stand will be used as an example of the technique used although it was also done for the cylinder. The front surface of the calibration plate was insulated with several layers of insulation and a guard heater was installed to further reduce heat loss (Figure 43). Cloth was used to keep stray fiberglass fibers from the gage and balsa wood strips were used to keep the gold film from being damaged. In operation, the center plate was heated to a given temperature and the power to the guard heater was adjusted until the thermocouple next to it reached the plate temperature. This process ensured that the air space above the gage was at the wall tmeperature, thereby reducing any error introduced by the film temperature being lowered by cooler air in the gap. Then the gage temperature and the two closest thermocouple temperatures (T-13 and T-18) were recorded along with the resistance from the IFA-100. The temperatures in the center region were found to be uniform to less than $\pm$ 0.1°C. A sample resistance-temperature curve generated from this method is shown in Figure 44. As the figure shows, the curve is very linear over the range calibrated.

However, shifts in the resistance-temperature curve were seen between the beginning and end of calibration tests (Figure 45). The nominal resistance of the gage consistently decreased during each test, which agreed with the fact that the gage thermocouple temperature increased over time even when the plate temperature and operating resistance were kept constant. This resistance shift occurred even after the gage had been operated for many hours. Although nothing could be done about the resistance drift, it was found that the gage thermocouple temperature

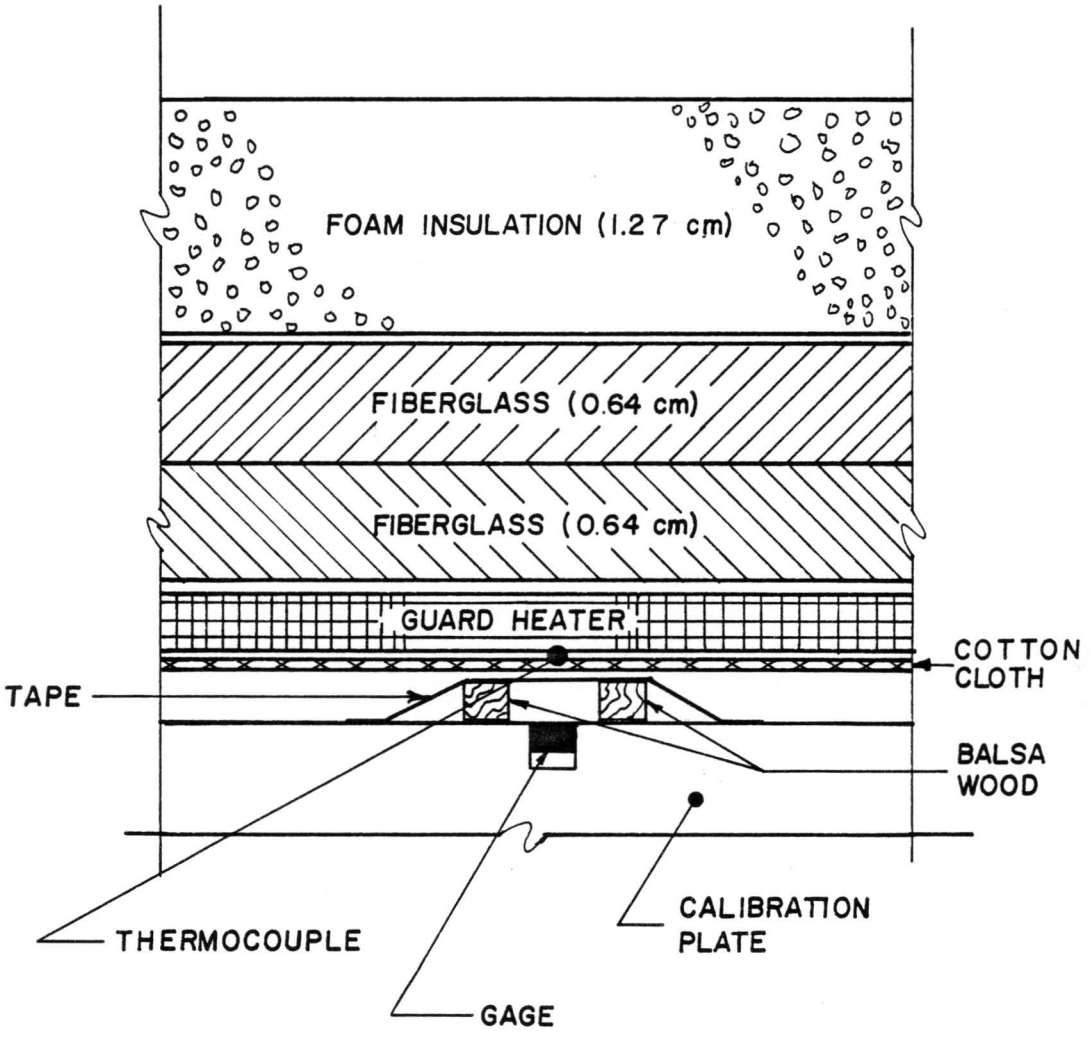

Figure 43. Insulation lay-up for resistance-temperature calibration.

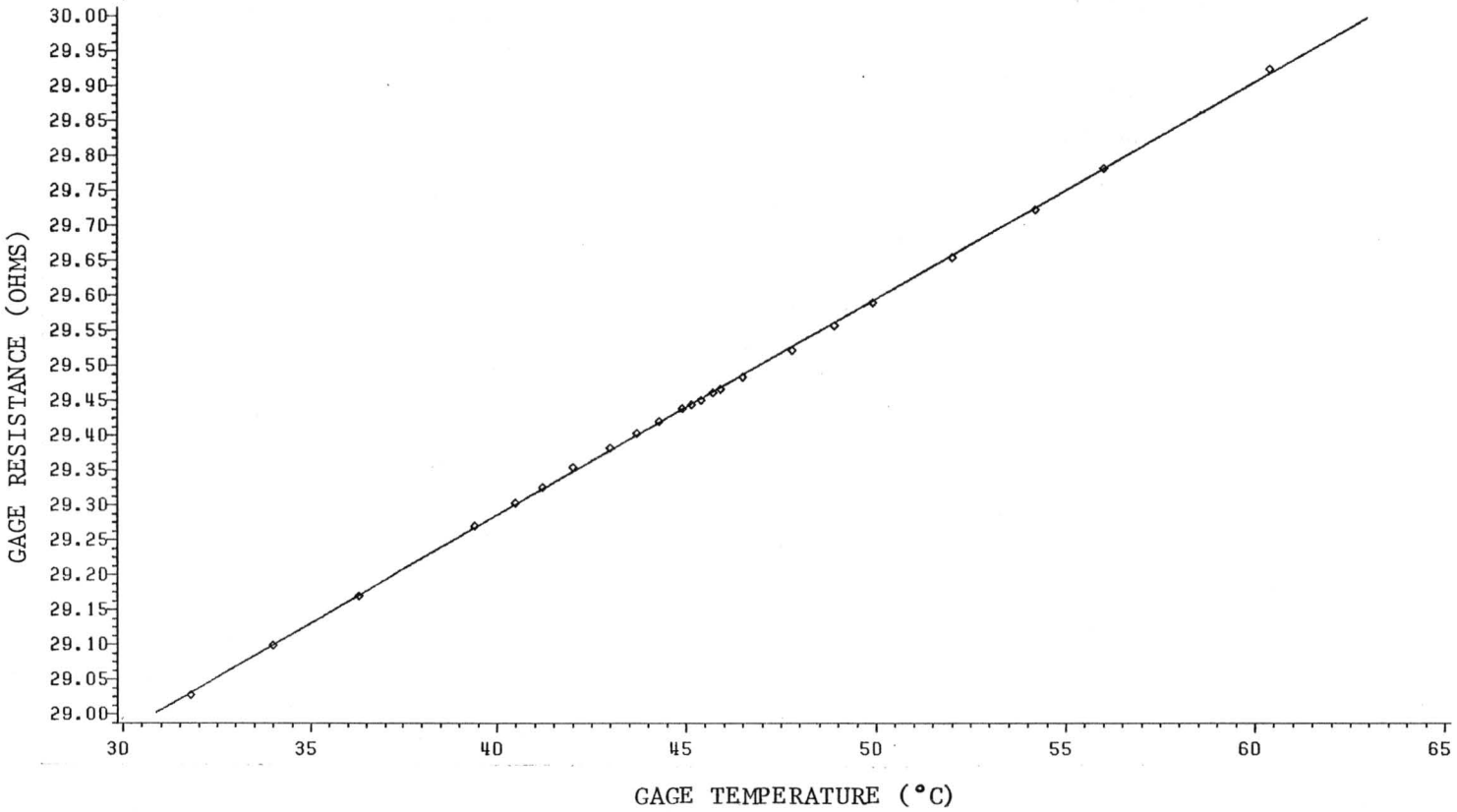

Figure 44. Resistance-temperature curve generated with in situ calibration process.

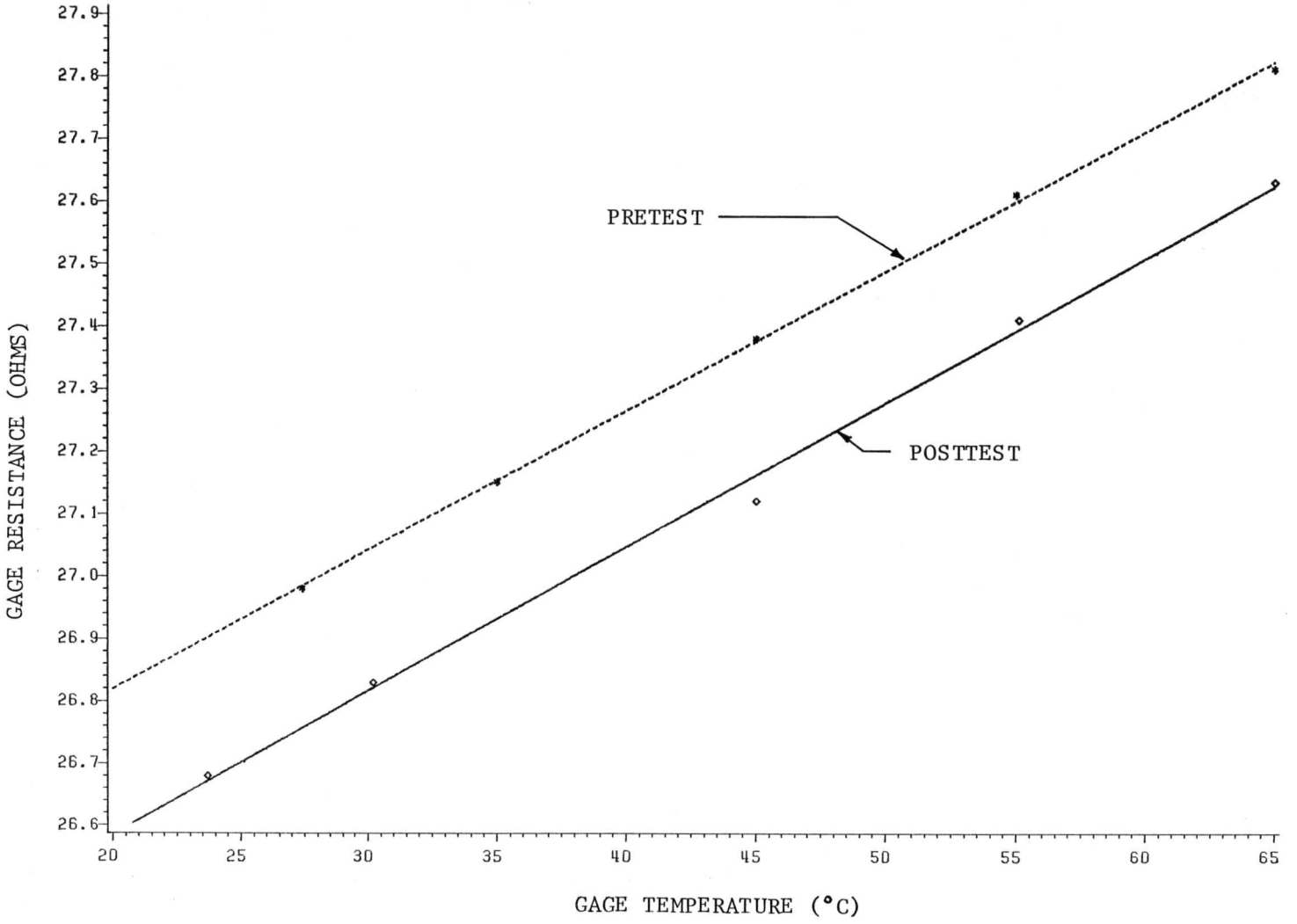

Figure 45. Variation of gage resistance over a test.

agreed to within $\pm$ 0.1°C when the gage was first operated after a calibration (with the boundary at the gage temperature). Therefore, the gage thermocouple was used as a direct measurement of the film temperature when the surrounding boundary temperature was matched to it. For cases when the boundary was at a lower temperature than the gage film temperature, the gage thermocouple registered a lower temperature. This is due to the temperature gradient in the substrate affecting the gage thermocouple temperature, since the thermocople junction is a finite distance below the film.

APPENDIX D. CALCULATION OF CONDUCTION LOSSES

This appendix describes the method used to determine the conduction losses from the gold film into the gage substrate due to a temperature mismatch between the film temperature and the surrounding boundary temperature. These losses needed to be quantified in order to determine the effect on the overall gage calibration uncertainty. The losses were determined using a finite difference solution to the 2-D heat conduction equation.

The formulation of the problem consists of breaking a given solid into a node mesh and performing an energy balance at each node point. A linear system of equations results, in which each node temperature is given in terms of the adjacent node temperature and any adjacent boundary conditions. To simplify the equations, the horizontal and vertical distances between the nodes were chosen to be equal. The system was solved for the nodal temperature using the Gauss-Sidel matrix reduction technique. A computer code (TWOD) was developed to simplify changing the size and geometry of the solid. The equations for a variety of node boundary conditions were loaded into the program. The program primarily consists of generating the coefficients associated with each nodal point. Each boundary condition is set by specifying the orientation, heating condition and the node range over which the boundary condition acts. The details of the program initialization are given at the end of this appendix along with the program listing. Further details on the development of this solution technique are given in Holman [42].

D.1 DETERMINATION OF CONDUCTION LOSSES

The conduction losses for the gage were determined for several temperature differences. The model used to approximate the gage is shown in Figure 46. The boundary conditions assumed were: 1) constant film temperature, 2) constant boundary temperature and 3) insulated back surface. The insulated back condition was assumed since there was an air gap between the back of the gage and the aluminum boundary. The constant temperature boundary conditions are imposed on the local surface nodes, which will give higher heat transfer results than for the actual gage. The heat transfer will actually be lower for the gage because of the thermal contact resistance between the gage and the slot walls.

The heat loss, Q_{cond}, was determined by summing the heat flow between each node along the constant temperature boundary between the gage and the boundary. The total heat lost was calculated by multiplying the unit heat loss by twice the gage length (1.27 cm (0.5 in.)), since heat is lost from both sides. The equation used was

$$Q_{cond} = k\, L \sum_{i=1}^{n} \Delta y_i \frac{\Delta T}{\Delta x} \tag{20}$$

Where Δx is the distance between node points. This value was recorded along with the equivalent heat transfer coefficient shift due to Q_{cond} for a 41°C difference in the wall and freestream temperature.

The results for the cases run are shown in Table 3. Since there were two slightly different gage widths used in the impinging flow calibration plate (0.08 in.) and the cylinder (0.075 in.), both were analyzed. How-

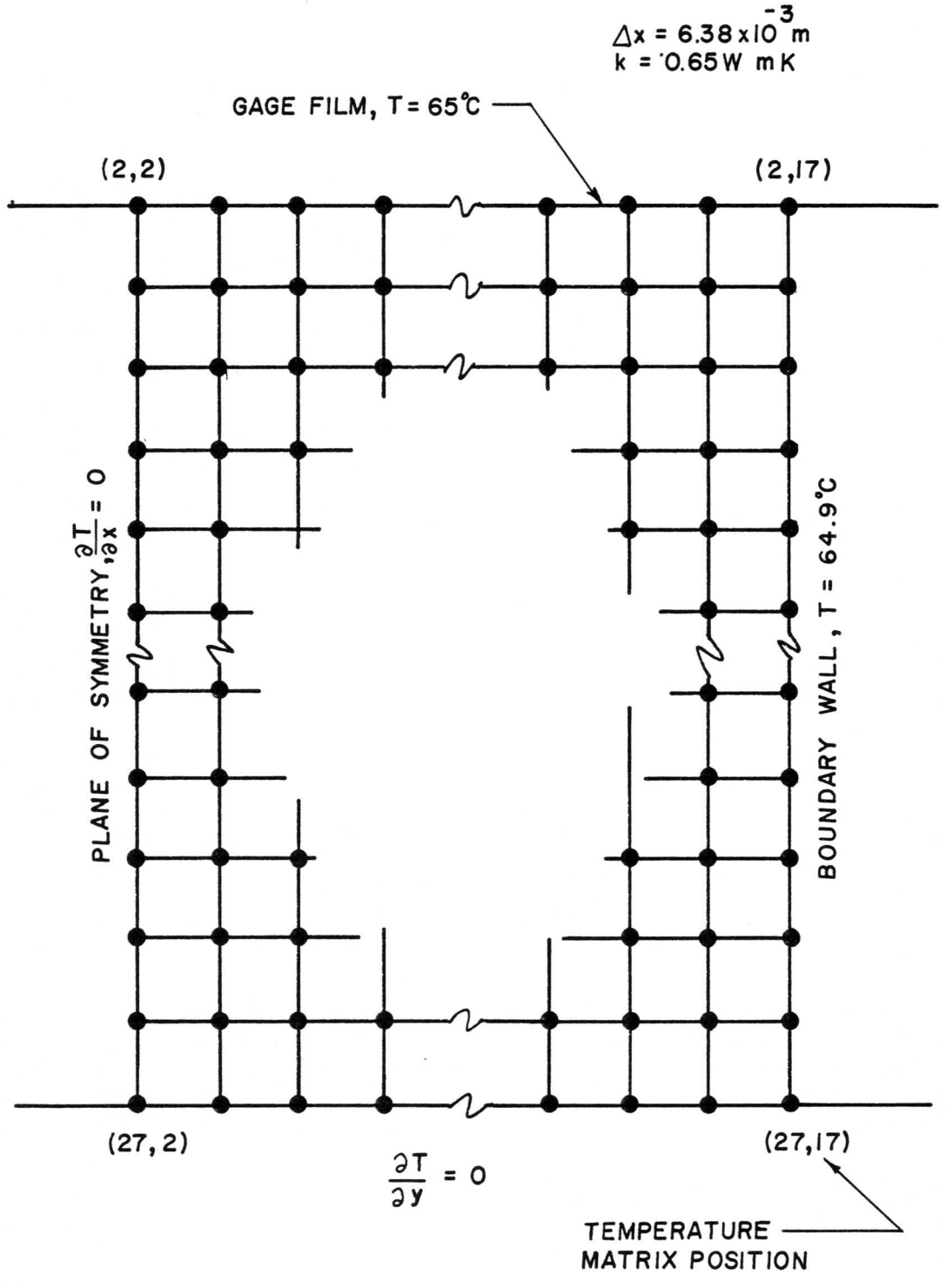

Figure 46. The finite difference grid used to calculate the losses from the 0.075 in. gage.

Table 3. Conduction loss summary

MISMATCH (°C)	0.075 in. WIDE GAGE			0.080 in. WIDE GAGE		
	$\sum \Delta T_i$ (°C)*	Q_{loss} (W)	Δh ** ($W/m^2 \cdot °C$)	$\sum \Delta T_i$ (°C)*	Q_{loss} (W)	Δh ** ($W/m^2 \cdot °C$)
0.1	.260	4.29×10^{-3}	4.3	.259	4.28×10^{-3}	4.0
0.2	.517	8.54×10^{-3}	8.6	.517	8.54×10^{-3}	8.1
0.5	1.290	2.13×10^{-2}	21.5	1.289	2.13×10^{-2}	20.1
2.0	5.153	8.51×10^{-2}	85.8	5.147	8.50×10^{-2}	80.4

* Area averaged sum (i.e. $\sum_{i=1}^{n} \Delta x_i \Delta T_i / \sum_{i=1}^{n} \Delta x_i$)

** Based on $T_{film} - T_\infty = 41\,°C$

ever, there was no significant variation in heat transfer between the gage dimensions analyzed. The loss associated with a 0.1°C mismatch was 4.29×10^{-3} W, corresponding to a 4 W/m^2-C shift in heat transfer coefficient. This value for Q_{cond} is used in the uncertainty calculations.

D.2 PROGRAM LOADING.

The step-by-step procedure for loading the TWOD code is given in the following paragraphs. The program can either be run interactively, with prompting from the screen, or the initialization data can be loaded into a file for more efficient operation. The program listing given in the following section is written for the latter case, with the prompting commented out.

The program has convection, prescribed heat flux and insulated boundary conditions built into it. For each boundary condition applied, the program requires that the orientation of the boundary be specified. The boundary orientation numbers are shown in Figure 47 along with the matrix coordinate axes. Also, for nodes with more than one boundary condition (ie. corners) the notation is slightly different. These orientation numbers are shown in Figure 47.

INPUT FORMAT

1. Error tolerance, the maximum allowable temperature difference between successive iterations for all nodes in the matrix. This is the convergence criteria.

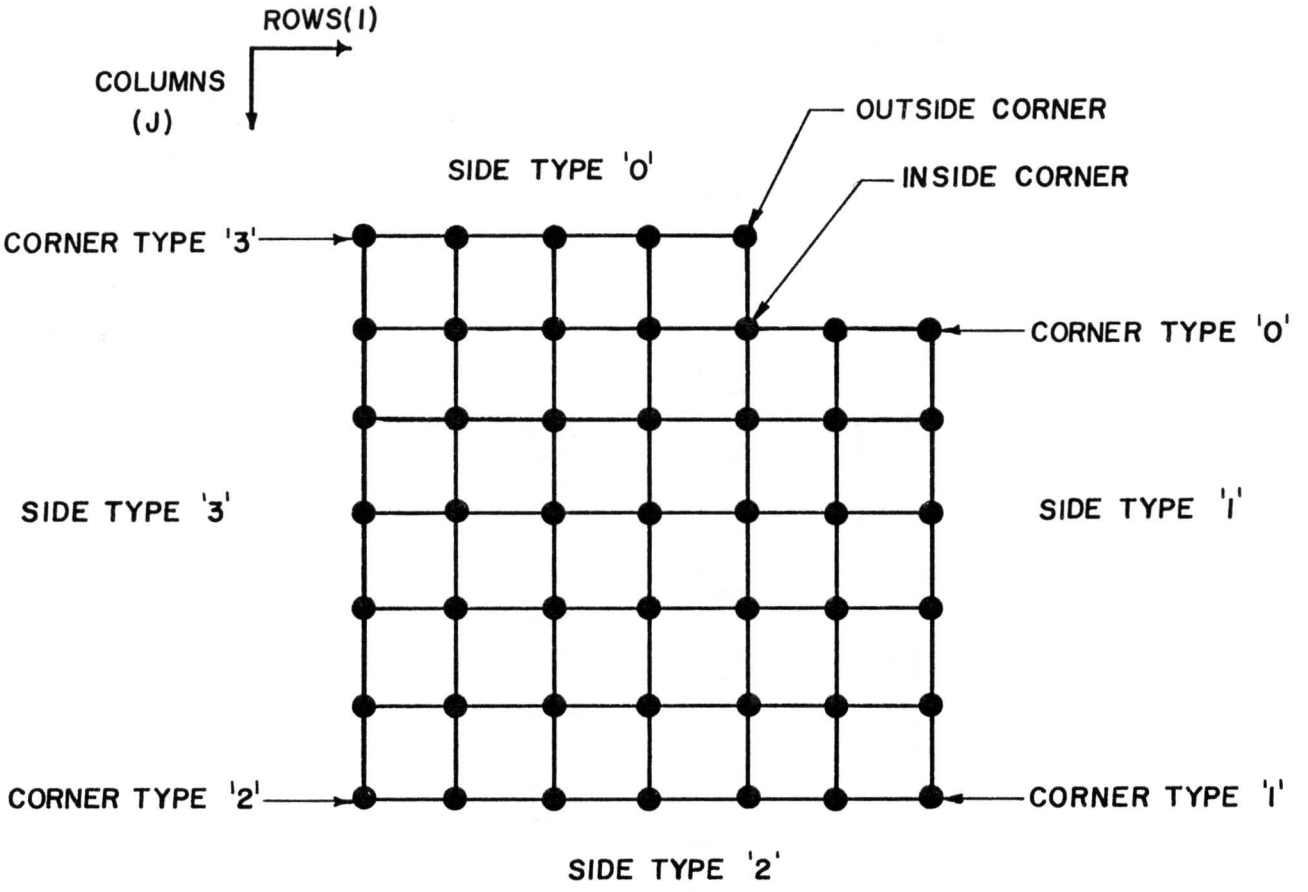

Figure 47. Detail of TWOD nomenclature, showing orientation numbers for side and corner pieces.

2. Number of rows, columns and distance between node points. This program was written for equal horizontal and vertical node spacing.

3. Conductivity of the solid and the maximum allowable number of iterations the program should be allowed to run.

4. Top face and bottom face temperatures. This is used to initialize the temperature matrix with a gradient. A good guess at this point can reduce the number of iterations.

5. Are there any constant temperature boundaries (1=yes, 0=no).
   - o if yes, how many
   - o input the temperature and the starting and ending columns and the starting and ending rows.

6. Are there any boundaries to be cut (yes/no).
   - o if yes, enter column and row bounds to be omitted as for item 5.

7. Are there any convective boundaries (yes/no).
   - o if yes, enter number of convective boundaries.
     - for each one, enter the column and row bounds (as in 5)
     - enter the boundary orientation, heat transfer coefficient and the freestream temperature.

8. Are there any prescribed heat flux boundary conditions (yes/no, only one is allowed).
   - o if yes, for each one enter the value of the heat flux (+ into the solid and - if out of it).
   - o enter the orientation, and the column and row bounds.

9. Are there any insulated boundaries (yes/no).
   - o if yes, enter how many.
     - for each one, enter the orientation and the column and row bounds.

10. Are there any heat flux-insulated corner pieces (yes/no).
    - o if yes, how many.
      - for each, enter the column and row point and the orientation.

11. Are there any convection-insulated corner pieces (yes/no).
    - o if yes, enter how many.
      - for each, enter the column and row point and the orientation.
      - also enter the heat transfer coefficient and the freestream temperature.

12. Are there any insulated inside corners, see Fig. 47 (yes/no). (only one type considered)
    - o if yes, enter how many.
      - for each corner enter the column and row point.

13. Are there any outside corners (yes/no).

    o if yes, enter how many.

        - for each corner enter the column and row point and the orientation.

The listing of the TWOD computer code is given on the following pages.

```
C  THIS PROGRAM CALCULATES THE TEMPERATURE IN A 2-D SOLID WITH
C  CONVECTIVE BOUNDARY AND A DEFINED WALL HEAT FLUX AND AN INSULATED
C  BOUNDARY.  THE SOLUTION IS OBTAINED BY PERFORMING AN ENERGY BALANCE
C  ON EACH GRID POINT IN THE SOLID.  THE RESULT IS A SYSTEM OF LINEAR
C  ALGEBRAIC EQUATIONS.  THIS SYSTEM IS SOLVED BY USING A GAUSS-SIDEL
C  ITERATION SCHEME.
C
C                          O  T(I,J-1)
C                          |
C            T(I-1,J)  O---O---O  T(I+1,J)
C                          |
C                          O  T(I,J+1)
C
C  PROGRAM VARIABLES
C      INPUT:  IGO(I) = CONDITION CHECKS (1=YES,0=NO)
C              ER = MAXIMUN TEMP CHANGE BETWEEN ITERATIONS
      DIMENSION A(51,27),B(51,27),C(51,27),D(51,27),AHTG(51,27),T(51,27)
      REAL H,K
C
C PROGRAM INITIALIZATION SECTION
C
      JSTART = 2
C     WRITE(6,210)
C 210 FORMAT(2X,'INPUT ERROR TOLERANCE ON TEMPERATURE ITERATIONS')
      READ(5,*) ER
C
C INPUT DATA SECTION
C
C     WRITE(6,160)
C160  FORMAT(2X,'WELCOME TO THE WORLD OF 2-D CONDUCTION',/)
C     WRITE(6,161)
C161  FORMAT(2X,'PLEASE ENTER THE NUMBER OF ROWS,COLUMNS AND DELTA')
      READ(5,*) NR,NC,DX
C     WRITE(6,162)
C162  FORMAT(//,2X,'ENTER CONDUCTIVITY AND MAX NUMBER OF LOOPS')
      READ(5,*) K,NLOOP
C
C INITIALIZE A,B,C,D AND AHTG MATRICIES
C
      NI = NC+1
      NJ = NR+1
      DO 10 I = 2,NI
      DO 11 J = 2,NJ
      A(I,J) = 0.2500
      B(I,J) = 0.2500
      C(I,J) = 0.2500
      D(I,J) = 0.2500
      AHTG(I,J) = 0.0
   11 CONTINUE
   10 CONTINUE
C
C INITIALIZE T MATRIX WITH GRADIENT
C
C     WRITE(6,163)
C163  FORMAT(2X,'ENTER ASSUMED TOP AND BOTTOM FACE TEMPS,C',/)
      READ(5,*) TTOP,TBOT
      NI = NC+2
      NJ = NR+2
      DO 1 I = 1,NI
      DO 2 J = 1,NJ
      T(I,J) = 0.0
    2 CONTINUE
    1 CONTINUE
      DTSET = (TTOP - TBOT)/(NR-1)
      NI = NC+1
```

```
      NJ = NR+1
      DO 5 J = 2,NJ
      DO 6 I = 2,NI
      T(I,J) = TTOP
    6 CONTINUE
      TTOP = TTOP - DTSET
    5 CONTINUE
C
C CONSTANT TEMPERATURE BOUNDARIES
C
C     WRITE(6,164)
C164  FORMAT(2X,'DO YOU HAVE ANY CONSTANT TEMP SURFACES: 1=YES: 0=NO',/)
      READ(5,*) IGO7
      IF(IGO7.EQ.0) GOTO 150
C     WRITE(6,165)
C165  FORMAT(2X,'HOW MANY ISOTHERMACES')
      READ(5,*) NCT
      DO 151 KCT = 1,NCT
C     WRITE(6,166) KCT
C166  FORMAT(2X,'SURFACE ',I2,' ENTER TEMPERATURE: COLUMN START AND FINI
C    1SH AND ROW START AND FINISH',/)
      READ(5,*) CT,NCTS,NCTF,NRTS,NRTF
      DO 152 I = NCTS,NCTF
      DO 153 J = NRTS,NRTF
      T(I,J) = CT
  153 CONTINUE
  152 CONTINUE
  151 CONTINUE
  150 CONTINUE
C
C CUT ANY BOUNDARIES THAT NEED TO BE CUT
C
C     WRITE(6,199)
C199  FORMAT(2X,'DO YOU WANT TO CUT ANY BOUNDARIES',/)
      READ(5,*) IGO1
      IF(IGO1.EQ.0) GOTO 22
C     WRITE(6,198)
C198  FORMAT(/,2X,'INPUT COLUMN AND ROW BOUNDS TO BE OMITTED')
      READ(5,*) NCBS,NCBF,NRBS,NRBF
      DO 20 I = NCBS,NCBF
      DO 21 J = NRBS,NRBF
      A(I,J) = 0.0
      B(I,J) = 0.0
      C(I,J) = 0.0
      D(I,J) = 0.0
      AHTG(I,J) = 0.0
   21 CONTINUE
   20 CONTINUE
   22 CONTINUE
C
C DETERMINE THE COEFFICIENTS OF THE A,B,C,D AND AHTG MATRICIES
C
C  FIRST THE CONVECTIVE HEATING BOUNDARIES
C
C     WRITE(6,167)
C167  FORMAT(2X,'DO YOU HAVE ANY CONVECTIVE BOUNDARIES')
      READ(5,*) IGO2
      IF(IGO2.EQ.0) GOTO 33
C     WRITE(6,168)
C168  FORMAT(2X,'HOW MANY',/)
      READ(5,*) NCB
      DO 34 KCB = 1,NCB
C     WRITE(6,169) KCB
C169  FORMAT(/,2X,'BOUNDARY ',I3,': INPUT COLUMN AND ROW BOUNDS')
      READ(5,*) NCCHS,NCCHF,NRCHS,NRCHF
C     WRITE(6,170)
C170  FORMAT(2X,'INPUT ORIENTATION,H AND AMBIENT TEMP',/)
```

```
      READ(5,*) ORC,H,TINF
      DO 30 I = NCCHS,NCCHF
      DO 31 J = NRCHS,NRCHF
C DENOTE TOP FACE BY A 0,RIGHT 1,BOTTOM 2,LEFT 3
      C1 = 1./(H*DX/K+2.)
      IF(ORC.EQ.2) GOTO 32
      A(I,J) = 0.0
      B(I,J) = C1/2.
      C(I,J) = C1
      D(I,J) = B(I,J)
      AHTG(I,J) = C1*H*DX*TINF/K
      GOTO 31
   32 A(I,J) = C1
      B(I,J) = C1/2.
      C(I,J) = 0.0
      D(I,J) = B(I,J)
      AHTG(I,J) = C1*H*DX*TINF/K
   31 CONTINUE
   30 CONTINUE
   34 CONTINUE
   33 CONTINUE
C
C NOW DO PRESCRIBED HEAT FLUX BOUNDARIES
C
C     WRITE(6,171)
C171  FORMAT(/,2X,'DO YOU HAVE ANY HEAT FLUX BOUNDARIES ?')
      READ(5,*) IGO3
      IF(IGO3.EQ.0) GOTO 43
C     WRITE(6,197)
C197  FORMAT(/,2X,'WHAT IS THE VALUE OF Q IN W/M**2')
      READ(5,*) Q
C     WRITE(6,172)
C172  FORMAT(/,2X,'PLEASE INPUT ORIENTATION AND COLUMN AND ROW BOUNDS')
      READ(5,*) ORHF,NCHFS,NCHFF,NRHFS,NRHFF
      DO 40 I = NCHFS,NCHFF
      DO 41 J = NRHFS,NRHFF
      IF(ORHF.EQ.0) GOTO 42
      A(I,J) = 0.50
      B(I,J) = 0.25
      C(I,J) = 0.0
      D(I,J) = 0.25
      AHTG(I,J) = Q*DX/(K*2.)
      GOTO 41
   42 A(I,J) = 0.0
      B(I,J) = 0.25
      C(I,J) = 0.50
      D(I,J) = 0.25
      AHTG(I,J) = Q*DX/(K*2.)
   41 CONTINUE
   40 CONTINUE
   43 CONTINUE
C
C NOW THE INSULATED BOUNDARIES
C
C     WRITE(6,173)
C173  FORMAT(/,2X,'DO YOU HAVE ANY INSULATED BOUNDARIES ?')
      READ(5,*) IGO
      IF(IGO.EQ.0) GOTO 56
C     WRITE(6,174)
C174  FORMAT(/,2X,'HOW MANY ?')
      READ(5,*) NINS
      DO 50 KI =1,NINS
C     WRITE(6,175) KI
C175  FORMAT(/,2X,'BOUNDARY ',I3,' INPUT ORIENTATION AND COLUMN AND ROW
C    1BOUNDS')
      READ(5,*) ORI,NCIS,NCIF,NRIS,NRIF
      DO 51 I = NCIS,NCIF
```

```
      DO 52 J = NRIS,NRIF
      AHTG(I,J) = 0.0
      IF(ORI.EQ.0) GOTO 53
      IF(ORI.EQ.1) GOTO 54
      IF(ORI.EQ.2) GOTO 55
      A(I,J) = 0.25
      B(I,J) = 0.50
      C(I,J) = 0.25
      D(I,J) = 0.0
      GOTO 52
 53   A(I,J) = 0.0
      B(I,J) = 0.25
      C(I,J) = 0.50
      D(I,J) = 0.25
      GOTO 52
 54   A(I,J) = 0.25
      B(I,J) = 0.0
      C(I,J) = 0.25
      D(I,J) = 0.50
      GOTO 52
 55   A(I,J) = 0.50
      B(I,J) = 0.25
      C(I,J) = 0.0
      D(I,J) = 0.25
 52   CONTINUE
 51   CONTINUE
 50   CONTINUE
 56   CONTINUE
C NOW THE ODDS AND ENDS... THE CORNER PIECES
C FIRST, HEAT FLUX AND INSULATED
C
C     WRITE(6,176)
C176  FORMAT(/,2X,'ARE THERE ANY CORNER PIECES-HEAT FLUX AND INSULATED')
      READ(5,*) IGO4
      IF(IGO4.EQ.0) GOTO 80
C     WRITE(6,177)
C177  FORMAT(/,2X,'HOW MANY ?')
      READ(5,*) NICHF
      DO 81 KIC = 1,NICHF
C     WRITE(6,178) KIC
C178  FORMAT(/,2X,'POINT ',I3,' :ORIENTATION, COLUMN AND ROW')
      READ(5,*) ORICHF,IHF,JHF
      IF(ORICHF.EQ.1) GOTO 82
      A(IHF,JHF) = 0.50
      B(IHF,JHF) = 0.50
      C(IHF,JHF) = 0.0
      D(IHF,JHF) = 0.00
      AHTG(IHF,JHF) = Q*DX/(2.*K)
      GOTO 81
 82   A(IHF,JHF) = 0.50
      B(IHF,JHF) = 0.00
      C(IHF,JHF) = 0.0
      D(IHF,JHF) = 0.50
      AHTG(IHF,JHF) = Q*DX/(2.*K)
 81   CONTINUE
 80   CONTINUE
C
C NOW, CONVECTION AND INSULATED
C
C     WRITE(6,179)
C179  FORMAT(/,2X,'ARE THERE ANY CONVECTION-INSULATED PIECES')
      READ(5,*) IGO5
      IF(IGO5.EQ.0) GOTO 90
C     WRITE(6,180)
C180  FORMAT(/,2X,'HOW MANY ?')
      READ(5,*) NICC
      DO 91 KIC = 1,NICC
```

```
C     WRITE(6,181) KIC
C181  FORMAT(/,2X,'PIECE ',I3,' : ORIENTATION, COLUMN AND ROW')
      READ(5,*) ORICC,ICON,JCON
C     WRITE(6,196)
C196  FORMAT(2X,'INPUT H AND T AMBIENT')
      READ(5,*) H,TINF
      C2 = 1./((H*DX/K)+2.)
      IF(ORICC.EQ.2) GOTO 93
      IF(ORICC.EQ.1) GOTO 92
      IF(ORICC.EQ.0) GOTO 94
      A(ICON,JCON) = 0.0
      B(ICON,JCON) = C2
      C(ICON,JCON) = B(ICON,JCON)
      D(ICON,JCON) = 0.0
      AHTG(ICON,JCON) = C2*TINF*H*DX/K
      GOTO 91
   94 A(ICON,JCON) = 0.0
      B(ICON,JCON) = 0.0
      C(ICON,JCON) = C2
      D(ICON,JCON) = C(ICON,JCON)
      AHTG(ICON,JCON) = C2*TINF*H*DX/K
      GOTO 91
   92 A(ICON,JCON) = C2
      B(ICON,JCON) = 0.0
      C(ICON,JCON) = 0.0
      D(ICON,JCON) = A(ICON,JCON)
      AHTG(ICON,JCON) = C2*TINF*H*DX/K
      GOTO 91
   93 A(ICON,JCON) = C2
      B(ICON,JCON) = A(ICON,JCON)
      C(ICON,JCON) = 0.0
      D(ICON,JCON) = 0.0
      AHTG(ICON,JCON) = C2*TINF*H*DX/K
   91 CONTINUE
   90 CONTINUE
C
C NOW, THE INSULATED CORNERS
C INSIDE
C
C     WRITE(6,182)
C182  FORMAT(/,2X,'ARE THERE ANY FULLY INSULATED INSIDE CORNERS')
      READ(5,*) IGO6
      IF(IGO6.EQ.0) GOTO 189
C     WRITE(6,183)
C183  FORMAT(/,2X,'FOR THE INSIDE CORNER,INPUT COLUMN AND ROW POINT')
      READ(5,*) IICI,JICI
      A(IICI,JICI) = 1./6.
      B(IICI,JICI) = 1./6.
      C(IICI,JICI) = 1./3.
      D(IICI,JICI) = 1./3.
      AHTG(IICI,JICI) = 0.0
C
C OUTSIDE
C
  189 CONTINUE
C     WRITE(6,184)
C 184 FORMAT(2X,'ARE THERE ANY FULLY INSULATED OUTSIDE CORNERS ?')
      READ(5,*) IGO7
      IF(IGO7.EQ.0) GOTO 99
C     WRITE(6,185)
C 185 FORMAT(2X,'HOW MANY ?')
      READ(5,*) NIOS
      DO 98 I = 1,NIOS
C     WRITE(6,186) I
```

```
C 186 FORMAT(2X,'PIECE ',I2,': INPUT ORIENTATION, COLUMN AND ROW')
      READ(5,*) ORICO,IICO,JICO
      AHTG(IICO,JICO) = 0.0
      IF(ORICO.EQ.3) GOTO 95
      IF(ORICO.EQ.2) GOTO 96
      IF(ORICO.EQ.1) GOTO 97
      A(IICO,JICO) = 0.0
      B(IICO,JICO) = 0.0
      C(IICO,JICO) = 0.5
      D(IICO,JICO) = 0.5
      GOTO 98
   95 A(IICO,JICO) = 0.0
      B(IICO,JICO) = 0.5
      C(IICO,JICO) = 0.5
      D(IICO,JICO) = 0.0
      GOTO 98
   96 A(IICO,JICO) = 0.5
      B(IICO,JICO) = 0.5
      C(IICO,JICO) = 0.0
      D(IICO,JICO) = 0.0
      GOTO 98
   97 A(IICO,JICO) = 0.5
      B(IICO,JICO) = 0.0
      C(IICO,JICO) = 0.0
      D(IICO,JICO) = 0.5
   98 CONTINUE
   99 CONTINUE
C
C THIS IS THE GAUSS-SIEDEL ITERATION SECTION
C
C     GOTO 900
C 903 CONTINUE
      DO 60 KL = 1,NLOOP
      DTMAX = 0.0
      JSTART = 2
      NI = NC + 1
      NJ = NR + 1
C     DO 61 I = 2,NI
      DO 61 I = 2,16
      IF(IGO1.EQ.0) GOTO 63
      IF(I.GT.NCBS) JSTART = NRBF
   63 CONTINUE
C     DO 62 J = JSTART,NJ
      DO 62 J = 3,26
      TOLD = T(I,J)
      T(I,J) = AHTG(I,J) + A(I,J)*T(I,J-1) + B(I,J)*T(I+1,J) + C(I,J)*T(
     1I,J+1) + D(I,J)*T(I-1,J)
C     WRITE(7,906) I,J
C 906 FORMAT(2X,2(I2,2X),/)
      DT = ABS(TOLD - T(I,J))
      IF(DT.GE.DTMAX) DTMAX = DT
   62 CONTINUE
   61 CONTINUE
      IF(DTMAX.LE.ER) GOTO 64
   60 CONTINUE
   64 CONTINUE
C
C THIS IS THE OUTPUT SECTION
C
      WRITE(6,507) KL
  507 FORMAT(2X,'*** PROGRAM ENDED IN LOOP ',I4,' ***',//)
      WRITE(6,908) K,H,TINF,Q,DX,ER
  908 FORMAT(2X,'K = ',F5.1,3X,'H = ',F6.2,3X,'TINF = ',F6.1,3X,'Q = ',F
     16.1,3X,'DX = ',F6.4,3X,'LOOP ERROR = ',F6.5,//)
      NI = NC + 1
      NJ = NR + 1
```

```
      DO 500 IL = 1,5
      ISTART = (IL-1)*10 + 2
      IEND = ISTART + 9
      WRITE(6,200) (I,I = ISTART,IEND)
      DO 120 KOUT = 1,NR
      JO = KOUT + 1
  120 WRITE(6,300) JO,(T(I,KOUT+1),I=ISTART,IEND)
  100 FORMAT(2X,'LOOP NUMBER ',I3,5X,'MAXIMUM TEMPERATURE DIFFERENCE ',F
     110.5)
  200 FORMAT('1',1X,'I = ',10(10X,I2))
  300 FORMAT(2X,'J = ',I2,10(3X,F9.3),/)
  500 CONTINUE
      GOTO 904
C
C  THIS IS THE DIAGNOSTIC OUTPUT DATA SECTION.  THE PARAMETER MATRICIES
C  ARE OUTPUT ALONG WITH THE INITIAL TEMPERATURE DISTRIBUTION.
C  ------------------------------------------------------------
C  ***  THE PROGRAM IS SET SUCH THAT IT IS NOT IN EFFECT ***
C  ------------------------------------------------------------
C
  900 CONTINUE
      WRITE(6,901)
      DO 910 J = 2,7
      WRITE(6,902) (A(I,J),I=2,11)
  910 CONTINUE
      WRITE(6,901)
      DO 920 J=2,7
      WRITE(6,902) (B(I,J),I=2,11)
  920 CONTINUE
      WRITE(6,901)
      DO 930 J=2,7
      WRITE(6,902) (C(I,J),I=2,11)
  930 CONTINUE
      WRITE(6,901)
      DO 940 J=2,7
      WRITE(6,902) (D(I,J),I=2,11)
  940 CONTINUE
      WRITE(6,901)
      DO 950 J=2,7
      WRITE(6,902) (AHTG(I,J),I=2,11)
  950 CONTINUE
      WRITE(6,901)
      DO 960 J=2,7
      WRITE(6,902) (T(I,J),I=2,11)
  960 CONTINUE
      WRITE(6,901)
  901 FORMAT('1')
  902 FORMAT(2X,12(2X,F8.4))
C     GOTO 903
  904 CONTINUE
      STOP
      END
```

E.0 EXTERNAL ERROR ANALYSIS

This appendix shows the derivation of the equations for calculating the external error of the heat transfer coefficient determined from the gage output and the cylinder stagnation point correlation. Although each system had many potential sources of error, several terms have been ignored because they are small relative to the other sources of error. The errors not considered are the physical property variations (viscosity, thermal conductivity, ect.) and the error associated with the accuracy of the digital voltmeter. The Klein and McClintock equation [41] for determining the uncertainty of a measured property, R, where R is composed of the independent variables x_1, x_2, ..., x_n, is given by

$$w_R = \left[\left(\frac{\partial R}{\partial x_1} w_{x_1} \right)^2 + \left(\frac{\partial R}{\partial x_2} w_{x_2} \right)^2 + (\cdots)^2 + \left(\frac{\partial R}{\partial x_n} w_{x_n} \right)^2 \right]^{\frac{1}{2}} \qquad (21)$$

where w_i is the uncertainty associated with each independent variable.

E.1 GAGE OUTPUT UNCERTAINTY

In this error analysis, the effects of conduction losses into the substrate due to temperature mismatch need to be considered. To simplify the equations, the analysis will be broken into determining the uncertainty in the power dissipated in the gage film and then determining the uncertainty in the heat transfer coefficient determined

from the gage output. The unit power dissipated by the gage is given by

$$Q_{film} = \frac{(E_{AC}^2 + E_{DC}^2) (R_{oper} - R_{gal})}{(R_A + R_{oper} + R_{cable})^2} \tag{22}$$

The error in the measurement due to E_{DC}, E_{AC}, R_{oper}, R_{gal} and R_{cable} will be determined. The required partial derivatives are:

$$\frac{\partial Q_{film}}{\partial E_{AC}} = \frac{2 E_{AC} (R_{oper} - R_{gal})}{(R_A + R_{oper} + R_{cable})^2} \tag{23}$$

$$\frac{\partial Q_{film}}{\partial E_{DC}} = \frac{2 E_{DC} (R_{oper} - R_{gal})}{(R_A + R_{oper} + R_{cable})} \tag{24}$$

$$\frac{\partial Q_{film}}{\partial R_{oper}} = \frac{(E_{AC}^2+E_{DC}^2) (R_{oper}+R_A+R_{cable}) -2(R_{oper}-R_{gal})(R_{oper}+R_A+R_{gal})}{(R_{oper} + R_A + R_{cable})^4} \tag{25}$$

$$\frac{\partial Q_{film}}{\partial R_{gal}} = \frac{- (E_{AC}^2 + E_{DC}^2)}{(R_A + R_{oper} + R_{cable})^2} \tag{26}$$

$$\frac{\partial Q_{film}}{\partial R_{cable}} = - \frac{2 (E_{AC}^2 + E_{DC}^2) (R_{oper} - R_{gal})}{(R_{cable} + R_{oper} + R_A)^3} \tag{27}$$

The uncertainties for each of these are as follows:

w_{EDC} = 0.02 v (plate)
0.01 v (cylinder)
; due to the uncertainty in taking a small number of samples to calculate the average. The turbulence intensity was less in the cylinder tests

w_{EAC} = 0.01 v (plate)
0.002 v (cylinder)
; same as above

w_{Roper} = 0.01 ohms ; due to uncertainty in CTA resistance measurement

wRgal = 0.05 ohms ; due to contact resistance uncertainty

w_{Rcable} = 0.01 ohms ; due to uncertainty in CTA resistance measurement

The gage heat transfer coefficient is found from the following equation (neglecting radiation losses since they are small relative to the uncertainty in the conduction losses).

$$h_{ga} = \frac{Q_{film}}{A_{ga} (T_{film} - T_{\infty})} \tag{29}$$

The error associated with all the terms will be considered. The partial derivative for each term is given below:

$$\frac{\partial h_{ga}}{\partial Q_{film}} = \frac{1}{A_{ga} (T_{film} - T_{\infty})} \tag{30}$$

$$\frac{\partial h_{ga}}{\partial A_{ga}} = \frac{- Q_{film}}{A_{ga}^2 (T_{film} - T_{\infty})} \tag{31}$$

$$\frac{\partial h_{ga}}{\partial T_{film}} = \frac{- Q_{film}}{A_{ga} (T_{film} - T_{\infty})^2} \tag{32}$$

$$\frac{\partial h_{ga}}{\partial T_{\infty}} = \frac{Q_{film}}{A_{ga} (T_{film} - T_{\infty})^2} \tag{33}$$

The uncertainties associated with each term are as follows:

w_{Qfilm} = determined above + $4.29 \times 10^{-3} / A_{ga}$; the conduction loss is treated as an uncertainty on the film power

$w_{Aga} = 8.0 \times 10^{-7}\ m^2$; uncertainty in gage dimensions

$w_{Tfilm} = 0.1\ C$; calibration accuracy of thermocouple readout

$w_{Ta} = 0.1\ C$; same as above

The calculations gave an error of about $\pm$ 7 W/m^2-C in the heat transfer coefficient determined from the gage output. Although most of the error terms were found to be insignificant, approximately 50 percent of the error was due to the uncertainty in the gage area. The other 50 percent was due to the conduction loss term. However, the gage area error can be neglected since the effect of this is removed through the calibration process. Therefore, the actual uncertainty, when the gage is calibrated, is approximately $\pm$ 4 W/m^2-C, due to the uncertainty of a 0.1 C temperature mismatch between the gage film and the boundary. See Appendix D for the details of the conduction loss analysis.

E.2 CYLINDER STAGNATION CORRELATION UNCERTAINTY

The equation for the heat transfer coefficient at the front stagnation point on a cylinder is

$$h_{theo} = \beta \, k \sqrt{V / \nu D} \tag{34}$$

where the constant, β, is approximately 0.955. However, a 3 percent variation of β has been assumed because of the test conditions. The correlation was developed from test data taken by Kraabel et al. [29] in a tunnel with 8 percent blockage and the cylinder temperature was operated about 10 C above the freestream air temperature. The blockage in the tunnel used for this research was about 25 percent and the cylinder was operated at about 40 C above the air temperature. The freestream turbulence level reported by Kraabel et al. was at 0.4 percent, which differs a small amount from the 0.2 percent present in the wind tunnel used in this research. It is because of these differences that a 3 percent uncertainty has been assigned to the correlation.

The variation of all the variables in equation (34), except for the fluid properties, will be considered. The uncertainty in the measured velocity is considered first. The velocity (for air) can be determined from

$$V = 4.8462 \sqrt{P_{stag} \, (\, 1.8 \, T_{\infty} + 460 \,) \, / \, P_{atm}} \tag{35}$$

which is purely in terms of the measured parameters. The required partial derivatives for the velocity equation are

$$\frac{\partial V}{\partial P_{stag}} = \frac{4.8462}{2} \sqrt{\frac{1.8 \, T_{\infty} + 460}{P_{atm} \, P_{stag}}} \tag{36}$$

$$\frac{\partial V}{\partial T_\infty} = \frac{1.8}{2}\ 4.8462 \sqrt{\frac{P_{stag}}{P_{atm}\ (\ 1.8\ T_\infty + 460)}} \tag{37}$$

$$\frac{\partial V}{\partial P_{atm}} = -\ \frac{4.8462}{2} \sqrt{\frac{P_{stag}\ (\ 1.8\ T_\infty + 460\ )}{P_{atm}^{\ 3}}} \tag{38}$$

The required partial derivatives for equation (34) are

$$\frac{\partial h_{theo}}{\partial \beta} = k \sqrt{V\ /\ \nu\ D} \tag{39}$$

$$\frac{\partial h_{theo}}{\partial V} = \frac{1}{2}\ \beta\ k \sqrt{\frac{1}{V\ \nu\ D}} \tag{40}$$

$$\frac{\partial h_{theo}}{\partial D} = -\ \frac{1}{2}\ \beta\ k \sqrt{\frac{V}{\nu\ D^3}} \tag{41}$$

The uncertainties for each of the variables are as follows:

$w_b = 0.03$; uncertainty due to different test conditions

w_{Pstag} = 0.01 in. H_2O ; uncertainty in reading inclined manometer

w_{Ta} = 0.1 C ; uncertainty of digital thermocouple readout

w_{Patm} = 0.01 in. Hg ; accuracy to which the mercury barometer could be read

The calculated error in the correlated heat transfer coefficient was approximately $\pm$ 3 W/m^2-C. This value was primarily determined by the uncertainty due to the different test conditions from those of Kraabel et al. [20], as reflected in the uncertainty of β. The flow measurement and other uncertainties contributed less than 1 percent to the overall uncertainty.

F.0 RAW DATA

This appendix contains the raw data collected for the test cases presented in the Results section. This data is reduced by computer as explained in section 3.6.

The impinging flow calibration data is given on the following pages. The format is explained below, using the nomencalture presented in the text.

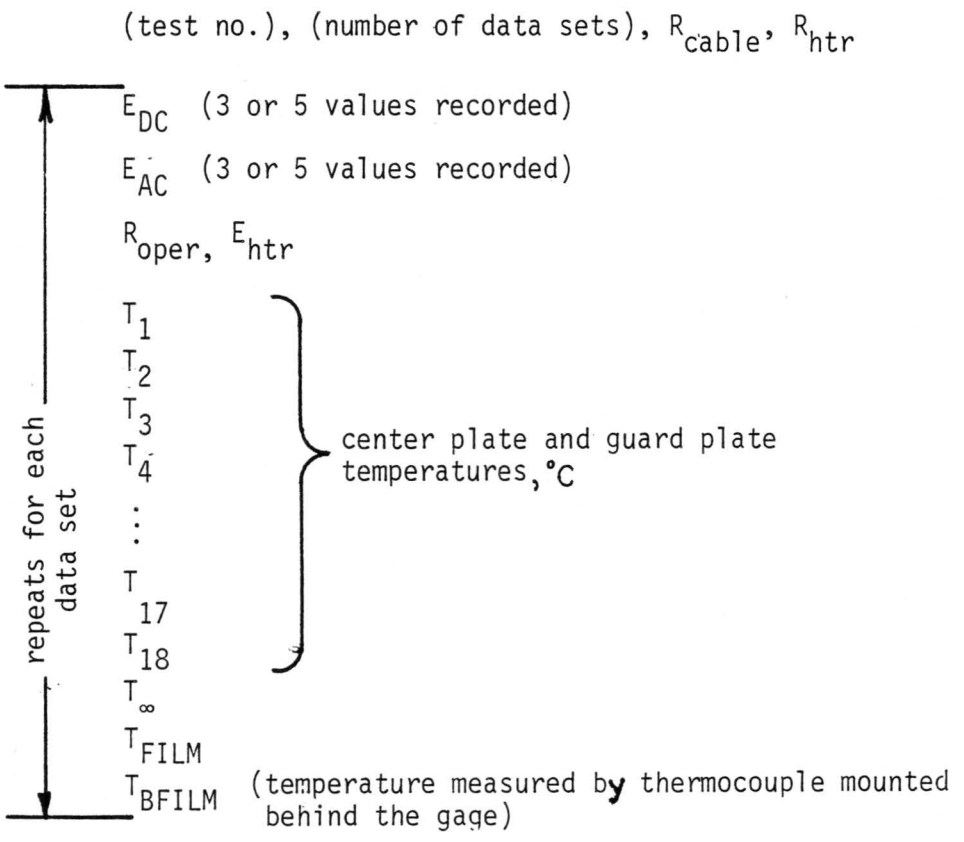

TEST P-2

```
2  4  .26  78.9
2.44  2.44  2.44
.16  .16  .16
27.59  83.3
64.1
64.7
64.4
64.3
65.4
65.3
65.9
65.1
64.7
64.9
65.0
64.4
65.0
66.7
64.8
64.6
65.2
65.0
31.2
65.1
65.2
2.40  2.40  2.40
.16  .16  .16
27.58  80.3
64.1
64.7
64.4
64.3
65.3
64.9
65.4
65.2
64.6
64.9
65.0
64.5
64.9
65.2
65.1
64.8
65.0
65.0
31.3
65.1
65.2
2.39  2.39  2.39
.16  .16  .16
27.59  80.3
64.2
64.8
64.6
64.4
65.3
65.1
65.5
65.0
64.6
64.8
65.0
64.5
65.0
65.1
64.8
65.0
65.0
65.1
30.1
65.1
65.2
2.29  2.29  2.29
.16  .16  .16
27.56  77.5
64.3
65.0
64.6
64.4
65.4
65.2
65.5
65.0
64.5
64.8
64.9
64.5
65.0
65.0
65.1
65.1
65.1
65.2
31.1
65.3
65.1
```

TEST P-3

```
3  2  .26  78.9
2.40  2.40  2.40
.16  .16  .16
27.84  81.2
63.9
64.6
64.5
64.3
64.4
64.8
65.4
65.2
64.3
64.7
64.9
64.3
64.9
64.5
64.9
65.1
65.1
64.9
30.0
65.0
65.0
2.42  2.42  2.42
.16  .16  .16
27.84  81.4
63.9
64.6
64.5
64.4
65.3
64.9
65.5
65.2
64.4
64.7
64.9
64.3
64.9
64.6
64.9
65.1
64.9
64.9
30.0
65.0
65.0
```

TEST P-4

```
4  3  .26  78.9
2.487  2.524  2.496
.163  .144  .172
27.42  83.52
64.2
64.7
64.5
64.3
65.4
64.6
65.2
65.0
63.8
64.1
64.8
64.5
64.9
65.1
65.8
65.1
64.9
65.0
30.7
65.4
65.4
2.417  2.410  2.410
.153  .175  .172
27.42  80.28
64.3
64.9
64.6
64.4
65.4
64.6
65.2
65.0
64.0
64.2
64.9
64.6
65.0
65.0
65.2
65.0
65.2
65.2
30.8
65.4
65.4
2.288  2.236  2.261
.178  .212  .165
27.42  77.7
64.4
64.9
64.6
64.4
65.3
64.7
65.1
64.9
64.0
64.2
64.9
64.7
65.0
65.0
65.3
65.0
65.0
65.1
30.7
65.4
65.4
```

TEST P-5

5 5 .26 78.76
2.473 2.474 2.435 2.504 2.479
.171 .172 .162 .169 .170
27.10 89.5 7.2
64.1
64.7
64.4
64.2
65.4
64.4
65.2
65.0
64.1
64.2
64.9
64.6
65.0
63.6
63.8
63.0
64.4
65.1
27.2
65.1
65.3
2.331 2.393 2.353 2.347 2.356
.211 .180 .171 .201 .184
27.10 85.9 5.4
64.3
64.9
64.6
64.4
65.4
64.6
65.1
65.1
64.2
64.4
64.9
64.6
65.0
63.4
65.0
64.9
64.0
65.1
27.3
65.2
65.4
2.231 2.299 2.247 2.277 2.278
.208 .222 .199 .222 .182
27.11 83.3 3.9
64.3
64.8
64.5
64.4
65.4
64.7
65.2
64.9
64.1
64.3
64.8
64.6
65.0
63.5
64.8
65.0
64.0
65.0
27.0
65.2
65.4
2.159 2.133 2.202 2.176 2.181
.213 .217 .236 .193 .172
27.11 80.1 3.1
64.3
64.9
64.5
64.4
65.3
64.7
65.1
64.8
64.0
64.4
64.8
64.5
65.0
63.5
64.7
64.7
64.0
65.0
27.7
65.0
65.2
2.153 2.146 2.133 2.175 2.133
.204 2.08 .228 .207 .210
27.10 76.1 2.30
64.3
64.8
64.5
64.4
65.2
64.7
65.0
64.8
64.1
64.4
64.8
64.5
65.0
63.5
64.8
64.7
64.0
65.0
27.4
65.1
65.2

TEST P-6

```
6  4  .26  78.76
2.492  2.458  2.464  2.462  2.448
.176  .158  .166  .165  .173
27.09  87.8  7.2
64.1
64.7
64.4
64.3
65.4
64.6
65.2
65.1
64.0
64.1
64.8
64.5
65.0
63.5
64.8
64.5
64.1
65.0
28.5
65.2
65.4
2.501  2.491  2.539  2.508  2.457
.165  .165  .164  .199  .177
27.08  87.9  7.2
64.0
64.9
64.7
64.5
65.6
64.8
65.6
65.1
63.8
63.9
64.7
64.5
65.0
63.4
64.2
63.9
64.0
65.0
28.4
65.2
65.4
2.332  2.291  2.338  2.266  2.345
.191  .193  .188  .222  .209
27.06  84.0  5.0
64.1
64.9
64.7
64.4
65.6
64.9
65.6
65.0
64.0
64.1
64.8
64.5
65.0
63.5
64.7
64.9
64.1
65.0
29.0
65.0
65.2
2.168  2.178  2.164  2.175  2.163
.208  .227  .237  .214  .221
27.07  79.8  3.30
64.2
64.8
64.6
64.5
65.3
64.9
65.4
64.8
63.9
64.0
64.7
64.5
65.0
63.4
64.7
64.7
64.1
65.0
29.2
65.0
65.2
```

The cylinder stagnation point data is given on the following pages. As for the previous data, the format is explained using the nomenclature presented in the text.

(test no.), (number of data sets), P_{amb}

repeats:

P_{stag}, R_{oper}, (angle from stagnation, 0 here)

T_1, T_2, T_3, T_4, T_∞, T_{film}

E_{DC} (3 or 5 values)

E_{AC} (3 or 5 values)

TEST C-1

```
1   10   27.52
1.12   24.11   0.
56.8   60.4   60.1   59.3   24.0   60.0
2.837   2.796   2.794
.0184   .0186   .0202
.96   24.09   0.
56.9   60.4   60.1   59.3   24.0   60.0
2.720   2.744   2.730
.0176   .0184   .0178
.81   24.09   0.
57.0   60.4   60.2   59.3   24.1   60.0
2.663   2.674   2.656
.0177   .0191   .0186
.72   24.08   0.
57.0   60.4   60.2   59.3   24.1   60.0
2.648   2.653   2.625
.0186   .0188   .0186
.54   24.07   0.
57.1   60.4   60.1   59.4   24.2   60.0
2.516   2.490   2.500
.0194   .0192   .0191
.45   24.06   0.
57.2   60.4   60.1   59.4   24.2   60.0
2.409   2.417   2.399
.0188   .0205   .0195
.36   24.06   0.
57.3   60.4   60.0   59.4   24.2   60.0
2.331   2.346   2.355
.0187   .0191   .0189
.28   24.06   0.
57.4   60.4   60.0   59.4   24.3   60.0
2.282   2.275   2.280
.0183   .0187   .0184
.22   24.05   0.
57.6   60.4   60.1   59.6   24.2   60.0
2.206   2.215   2.209
.0189   .0189   .0193
.13   24.05   0.
57.8   60.4   60.0   59.4   23.7   60.0
2.125   2.125   2.125
.0196   .0196   .0196
```

TEST C-2

```
2   7   27.52
1.14   24.17   0.
56.6   60.4   60.5   60.1   21.3   60.0
2.931   2.885   2.871
.0133   .0124   .0128
.94   24.16   0.
56.8   60.4   60.6   60.1   21.6   60.0
2.775   2.753   2.787
.0105   .0087   .0112
.85   24.13   0.
57.0   60.4   60.6   60.0   21.7   60.0
2.707   2.695   2.711
.0084   .0068   .0109
.68   24.12   0.
57.1   60.4   60.6   59.9   21.7   60.0
2.612   2.596   2.600
.0126   .0078   .0075
.54   24.11   0.
57.3   60.4   60.6   59.9   21.7   60.0
2.524   2.518   2.514
.0088   .0073   .0079
.29   24.11   0.
57.6   60.4   60.4   59.8   21.8   60.0
2.310   2.314   2.310
.0066   .00798   .0069
.230   24.08   0.
57.7   60.4   60.4   59.8   22.0   60.0
2.204   2.211   2.214
.0077   .0063   .0077
```

TEST C-3

```
___3  10  27.92
   1.15  24.05  0.
   56.0  59.1  60.8  59.6  20.7  59.4
   2.880  2.880  2.890
___.0091  .0082  .0077
___.95  24.03  0.
   56.1  59.0  60.8  59.5  21.0  59.3
   2.787  2.774  2.758
___.0467  .0442  .0451
___.86  24.02  0.
   56.2  59.0  60.8  59.5  21.0  59.3
   2.698  2.684  2.677
___.0235  .0392  .0441
___.69  24.01  0.
   56.5  59.0  60.8  59.3  20.9  59.2
   2.545  2.535  2.548
___.0362  .0374  .0423
___.52  24.00  0.
   56.6  59.0  60.8  59.3  21.0  59.2
   2.428  2.415  2.428
___.0374  .0446  .0463
___.36  23.99  0.
   56.9  59.0  60.8  59.3  21.0  59.2
   2.307  2.283  2.293
___.0441  .0453  .0422
___.26  23.99  0.
   57.1  59.0  60.8  59.3  21.1  59.1
   2.156  2.154  2.158
___.0576  .0581  .0619
___.190  23.98  0.
   57.3  59.0  60.8  59.2  21.0  59.1
   2.051  2.044  2.053
___.0391  .0361  .0442
___.160  23.97  0.
   57.3  59.0  60.8  59.2  21.0  59.1
   2.035  2.026  2.024
___.0719  .0479  .0742
___.085  23.97  0.
   57.6  59.1  60.8  59.2  21.0  59.2
   1.867  1.848  1.832
___.0447  .0492  .0512
```

TEST C-4

```
4  4  28.00
1.12  23.90  0.
57.0  59.7  61.5  60.0  24.7  59.9
2.738  2.737  2.742
.0393  .0390  .0175
.72  23.89  0.
57.5  59.9  61.8  60.1  24.6  60.0
2.494  2.505  2.484
.0393  .0300  .0376
.53  23.89  0.
57.7  59.8  61.8  60.0  24.6  59.9
2.324  2.319  2.320
.0301  .0382  .0341
.27  23.89  0.
58.0  59.9  61.8  60.1  24.5  60.0
2.104  2.107  2.102
.0312  .0289  .0310
```

TEST C-6

```
___6  4    27.93
   1.08   24.98   0.
   61.7 60.0   60.1   59.9   24.7   61.7
   3.292   3.289   3.298
___.0282   .0292   .0235
___.78   24.95   0.
   61.7   60.0   60.1   59.7   24.9   61.7
   3.128   3.142   3.135
___.0278   .0219   .0241
___.52   24.95   0.
   61.5   60.0   60.0   59.6   25.0   61.5   61.5
   2.945   2.953   2.950
___.0194   .0199 .0184
___.31   24.93   0.
   61.4   60.0   59.8   59.4   24.3   61.4
   2.781   2.744   2.768
___.0187   .0184   .0171
```

TEST C-8

```
8  12  27.70
1.09  24.32  0.
0.  65.0  64.8  64.2  22.6  64.2
2.867  2.862  2.870  2.875  2.873
.022  .027  .023  .025  .029
1.09  24.25  0.
0.  65.0  63.9  64.0  22.8  64.0
2.843  2.846  2.851  2.839  2.863
.029  .025  .027  .025  .026
1.00  24.24  0.
0.  65.0  63.9  64.1  22.8  64.1
2.828  2.819  2.824  2.829  2.830
.026  .022  .025  .023  .029
0.90  24.23  0.
0.  65.0  64.0  64.1  22.8  64.1
2.778  2.771  2.763  2.768  2.769
.022 .024  .028  .023  .019
0.73  24.22  0.
0.  65.0  64.0  64.0  22.9  64.0
2.679  2.675  2.675  2.676  2.677
.021  .024  .026  .024  .020
0.58  24.22  0.
0.  65.0  64.2  64.0  22.8  64.0
2.575  2.589  2.580  2.584  2.592
.025  .021  .018  .020  .020
.52  24.21  0.
0.  65.0  64.1  64.0  22.7  64.0
2.536  2.538  2.536  2.538  2.535
.026  .022  .024  .025  .021
0.39  24.21  0.
0.  65.0  64.2  64.0  22.8  64.0
2.448  2.450  2.464  2.457  2.453
.021  .023  .023  .025  .024
0.31  24.20  0.
0.  65.0  64.2  64.1  22.6  64.1
2.348  2.356  2.352  2.357  2.356
.025  .023  .022  .024  .022
0.23  22.19  0.
0.  65.0  64.3  64.0  22.5  64.0
2.255  2.257  2.255  2.246  2.258
.026  .026  .027  .024  .027
0.17  24.18  0.
0.  65.0  64.3  64.1  22.4  64.1
2.143  2.146  2.142  2.147  2.146
.025  .023  .025  .022  .026
0.08  24.17  0.
0.  65.0  64.3  64.1  22.2  64.1
1.881  1.890  1.886  1.879  1.877
.028  .028  .028  .029  .029
```

The vita has been removed from the scanned document